Hydrodynamic and Microscopic Investigations of Polysaccharides and Glycopeptide Antibiotics of Ophthalmological Importance

By

Taewoo Chun, BSc, MD, MSc

Thesis submitted to University of Nottingham for the degree of Doctor of Philosophy

National Centre of Macromolecular Hydrodynamics (NCMH)

School of Biosciences, University of Nottingham

Sutton Bonington Campus, Loughborough LE12 5RD, UK

May 2023

List of Contents

List of Figures

List of Tables

List of Abbreviations

AMR: antimicrobial resistance

BSM: bovine submaxillary mucin

DLS: dynamic light scattering

ESEM: environmental scanning electron spectroscopy

HA: hyaluronic acid

MRSA: methicillin-resistant *Staphylococcus aureus*

NHS: National Health Service

NMR: nuclear magnetic resonance

SE-AUC: sedimentation equilibrium in the analytical ultracentrifuge

SEC-MALS: size exclusion chromatography coupled to multi-angle light scattering

SV-AUC: sedimentation velocity in the analytical ultracentrifuge

TSP: tamarind seed polysaccharides

VRE: vancomycin-resistant enterococci

Abstract

The thesis consists of two main themes: the eye-drop study for dry eye syndrome and the antibiotic study for antibiotic resistance. Hyaluronic acid (HA) has been commonly used in eyedrop formulations. A difficulty has been its short residence time on ocular surfaces due to ocular clearance mechanisms which remove the polysaccharide almost immediately. To prolong its retention time, tamarind seed gum polysaccharide (TSP) is mixed as a helper biopolymer with HA. Here I look at the hydrodynamic characteristics of HA and TSP (weight average molar mass M_w and viscosity [η]) and then explore the compatibility of these polymers, including the possibility of potentially harmful aggregation effects. The research is based on a novel combination of three methods: sedimentation velocity in the analytical ultracentrifuge (SV-AUC), size-exclusion chromatography coupled to multiangle light scattering (SEC-MALS) and capillary viscometry. For the mixed HA-TSP systems, SEC-MALS indicates the possibility of a weak interaction. However, further investigation using sedimentation coefficient (s) distributions obtained from SV-AUC measurements together with intrinsic viscosity demonstrated no evidence of any significant aggregation phenomenon, reassuring in terms of eye-drop formulation technology involving these substances.

The other topic is about the natural glycopeptide antibiotic teicoplanin used for the treatment of serious Gram-positive related bacterial infections and it can be

administered intravenously, intramuscularly, topically (ocular infections), or orally. The hydrodynamic properties of teicoplanin A2 (M_1 = 1879.7 g/mol) were examined in phosphate chloride buffer using sedimentation velocity and sedimentation equilibrium in an analytical ultracentrifuge together with capillary (rolling ball) viscometry. In the concentration range, 0-10 mg/mL teicoplanin A2 was found to self-associate plateauing > 1 mg/mL to give a molar mass of (35400 ± 1000) g/mol corresponding to ~ (19 ± 1) mers, with a sedimentation coefficient $s_{20,w}$ = ~ 4.65 S.

Methicillin-resistant *Staphylococcus aureus* (MRSA) and enterococci have managed to avoid the antimicrobial activity of glycan antibiotics. Aggregations of antibiotics with mucins lead to long exposure and selection pressure to push forward further increases in resistant species in microbes. This study was focused on any potential interactions of teicoplanin with bovine submaxillary mucin (BSM) as an ocular mucin model, based on the relatively novel combination of hydrodynamic and microscopic techniques: SV-AUC, dynamic light scattering (DLS), and environmental scanning electron microscopy (ESEM). For the mixture of teicoplanin with the lowest concentration (0.125 mg/mL) and BSM, SV-AUC showed no interactions, while for higher concentrations (1.25 mg/mL and 12.5 mg/mL), teicoplanin was shown to have weak interactions with BSM and aggregates in the distributions of both sedimentation coefficients by SV-AUC and hydrodynamic radii by DLS.

Acknowledgments

First, I, Taewoo Chun, must thank my supervisor, Professor Stephen E. Harding for his continuous support during my PhD journey at National Centre for Macromolecular Hydrodynamics (NCMH). He has continuously provided the best and kindest guidance for the student whose speaking English skill is insufficient. I also express my deep gratitude to my co-supervisor, Professor Anthony P. Corfield for his information and advice on my PhD thesis.

I should extend my thanks to all staff (present and past) in the NCMH and the Biomaterials group in the University of Nottingham. Professor Mary K. Phillips-Jones gave me her expertise in antibiotic resistance. Professor Gleb E. Yakubov provided his suggestions about the data interpretation of experimental results. Assistant Professor Vlad T. Dinu and Dr Thomas MacCalman taught me how to perform hydrodynamic experiments and analyse the obtained data. Dr Jacob Pattem kindly performed microscopic experiments and proofread Chapters of my PhD thesis. Dr Richard B. Gillis demonstrated how to conduct the conformational analysis. Dr Jennifer Wakefield advised me how to manage long Word documents including PhD theses.

Finally, I would like to thank my parents, paying the PhD tuition fee, for their endless love and support.

Chapter 1: General introduction

1.1. Polysaccharides in ophthalmology

A polysaccharide is typically a large glycan formed by repeating motifs of mono- or oligosaccharides. The term 'glycan' usually includes both polysaccharides and glycoconjugates, such as glycoproteins and glycolipids (Harding et al., 2017). A monosaccharide is a carbohydrate represented by $C_x(H_2O)_y$ in a chemical formula. A typical example is β-D-glucose. Figure 1-1 shows the open-chain (Fischer) and ring (Haworth and chair) forms of β-D-glucose. In the ring form, D-glucose has one of two orientations of a hydroxy group on C1 notated by either α (below the ring) or β (above the ring). These differences in orientation generate diversity in polysaccharides. For example, cellulose is a homopolymer composed of β-D-glucose residues linked by β(1→4) throughout, while amylose is composed of α(1→4) linked α-D-glucose residues (Varki and Kornfeld, 2017). There is also a range of ways of producing diverse polysaccharides, such as branching (e.g., amylose vs. amylopectin) and the result of substitution reactions (e.g., N-acetyl-D-glucosamine). Consequently, it is no surprise that the roles of polysaccharides are diverse (Harding et al., 2017). For instance, cellulose is the main ingredient of plant cell walls while starch is one of the storage polysaccharides (Harding et al., 2017). Additionally, glucosamine including N-acetyl-D-glucosamine (β-D-glucose with

C2 of the hydroxy group substituted by the acetylamino group) is used to alleviate symptoms of osteoarthritis, in which articular cartilage of the knee or/and hip is eroded with ageing (Seeberger and Cummings, 2017).

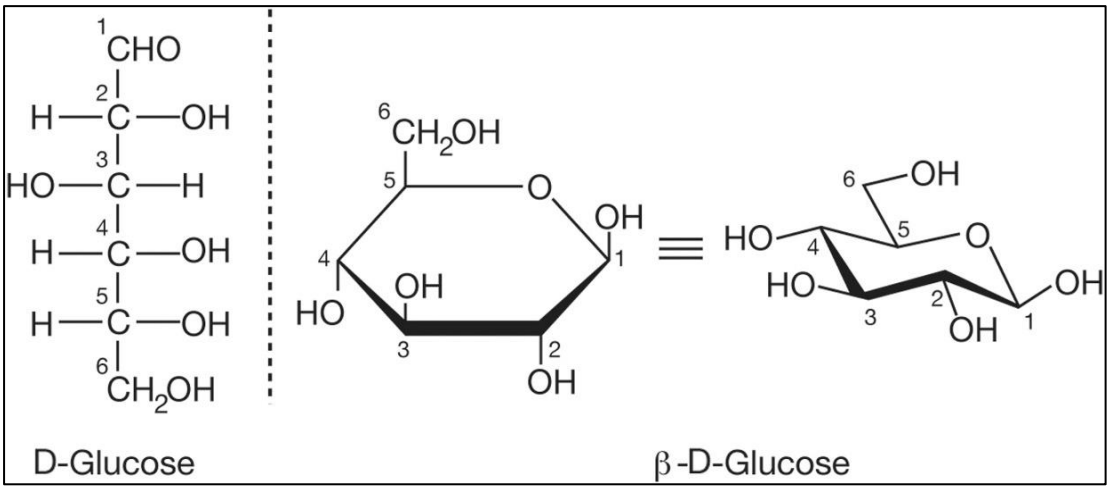

Figure 1-1: The open-chain (left), Haworth (middle), and chair (right) forms of β-D-glucose (Varki and Kornfeld, 2017).

Similarly, polysaccharides are used widely to relieve ocular problems including dry eye syndrome (*keratoconjunctivitis sicca* in medical terms). The causes of dry eye are classified as evaporative or aqueous-tear deficient dry eyes (Golden et al., 2022). Evaporative dry eye is caused by exacerbated evaporation of tears (Golden et al., 2022). This results from the dysfunction of meibomian glands secreting oils which remain on the top of the tear film – the lipid layer of the three layers composing the tear film and prevent evaporation. Other factors are insufficient blinking and environmental factors, such as low humidity and high flow of air. Aqueous-tear deficient dry eye is subclassified into two categories: Sjögren's syndrome, and non-Sjögren's syndrome, the latter mostly because of age-related lachrymal dysfunction (Barabino, 2013). No matter what the cause, a tear supplement is the only treatment for dry eye (Barabino, 2013).

Artificial tear products to replace mucins of tear films have been invented using various biopolymers including polyvinyl alcohol, polyacrylic acid (Carbomer), and semisynthetic celluloses: carboxymethylcellulose and hydroxypropyl methylcellulose, known as Hypromellose (Forrester et al., 2016a). Figure 1-2 shows the chemical structures (chair forms) of these semisynthetic celluloses. Cellulose derivatives are the first group of polysaccharides available for eye drops and are still used in ophthalmology (Patchan et al., 2013). One of their drawbacks is the

unclear threshold between a viscous solution and an unwanted gel phase because of a lack of data on hydrodynamic properties including viscosities (Dubashynskaya et al., 2019). As a result, the scope of eye drop development has extended to other types of polysaccharides, such as chitosan, alginate, and hyaluronic acid (HA). HA has a longer retention time than cellulose derivatives and polyvinyl alcohol (Forrester et al., 2016). That is one of the main reasons why the NHS Trusts recommend HA and cellulose derivatives rather than any other polysaccharides. Table 1-1 summarises eye drop products recommended by the NHS Trusts.

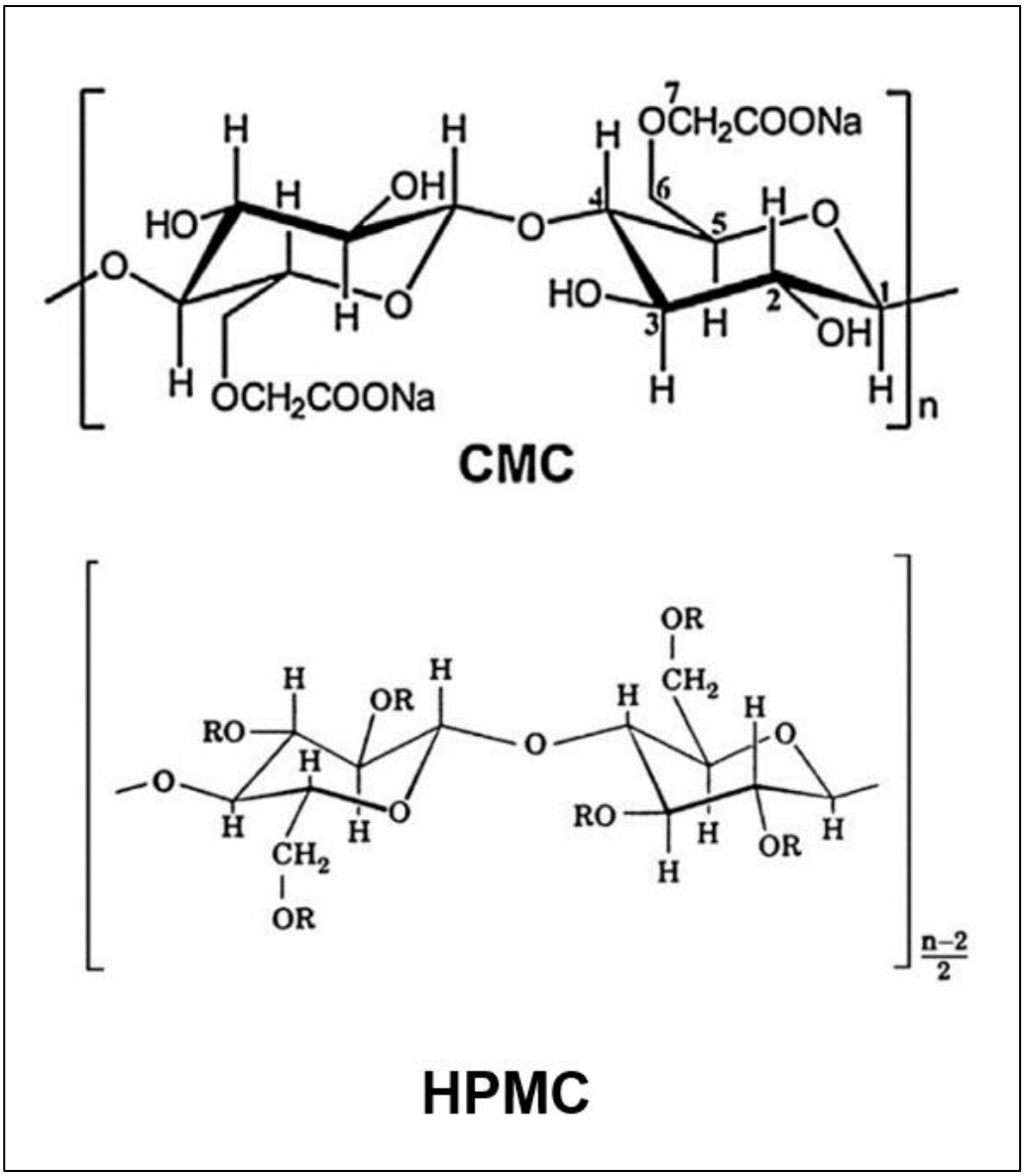

Figure 1-2: The chemical structures of CMC – sodium carboxymethyl cellulose (Ghorpade et al., 2017) and HPMC – hydroxypropyl methylcellulose (Siepmann and Peppas, 2012). The R group is either CH_3, $CH_2CH(CH_3)OH$, or H. Types of HPMC are classified according to the degree of methoxy- and hydroxypropoxy-groups (Siepmann and Peppas, 2012).

Table 1-1: the eye products recommended by the NHS Trusts (NHS, 2020, 2022)

The type of ingredients such as polysaccharides	Products listed by Imperial College Healthcare NHS Trust (Not related to disease severity)	Products, depending on disease severity, recommended by NHS West Essex CCG (Clinical Commissioning Group)
Hypromellose	Hypromellose 0.3%, 0.5%	Hypromellose 0.3% for mild symptoms
carboxymethylcellulose	carboxymethylcellulose 0.5%, 1%	carboxymethylcellulose 0.5% for mild symptoms
Carbomer	Carbomer 0.2% (GelTears® / Viscotears®) 0.36% (Blephagel®)	Carbomer 0.2% for mild and moderate symptoms
Hyaluronic acid (HA)	Sodium Hyaluronate 0.1% (Hylo-Tear®) 0.2% (HydraMed®)	Sodium Hyaluronate 0.1% for moderate symptoms
Lipid paraffin	Lipid paraffin (Lacri-Lube eye ointment®)	carboxymethylcellulose 1% for moderate symptoms
Retinal palmitate with paraffin and wool fat (VitA-POS®)	Retinal palmitate with paraffin and wool fat (VitA-POS®)	-
Hyaluronic acid (HA)	-	Sodium Hyaluronate 0.1% for severe symptoms
Hyaluronic acid (HA)	-	Sodium Hyaluronate 0.2% for severe symptoms
Vitamin A	-	Retinol (vitamin A) with paraffin and wool fat ointment for severe symptoms

HA, also known as hyaluronan, has the repeating unit of N-acetyl-D-glucosamine (GlcNAc) β(1→4)-linked with glucuronic acid (GlcA). This is represented by:

…→3) β-D-Glc*p*NAc (1→4) β-D-Glc*p*A(1→…

where *p* means pyranose, a six-membered ring including an oxygen atom (see Figure 1-1), while furanose, *f*, is a five-membered ring (Harding et al., 2017). Figure 1-3 shows the chair form of HA. HA has numerous desirable features for eye drops. For example, there are enhancing tear film stability (Forrester et al., 2016), good biocompatibility (Dubashynskaya et al., 2019), and pseudoplastic behaviour (shear-thinning). When a shear rate or stress increases, its viscosity decreases. Excessive viscosity is not excellent, leading to blurred vision and low compliance of patients (Snibson et al., 1990).

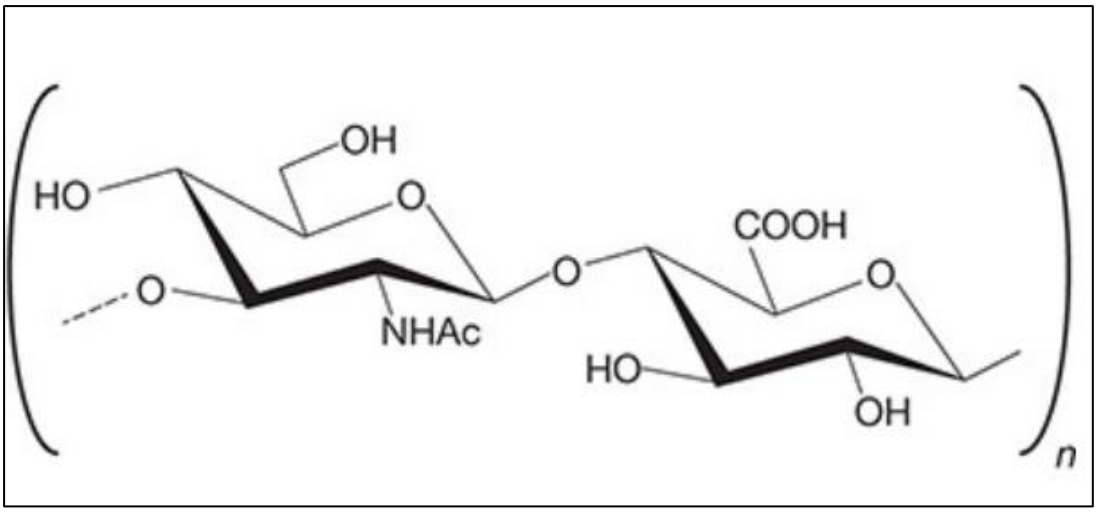

Figure 1-3: The chemical structure of HA. n=250-25000 (Hascall and Esko, 2017).

However, the undesired point of topical installation is that most of the amount of an ocular drug is shed by anatomical and physiological factors (Forrester et al., 2016). After that, the eye drop is exposed to blinking, further decreasing its volume on the conjunctival sac (Lee, et al., 2017). Consequently, increasing the retention time of eye drops is essential for improving their bioavailability, which is the actual amount of a drug delivered on-site (Harding et al., 2017). In contrast, a far viscous eye drop (e.g., 1 % w/v HA) leads to discomfort and a greater blink rate (Dubashynskaya et al., 2019). Therefore, a firm interaction of polysaccharides with ocular mucins is a key strategy to resist blinking.

A range of products aims to improve the interaction of ingredients of eye drops with ocular glycans. For instance, chitosan-*N*-acetylcysteine (Lacrimera®) is the chitosan derivative, whose mucoadhesive property is more improved by the thiol group of *N*-acetylcysteine (Schmitz et al., 2008). The other way of enhancing mucoadhesion is the combination of two different polysaccharides. One example is a combination of HA and carboxymethylcellulose (Carmellose), which has a synergistic effect and thus increases its retention time (Simmons et al., 2015). A successful alternative combination is a mixture of HA and tamarind seed polysaccharide (TSP), released into the market as HydraMed®. TSP is a neutral xyloglucan composed of the backbone of β(1→4) linked β-D-glucan with branches of mainly α(1→6) linked α-

D-xylose and partially β(1→2) linked β-D-galactoxylose (Miyazaki et al., 1998). TSP has been intensively investigated regarding its mucoadhesive property (Uccello-Barretta et al., 2011) and synergistic interactions with HA (Uccello-Barretta et al., 2010). They showed using nuclear magnetic resonance (NMR) spectroscopy mucoadhesive interactions of TSP with bovine submaxillary mucin (BSM) as model mucin (Uccello-Barretta et al., 2013). However, prior to the present study, there has been no published paper that presents hydrodynamic data, which provides a different and new aspect from molecular hydrodynamics.

The second aspect of this thesis also considers the hydrodynamic properties of glycopeptide antibiotics used in the treatment of more serious ocular and other diseases.

1.2. Glycopeptide antibiotics and drug delivery in ophthalmology

The history of glycopeptide antibiotics comes from the discovery of vancomycin. Vancomycin was approved for clinical use in 1958 (see, e.g., Griffith, 1984). Vancomycin is included in first-generation glycopeptide antibiotics, as well as teicoplanin approved in 1988 in Europe (Blaskovich et al., 2018). Second-generation antibiotics are telavancin, dalbavancin, and oritavancin, which are semi-synthetic glycans (van Groesen et al., 2022). Figure 1-4 shows the chemical structures of these glycans with noticeable differences and similarities. Both vancomycin and teicoplanin have heptapeptide backbones, though vancomycin has a disaccharide residue (glucose and vancosamine) attached to amino acid 4, while teicoplanin has *N*-acylglucosamine, *N*-acetylglucosamine, and mannose, attached to amino acid 4, 6, and 7, respectively. *N*-acylglucosamine includes a long acyl chain (the R group in Figure 1-4). Both glycopeptides inhibit peptidoglycan synthesis through Lipid II, a precursor of peptidoglycan necessary for the construction of bacterial cell walls (Blaskovich et al., 2018). This class of antibiotics is mainly used to treat Gram-positive infections (Vazquez-Guillamet and Kollef, 2014).

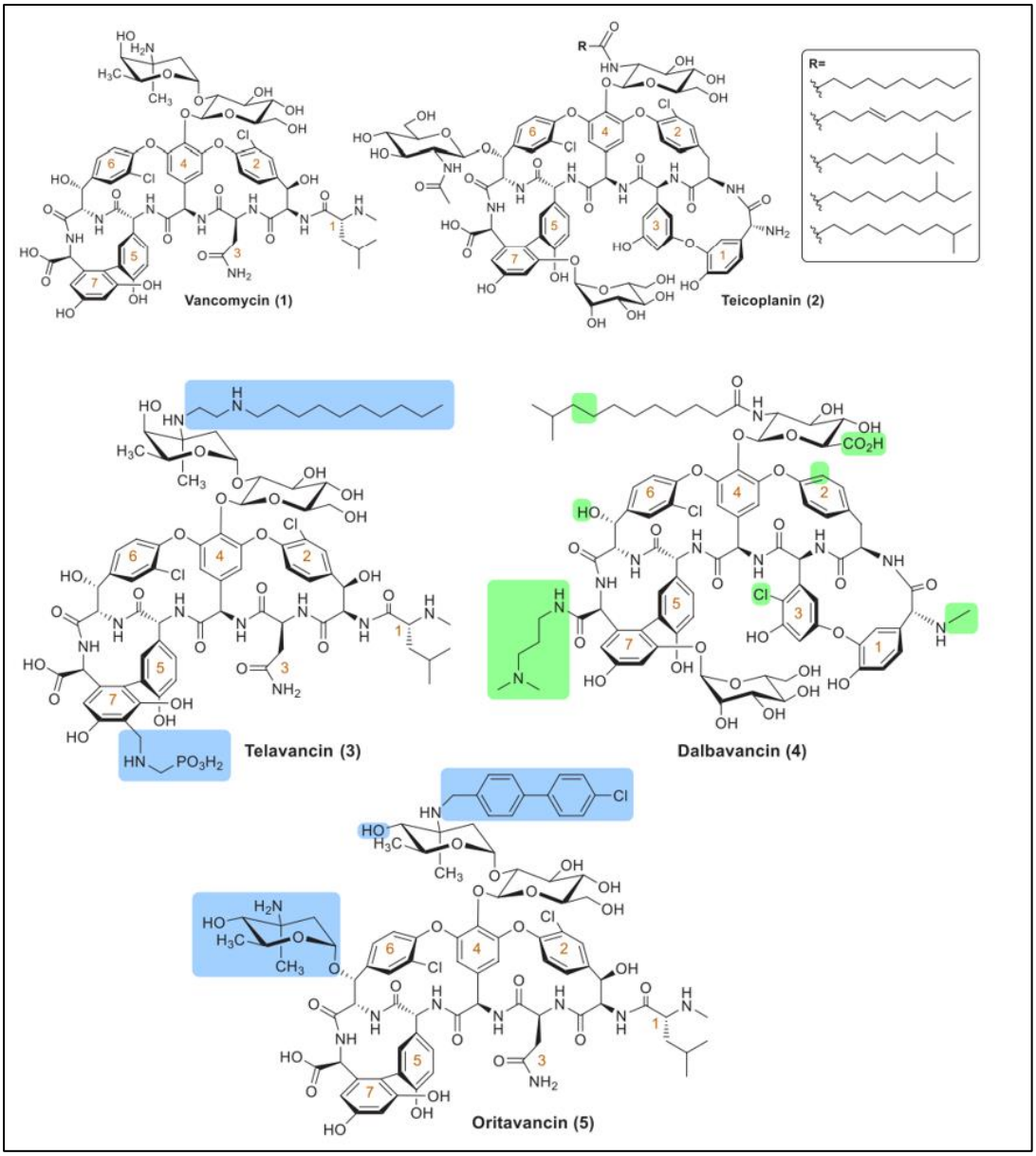

Figure 1-4: The structure of (1) vancomycin, (2) teicoplanin, (3) telavancin, (4) dalbavancin, and (5) oritavancin (van Groesen et al., 2022). Blue areas indicate the structural differences with vancomycin and green areas indicate the differences with teicoplanin.

Bacterial infections of the eyes lead to devastating effects on patients' quality of life. Although conjunctivitis and blepharitis (inflammation of eyelids) rarely affect vision, keratitis (inflammation of the cornea) and endophthalmitis (inflammation of intraocular tissues) result in severe visual impairment (Forrester et al., 2016). Post-operative (cataract) endophthalmitis accounts for 40-80% of major cases, which are caused by coagulase-negative staphylococci (Durand, 2017). Since pathogens are undetermined in 20-30% of cases (Durand, 2017), immediate and empiric treatment is needed after sampling. The first choice of drugs is the intravitreal or intravenous injection of vancomycin and ceftazidime (or amikacin for patients with penicillin anaphylaxis), which are broad-spectrum antibiotics (NHS, 2017). Keratitis is caused by *S. aureus*, the second most common bacteria (Ross et al., 2021), following *Pseudomonas aeruginosa*, the Gram-negative bacteria (Forrester et al., 2016). While *P. aeruginosa* leads to more severe outcomes than *S. aureus*, methicillin-resistant *S. aureus* (MRSA) is more challenging (Forrester et al., 2016). For MRSA keratitis, vancomycin (1.2, 2, or 5%) eye drops are recommended (Lin et al., 2019).

To prevent infections, the ocular surface has developed host defence mechanisms. Of these host defences, tear films play important roles in removing pathogens. The tear film consists of two layers – an outer lipid layer and a mucous-aqueous layer,

covering a glycocalyx layer of the ocular epithelium (Gipson, 2004). Figure 1-5 shows these two layers between the ocular surface and the environment. In this thin (3μm) film, there are more than 1500 proteins (Zhou et al., 2012), including over twenty mucins (Dartt and Willcox, 2013). These proteins, such as secretory immunoglobulin A (IgA), IgG, and complement, prevent bacteria invading further (Forrester et al., 2016). Lysozyme and lactoferrin also contribute to antimicrobial effects (Wiesner and Vilcinskas, 2010). This might be the reason why unstable or insufficient tear films cause dry eye syndrome, leading to more susceptibility to infections. Moreover, the epithelial cells under the tear film provide an effective physical barrier against microorganisms – tight junctions. Superficial cells of the stratified epithelium adhere to each other via desmosomes between the lateral membranes (Forrester et al., 2016). These barriers are effective against bacterial infections. As a result, microorganisms cannot colonise in the eye surface, compared with different mucosal surfaces including the oral and intestinal cavities (Dartt and Willcox, 2013). On the other hand, such barriers also make ocular drug delivery harder.

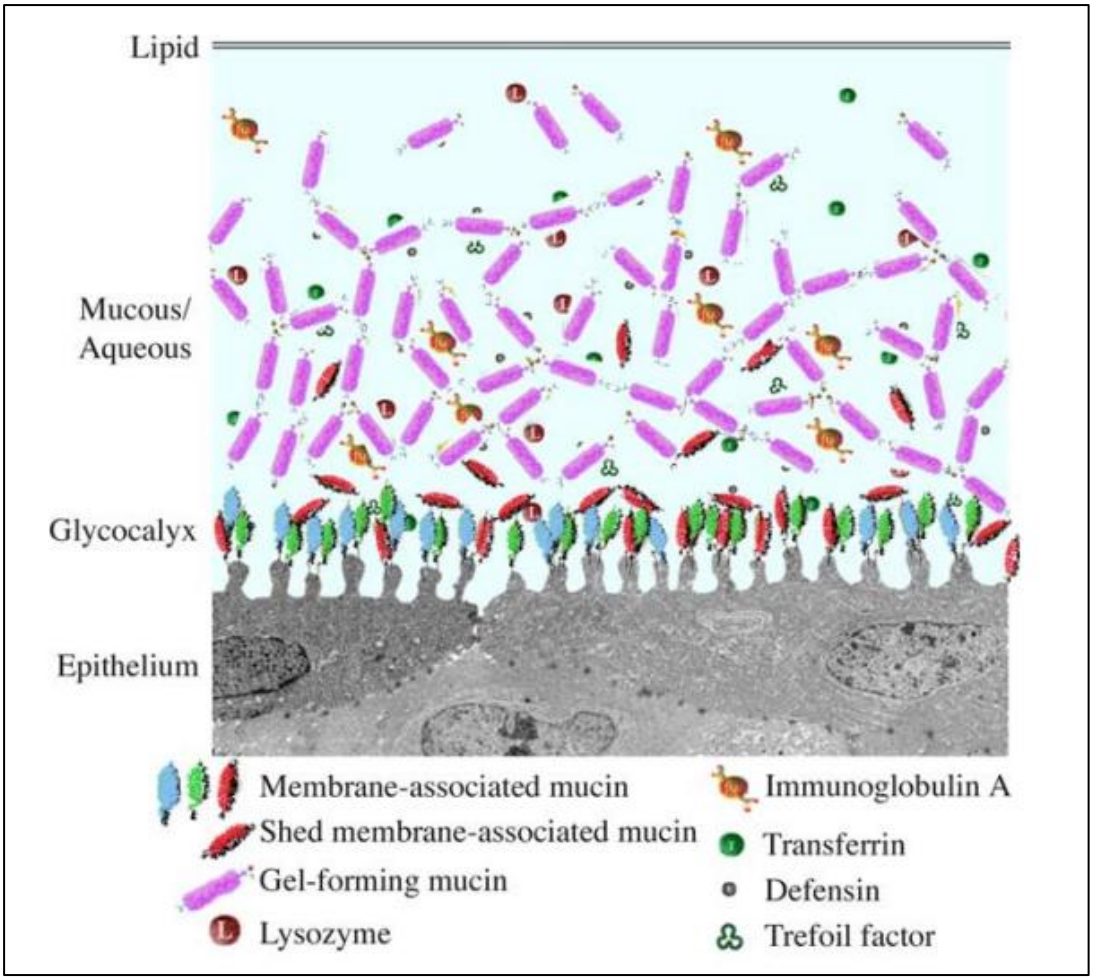

Figure 1-5: The tear film and the glycocalyx (the layer of transmembrane proteins of the ocular epithelial cells). In the tear film, there are various types of mucins, such as MUC5AC (purple); a secreted mucin, MUC1 (blue), MUC4 (green), and MUC16 (red); membrane-associated mucins (Gipson, 2004).

Beyond the tight junctions between the ocular epithelial cells, there is a variety of factors affecting drug absorption, such as ionisation, lipophilicity, and the biological form of drugs. The first point of these factors to affect drug delivery is the pH of tear films, normally 6.5-7.5 (Forrester et al., 2016). The degree of ionisation under a certain pH is determined by the Henderson-Hasselbalch equation for weak acid and base:

$$pH = pK_a + log\left\{\frac{[A^-]}{[HA]}\right\} \quad (1\text{-}1)$$

$$pH = pK_a + log\left\{\frac{[B]}{[BH^+]}\right\} \quad (1\text{-}2)$$

where pK_a is the point where half (50%) of the molecules are ionised, and A^-/HA and B/BH^+ represent an acid and base, respectively (Forrester et al., 2016). The pK_a values of vancomycin and teicoplanin A2 are 7.75 (Jia et al., 2013; Takács-Novák et al., 1993) and 5.66 (Bardone et al., 1978; Cavalleri et al., 1983; Jin et al., 2021), respectively. As a result, in the tear film, vancomycin molecules are more inclined to be un-ionised, and thus lipophilic, than teicoplanin A2. The un-ionised form is favourable for corneal penetration because the corneal epithelium is lipophilic.

In terms of clinical use in ophthalmology, many papers have reported favourable corneal absorption of vancomycin, rather than teicoplanin. For example, one paper (Alster et al., 2000) showed that 50 mg/mL of vancomycin eye drops reached 1.5-2 μg/mL in the anterior chamber (Figure 1-6), being more than the therapeutic

concentration; MIC90 (minimum inhibitory concentration which kills 90% of bacteria) = 1 μg/mL for both vancomycin and teicoplanin (Xu et al., 2021). Another study reported that, after applying 33 mg/mL of topical drugs, the vancomycin concentration was ~46.4 μg/mL in the corneal stroma (Cahane et al., 2004). In contrast, nearly all reports indicate poor corneal penetration of teicoplanin (Antoniadou et al., 1998; Kaye et al., 2009), and therefore, there is no clinical use of teicoplanin by the topical route. The difference in drug absorption would result from the biological form in tear films because teicoplanin aggregates in solution (Bardsley et al., 2002). This aggregation additionally becomes a physical barrier to corneal penetration of teicoplanin. Furthermore, the aggregation would prevent teicoplanin from working, since teicoplanin uniquely works as a monomer form, compared with vancomycin needing cooperative back-to-back dimerization during the inhibition of bacterial cell wall synthesis (Beauregard et al., 1995).

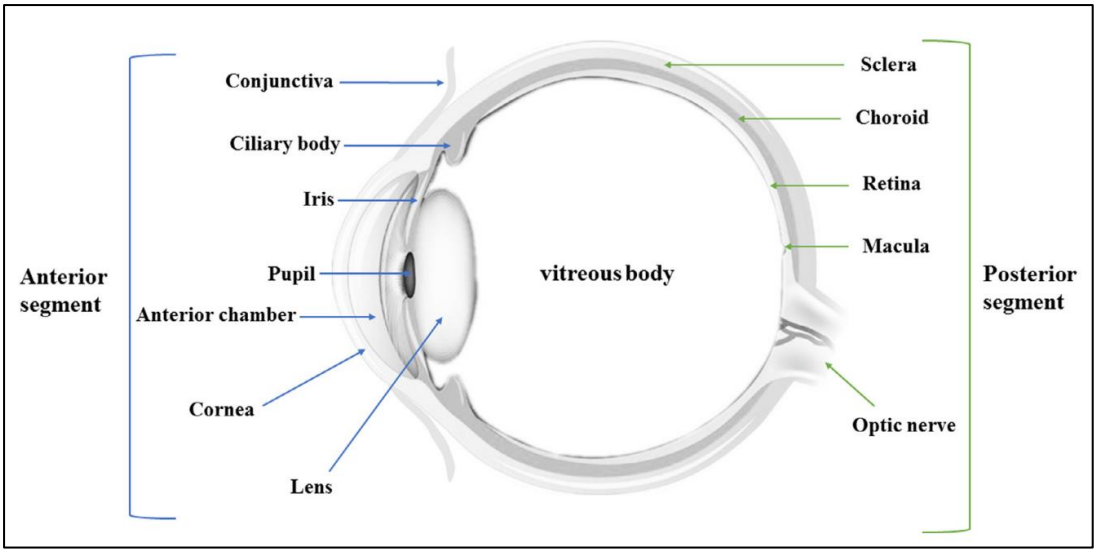

Figure 1-6: The diagram of a sagittal plane of ocular anatomy (Wu et al., 2018).

1.3. Mucins and ocular mucins

Structures of mucins are diverse. Mucins are classified as glycoproteins containing heterogeneous O-linked N-acetylgalactosamine (GalNAc) glycans attached to the protein backbone (Brockhausen and Stanley, 2017). In eukaryotic cells, N- or O-linkages are typically used for the covalent binding of glycans with the protein scaffold (Guzman-Aranguez and Argüeso, 2010). As for the O-linkage, GalNAc covalently binds with the hydroxyl group of serine (Ser) or threonine (Thr) amino acids. O-GalNAc glycans form one of four common structures, called ‘core’, and each core may extend further by adding sugar residues (Brockhausen and Stanley, 2017). Figure 1-7 shows four types of core structures and the model of a secreted mucin resembling a bottle brush. It is well-known that O-GalNAc glycans (also called ‘mucin-type O-glycans’) are relatively shorter in tear films than in other sites, such as the respiratory and intestinal tracts (Podolsky, 1985). This could be because of the characteristic conditions of the eyes (Guzman-Aranguez and Argüeso, 2010). Humans have about twenty mucin genes (Brockhausen and Stanley, 2017), though around five ocular mucins are well-investigated, namely, secreted mucins; MUC5AC and MUC7, and membrane-associated mucins; MUC1, MUC4, and MUC16 (Forrester et al., 2016).

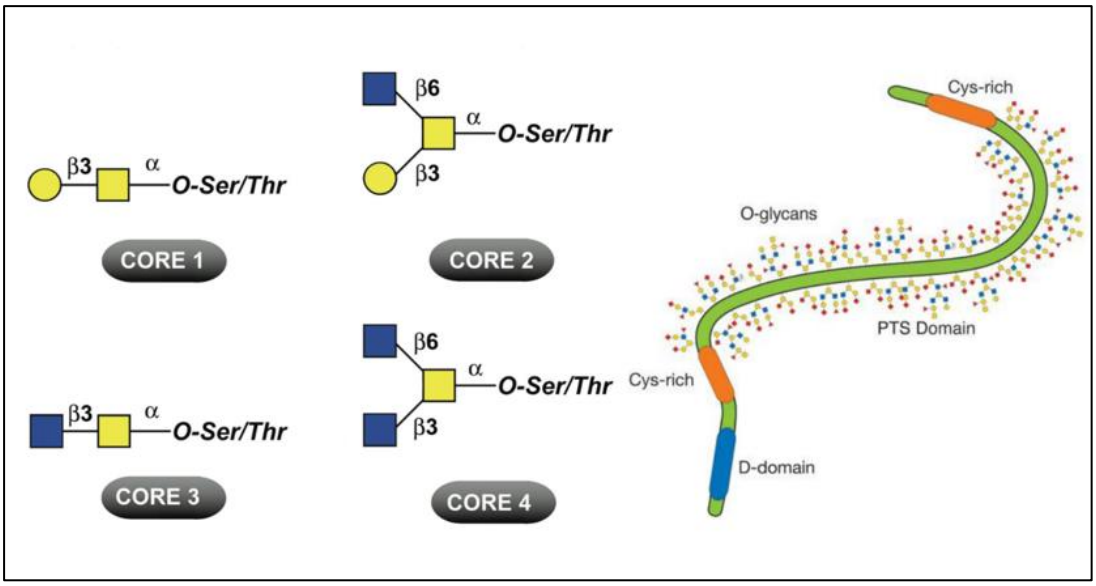

Figure 1-7: Four types of 'Core' structures and the diagram of a bottle-brush mucin (Brockhausen and Stanley, 2017; Guzman-Aranguez and Argüeso, 2010). Symbols represent galactose (yellow round), GalNAc (yellow square), and GlcNAc (blue square). A PTS domain is a proline, threonine, and serine-rich region which is heavily glycosylated. A D-domain is a dimerization domain.

Secreted mucins are subclassified as gel-forming mucin; MUC5AC and small secretary mucin; MUC7. MUC5AC is produced by goblet cells of the conjunctival epithelium as a large glycoprotein with a molar mass of around 40 MDa (Gipson and Argüeso, 2003). MUC5AC includes a tandem repeat of cysteine-rich D domains causing multimerization through disulfide bonds (Gipson and Argüeso, 2003; Hodges and Dartt, 2013). This multimerization allows MUC5AC to form a gel (Gipson and Argüeso, 2003). On the other hand, MUC7 is a small soluble and monomeric glycoprotein produced by the lacrimal gland. Its molar mass is about 180 kDa (Gomes et al., 2011). MUC7 has a single polypeptide backbone containing five domains (Gururaja et al., 1998), such as a histatin (histidine-rich polypeptide)-like domain (Domain 1) and five to six tandem repeats of mucins (Domain 3). MUC7 is not found in tear fluid (Spurr-Michaud et al., 2007), whereas MUC5AC is the most abundant mucin. Figure 1-8 shows the diagrams of each secretory mucin. Secretory mucins must be transparent so that vision is normal due to a transparent tear film. Mantelli and Argüeso (2008) suggested that the feature, that is, a relatively low molar mass of the ocular mucin, might be uniquely required just for ocular surfaces because a highly polymerised and viscous layer would damage visional functions.

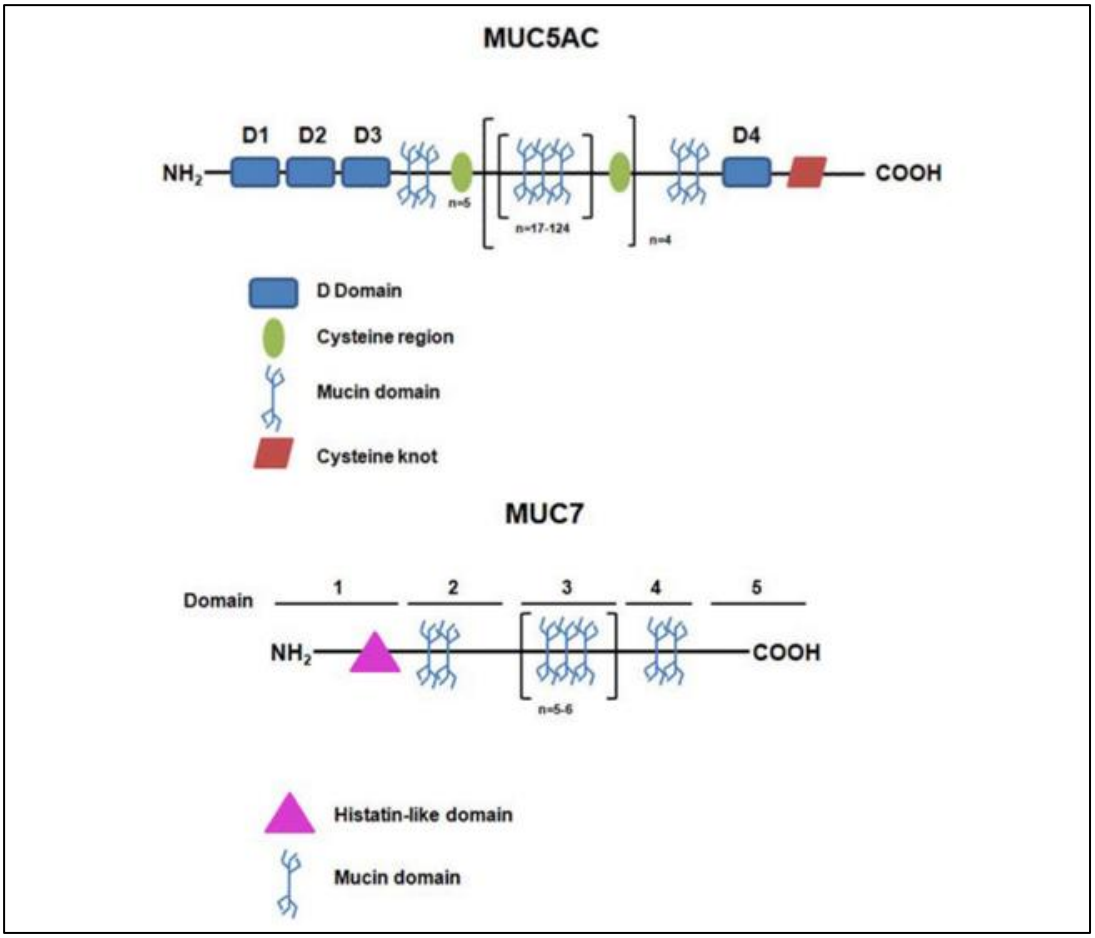

Figure 1-8: The diagrams of the structure of MUC5AC and MUC7 (Hodges and Dartt, 2013).

The structures of membrane-associated mucins are more complex than secretory mucins. Transmembrane mucins are usually composed of two heterodimers linked together through a noncovalent bond (Hattrup and Gendler, 2008). The larger one is extracellular and highly glycosylated, while the smaller one has a transmembrane area and a short cytoplasmic tail (CT). Consequently, these transmembrane mucins also have each cleavage site targeted by enzymes, leading to soluble forms detected in tear fluid (Spurr-Michaud et al., 2007). MUC1 is the smallest mucin of three membrane-associated mucins with a molar mass of 200-500 kDa (Brayman et al., 2004). The molar mass of MUC4 is 900 kDa (Hattrup and Gendler, 2008). MUC4 contains several characteristic domains, such as EGF (epidermal growth factor)-like domains and a D domain (Hodges and Dartt, 2013). MUC16 is the largest mucin of the three with a molar mass of over 2.5 MDa (Hattrup and Gendler, 2008). Both the cornea and the conjunctivae express these three mucins (Gipson and Argüeso, 2003), while the goblet cells of the conjunctivae express MUC5AC. Figure 1-9 shows the diagrams of each membrane-associated mucin. Both secretory and transmembrane mucins prevent bacterial adhesion and colonisation on ocular surfaces (Hodges and Dartt, 2013).

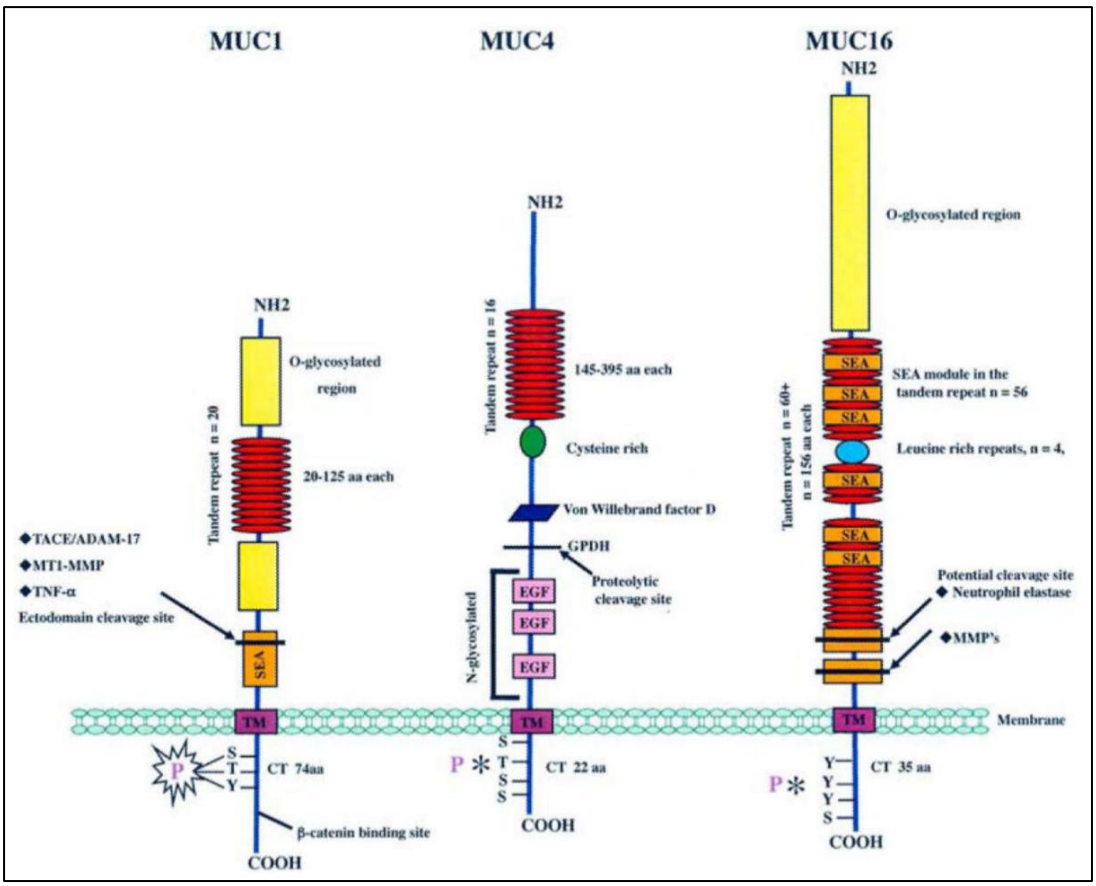

Figure 1-9: The diagrams of MUC1, MUC4, and MUC16 (Hodges and Dartt, 2013).

However, recent research has provided new insight into the relationship between mucins and antimicrobial resistance (AMR). While gastrointestinal mucins prevent a range of microbes from causing infections (McGuckin et al., 2011), mucin binding to vancomycin exacerbates AMR because pathogens are exposed to the aggregates of vancomycin (Dinu et al., 2020). Glycopeptide antibiotics inhibit peptidoglycan synthesis by attaching a Lipid II precursor through five hydrogen bonds (Blaskovich et al., 2018). To avoid the attachment of antibiotics, bacteria, such as vancomycin-resistant enterococci (VRE), transform the binding sites (D-Ala-D-Ala) of Lipid II. D-Ala-D-Ala is modified into D-Ala-D-Lac for *vanA*, *vanB*, *vanD*, *vanF*, and *vanM*, or D-Ala-D-Ser for *vanC*, *vanE*, *vanG*, *vanL*, and *vanN* (Stogios and Savchenko, 2020). Figure 1-10 shows the structure of Lipid II, its binding sites (D-Ala-D-Ala), and the modification of the binding sites (D-Ala-D-Lac). This transformation results from the plasmid-mediated gene cluster, such as *vanA* and *vanB*, between bacterial cells (van Groesen et al., 2022). Consequently, the increased exposure to vancomycin may be responsible for the further activation of AMR in bacteria and selection for VRE populations among gut microbes (Dinu et al., 2020).

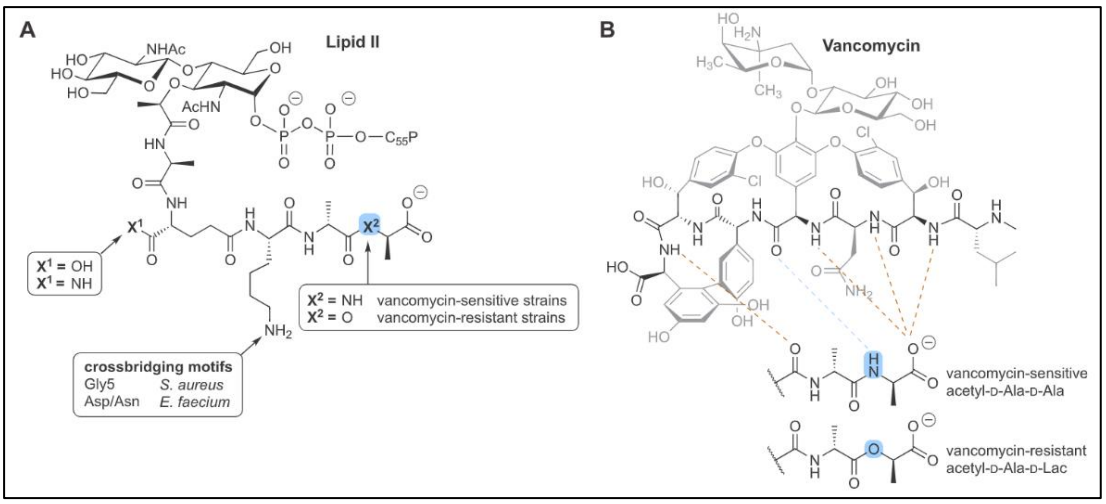

Figure 1-10: The structure of Lipid II (A) and binding of vancomycin to D-Ala-D-Ala through the five hydrogen bonds (dotted lines). One (blue line) of them is lost in D-Ala-D-Lac (van Groesen et al., 2022).

Teicoplanin also may be involved in aggregation with mucins, resulting in higher acquisition of AMR among ocular and gastrointestinal microbes in the healthy and infected sites. Bovine submaxillary mucin (BSM) is used as model mucin in this thesis. Both MUC5AC, the most abundant ocular mucins, and BSM are gel-forming mucins (Carpenter et al., 2021; Hodges and Dartt, 2013). The molar mass of MUC5AC is 2.2 MDa for monomer (Thornton et al., 1996) and 40 MDa for polymer (Sheehan et al., 2000) while that of BSM is 0.8-2 MDa for monomer and 21-25 MDa for polymer (Sandberg et al., 2009). The carbohydrate content of ocular mucins including MUC5AC is ~70% (Hodges and Dartt, 2013) whereas BSM is 60% (Tsuiki et al., 1961). Both MUC5AC and BSM are structurally similar, and as a result, it would be reasonable to use BSM as model mucin. Moreover, the interaction of vancomycin was examined using BSM (Dinu et al., 2020), and thus, a study on the interactions of teicoplanin which also used BSM would be comparable with the previous study on vancomycin. However, it should be noted that the glycan patterns for BSM and MUC5AC are different because these patterns vary with species and tissues (Hattrup and Gendler, 2008; Guzman-Aranguez et al., 2012), and consequently, this difference might affect the behaviour of each mucin.

1.4. PhD project and the scope of the study

The PhD thesis is designed to cover hydrodynamic investigation of the behaviours of glycans, such as interactions and aggregation, related to ophthalmology. The first theme is the ocular mucin supplement to relieve dry eye symptoms. The combination of HA and TSP as an eye drop has been thoroughly investigated, although there is little data derived from molecular hydrodynamics. In this theme, I will attempt to explore the interaction between these polysaccharides in a solution, which is closer to the actual physiological conditions of eye drops. The hydrodynamic methods used were sedimentation velocity in the analytical ultracentrifugation (SV-AUC) and then size-exclusion chromatography coupled to multi-angle light scattering (SEC-MALS). These methods would be complementary to previous research using NMR spectroscopy with dry samples. The study will be also focused on the hydrodynamic properties, such as intrinsic viscosity, using the capillary viscometer. Together with molar masses obtained from SEC-MALS, I will estimate the shapes of HA, TSP, and their mixture, which is of importance to eye drop formulation.

The following theme is the aggregation of glycan antibiotic teicoplanin in a solution. A study on the biological form of teicoplanin in tear fluid is interesting because that is one of several factors affecting corneal penetration of antibiotics. Sedimentation

equilibrium in the analytical ultracentrifugation (SE-AUC) is used to explore the aggregation/self-association of teicoplanin A2, together with SV-AUC and dynamic light scattering (DLS). Both SV-AUC and SE-AUC apply the same principle; sedimentation of samples under a centrifugal field, though SE-AUC provides accurate molar masses over a wide range of concentrations. This technique will give information on the aggregational behaviours of teicoplanin in an aqueous solution. DLS is another hydrodynamic method complementary to the results provided by AUC in terms of molecular size and shape. This investigation may offer insights into poor corneal absorption of teicoplanin.

Finally, this thesis will also focus on teicoplanin's interactions with model mucins. It is reported that vancomycin interacts with gastrointestinal mucins, such as BSM, resulting in aggregates. The comparative study of two glycan antibiotics contributes to the further understanding of long exposure to antibiotics resulting in AMR, exploring differences and similarities in interactions with BSM. Scanning electron spectroscopy (SEM) may consolidate the results of SV-AUC. Together with SV-AUV and SEM, this thesis will give more insight into mucin complexation with teicoplanin, which leads to a selection of resistant strains in mucous layers.

In the following chapter we review hydrodynamic and high resolution microscopic methods for the evaluations of glycans.

1.5. References

Alster, Y., Herlin, L., Lazar, M., Loewenstein, A., 2000. Intraocular penetration of vancomycin eye drops after application to the medial canthus with closed lids. Brit J Ophthalmol 84, 300.

Antoniadou, A., Vougioukas, N., Kavouklis, E., Chrissouli, Z., Giamarellou, H., 1998. Penetration of teicoplanin (TEC) into human aqueous humor (AH) after subconjunctival (SCJ) and IV administration. Clinical Infectious Diseases 27, 967.

Barabino, S., 2013. Causes and pathophysiology. In: Yokoi, N. (Ed.), Dry eye syndrome : basic and clinical perspectives. Future Medicine Ltd, London, pp. 21–30.

Bardone, M.R., Paternoster, M., Coronelli, C., 1978. Teichomycins, new antibiotics from *Actinoplanes Teichomycetinus* NOV. SP. J Antibiotics 31, 170–177.

Bardsley, B., Zerella, R., Williams, D.H., 2002. Aggregation, binding, and dimerisation studies of a teicoplanin aglycone analogue (LY154989). J Chem Soc Perkin Transactions 2 0, 598–603.

Beauregard, D.A., Williams, D.H., Gwynn, M.N., Knowles, D.J., 1995. Dimerization and membrane anchors in extracellular targeting of vancomycin group antibiotics. Antimicrob Agents Ch 39, 781–785.

Blaskovich, M.A.T., Hansford, K.A., Butler, M.S., Jia, Z., Mark, A.E., Cooper, M.A., 2018. Developments in glycopeptide antibiotics. Acs Infect Dis 4, 715–735.

Brayman, M., Thathiah, A., Carson, D.D., 2004. MUC1: A multifunctional cell surface component of reproductive tissue epithelia. Reprod Biol Endocrin 2, 4.

Brockhausen, I., Stanley, P., 2017. Chapter 10 O-GalNAc glycans. In: Varki, A., Cummings, R.D., Esko, J.D., Stanley, P., Hart, G.W., Aebi, M., Darvill, A.G., Kinoshita, T., Packer, N.H., Prestegard, J.H., Schnaar, R.L., Seeberger, P.H. (Eds.), . Cold Spring Harbor Laboratory Press, New York, pp. 113–123.

Cahane, M., Simon, G.J.B., Barequet, I.S., Grinbaum, A., Diamanstein-Weiss, L., Goller, O., Rubinstein, E., Avni, I., 2004. After consecutive doses of topically applied 3.3% vancomycin, human corneal stromal tissue concentration. Brit J Ophthalmol 88, 22.

Carpenter, J., Wang, Y., Gupta, R., Li, Y., Haridass, P., Subramani, D.B., Reidel, B., Morton, L., Ridley, C., O'Neal, W.K., Buisinee, M.-P., Ehre, C., Thornton, D.J., Kesimer, M., 2021. Assembly and organization of the N-terminal region ofmucin MUC5AC: Indications for structural and functional distinction from MUC5B. PNAS 118, e2104490118.

Cavalleri, B., Pagani, H., Volpe, G., Selva, E., Parenti, F., 1983. A-16686, A new antibiotic from Actinoplanes. J Antibiotics 37, 309–317.

Dartt, D.A., Willcox, M.D.P., 2013. Complexity of the tear film: Importance in homeostasis and dysfunction during disease. Exp Eye Res 117, 1–3.

Dinu, V., Lu, Y., Weston, N., Lithgo, R., Coupe, H., Channell, G., Adams, G.G., Gómez, A.T., Sabater, C., Mackie, A., Parmenter, C., Fisk, I., Phillips-Jones, M.K., Harding, S.E., 2020. The antibiotic vancomycin induces complexation and aggregation of gastrointestinal and submaxillary mucins. Sci Rep-uk 10, 960.

Dubashynskaya, N., Poshina, D., Raik, S., Urtti, A., Skorik, Y.A., 2019. Polysaccharides in ocular drug delivery. Pharm 12, 22.

Durand, M.L., 2017. Bacterial and fungal endophthalmitis. Clin Microbiol Rev 30, 597–613.

Forrester, J.V., Dick, A.D., McMenamin, P.G., Roberts, F., Pearlman, E., 2016. The eye basic sciences in practice, Fourth. ed. Elsevier, London.

Ghorpade, V.S., Yadav, A.V., Dias, R.J., 2017. Citric acid crosslinked β-cyclodextrin/carboxymethylcellulose hydrogel films for controlled delivery of poorly soluble drugs. Carbohyd Polym 164, 339–348.

Gipson, I.K., 2004. Distribution of mucins at the ocular surface. Exp Eye Res 78, 379–388.

Gipson, I.K., Argüeso, P., 2003. Role of mucins in the function of the corneal and conjunctival epithelia. International Review of Cytology 231, 1–49.

Golden, M.I., Meyer, J.J., Patel, B.C., 2022. Dry eye syndrome. StatPearls Publishing, Treasure Island (FL).

Gomes, G.P., Assis, M.A.L., Fonseca, J.S.S., Souza, P.E.A. de, Zenóbio, E.G., Oliveira, D.D., Soares, R.V., 2011. Genetic polymorphism of MUC7 in individuals with aggressive or chronic periodontitis. J Oral Sci 53, 445–449.

Griffith, R.S., 1984. Vancomycin use--an historical review. J Antimicrob Chemoth 14, 1–5.

Groesen, E. van, Innocenti, P., Martin, N.I., 2022. Recent advances in the development of semisynthetic glycopeptide antibiotics: 2014–2022. Acs Infect Dis 8, 1381–1407.

Gururaja, T.L., Ramasubbu, N., Venugopalan, P., Reddy, M.S., Ramalingam, K., Levine, M.J., 1998. Structural features of the human salivary mucin, MUC7. Glycoconjugate J 15, 457–467.

Guzman-Aranguez, A., Argüeso, P., 2010. Structure and biological roles of mucin-type O-glycans at the ocular Surface. The ocular surface 1, 8–17.

Guzman-Aranguez, A., Woodward, A. M., Pintor, J., Argüeso, P. Targeted disruption of Core 1 B1,3-Galactosyltransferase (C1galt1) induces apical endocytic trafficking in human corneal keratinocytes/ PLOS ONE 7(5), No. e36628.

Harding, S.E., Tomb, M.P., Adams, G.G., Paulsen, B.S., Inngjerdingen, K.T., Barsett, H., 2017. An introduction to polysaccharide biotechnology, Second. ed. CRC Press, Boca Raton, pp.1-46.

Hascall, V., Esko, J.D., 2017. Hyaluronan. In: Varki, A., Cummings, R.D., Esko, J.D., Stanley, P., Hart, G.W., Aebi, M., Darvill, A.G., Kinoshita, T., Packer, N.H., Prestegard, J.H., Schnaar, R.L., Seeberger, P.H. (Eds.), Essentials of glycobiology. Cold Spring Harbor Laboratory Press, New York, pp. 197–206.

Hattrup, C.L., Gendler, S.J., 2008. Structure and function of the cell surface (tethered) mucins. Annu Rev Physiol 70, 431–457.

Hodges, R.R., Dartt, D.A., 2013. Tear film mucins: Front line defenders of the ocular surface; comparison with airway and gastrointestinal tract mucins. Exp Eye Res 117, 62–78.

Jia, Z., O'Mara, M.L., Zuegg, J., Cooper, M.A., Mark, A.E., 2013. Vancomycin: ligand recognition, dimerization and super-complex formation. Febs J 280, 1294–1307.

Jin, H., Zhao, C., Yin, Y., Zheng, G., li, L., Shan, Q., Zhang, M., Wei, L., Shi, X., Huang, H., Zhang, W., Liu, S., 2021. Simultaneous determination of active clinical components of teicoplanin and ramoplanin in environmental water by LC-MS/MS coupled with cascade elution. Frontiers Environ Sci 9, 785408.

Kaye, S.B., Neal, T., Nicholson, S., Szkurlat, J., Bamber, S., Baddon, A.C., Anderson, S., Seddon, K., Dwyer, N., Lovering, A.M., Smith, G., 2009. Concentration and bioavailability of ciprofloxacin and teicoplanin in the cornea. Investigative Opthalmol Vis Sci 50, 3176.

Lee, D., Lu, Q., Sommerfeld, S.D., Chan, A., Menon, N.G., Schmidt, T.A., Elisseeff, J.H., Singh, A., 2017. Targeted delivery of hyaluronic acid to the ocular surface by a polymer-peptide conjugate system for dry eye disease. Acta Biomater 55, 163–171.

Lin, A., Rhee, M.K., Akpek, E.K., Amescua, G., Farid, M., Garcia-Ferrer, F.J., Varu, D.M., Musch, D.C., Dunn, S.P., Mah, F.S., Panel, A.A. of O.P.P.P.C. and E.D., 2019. Bacterial keratitis preferred practice pattern®. Ophthalmol 126, P1–P55.

Mantelli, F. and Argüeso, P. 2008. Functions of ocular surface mucins in health and disease. Curr Opin Allergy Clin Immunol 8(5): 477–483.

McGuckin, M.A., Lindén, S.K., Sutton, P., Florin, T.H., 2011. Mucin dynamics and enteric pathogens. Nat Rev Microbiol 9, 265–278.

Miyazaki, S., Suisha, F., Kawasaki, N., Shirakawa, M., Yamatoya, K., Attwood, D., 1998. Thermally reversible xyloglucan gels as vehicles for rectal drug delivery. J Control Release 56, 75–83.

NHS, 2017. SWBH-Guidelines-for-the-Management-of-Endogenous-Endophthalmitis-June-2014.pdf.

NHS, 2020. Eye preparations that can be bought over the counter (1).pdf. Imperial College Healthcare NHS Trust.

NHS, 2022. Dry eye treatment guidelines. NHS West Essex CCG (Clinical Commissioning Group).

Patchan, M., Graham, J.L., Xia, Z., Maranchi, J.P., McCally, R., Schein, O., Elisseeff, J.H., Trexler, M.M., 2013. Synthesis and properties of regenerated cellulose-based hydrogels with high strength and transparency for potential use as an ocular bandage. Mater Sci Eng C 33, 3069–3076.

Podolsky, D.K., 1985. Oligosaccharide structures of human colonic mucin. J Biol Chem 260, 8262–8271.

Ross, C., Syed, B., Pak, J., Jhanji, V., Yamaki, J., Sharma, A., 2021. Stability evaluation of extemporaneously compounded vancomycin ophthalmic drops: effect of solvents and storage conditions. Pharm 13, 289.

Sandberg, T., Blom, H., Caldwell, K.D., 2009. Potential use of mucins as biomaterial coatings. I. Fractionation, characterization, and model adsorption of bovine, porcine, and human mucins. J Biomed Mater Res A 91A, 762–772.

Schmitz, T., Grabovac, V., Palmberger, T.F., Hoffer, M.H., Bernkop-Schnürch, A., 2008. Synthesis and characterization of a chitosan-N-acetyl cysteine conjugate. Int J Pharmaceut 347, 79–85.

Seeberger, P.H., Cummings, R.D., 2017. Chapter 57 Glycans in biotechnology and the pharmaceutical industry. In: Varki, A., Cummings, R.D., Esko, J.D., Stanley, P., Hart, G.W., Aebi, M., Darvill, A.G., Kinoshita, T., Packer, N.H., Prestegard, J.H., Schnaar, R.L., Seeberger, P.H. (Eds.), . Cold Spring Harbor Laboratory Press, New York, pp. 729–741.

Sheehan, J.K., Brazeau, C., Kutay, S., Pigeon, H., Kirkham, S., Howard, M., Thornton, D.J., 2000. Physical characterization of the MUC5AC mucin: a highly oligomeric glycoprotein whether isolated from cell culture or in vivo from respiratory mucous secretions. Biochem J 347, 37–44.

Siepmann, J., Peppas, N.A., 2012. Modeling of drug release from delivery systems based on hydroxypropyl methylcellulose (HPMC). Adv Drug Deliver Rev 64, 163–174.

Simmons, P.A., Liu, H., Carlisle-Wilcox, C., Vehige, J.G., 2015. Efficacy and safety of two new formulations of artificial tears in subjects with dry eye disease: a 3-

month, multicenter, active-controlled, randomized trial. Clin Ophthalmol Auckl N Z 9, 665–675.

Snibson, G.R., Greaves, J.L., Soper, N.D.W., Prydal, J.I., Wilson, C.G., Bron, A.J., 1990. Precorneal residence times of sodium hyaluronate solutions studied by quantitative gamma scintigraphy. Eye 4, 594–602.

Spurr-Michaud, S., Argüeso, P., Gipson, I., 2007. Assay of mucins in human tear fluid. Experimental Eye Research 5, 939–950.

Stogios, P.J., Savchenko, A., 2020. Molecular mechanisms of vancomycin resistance. Protein Sci 29, 654–669.

Takács-Novák, K., Noszál, B., Tókés-Kövesdi, M., Szász, G., 1993. Acid-base properties and proton-speciation of vancomycin. Int J Pharmaceut 89, 261–263.

Thornton, D.J., Carlstedt, I., Howard, M., Devine, P.L., Price, M.R., Sheehan, J.K., 1996. Respiratory mucins: identification of core proteins and glycoforms. The Biochemical Journal 967–975.

Tsuiki, S., Hashimoto, Y., Pigman, W., 1961. Comparison of procedures for the isolation of bovine submaxillary mucin. J Biol Chem 236, 2172–2178.

Uccello-Barretta, G., Balzano, F., Vanni, L., Sansò, M., 2013. Mucoadhesive properties of tamarind-seed polysaccharide/hyaluronic acid mixtures: A nuclear magnetic resonance spectroscopy investigation. Carbohyd Polym 91, 568–572.

Uccello-Barretta, G., Nazzi, S., Balzano, F., Sansò, M., 2011. A nuclear magnetic resonance approach to the comparison of mucoadhesive properties of polysaccharides for ophthalmic uses. Int J Pharmaceut 406, 78–83.

Uccello-Barretta, G., Nazzi, S., Zambito, Y., Colo, G.D., Balzano, F., Sansò, M., 2010. Synergistic interaction between TS-polysaccharide and hyaluronic acid: Implications in the formulation of eye drops. Int J Pharmaceut 395, 122–131.

Varki, A., Kornfeld, S., 2017. Chapter 1 Historical background and overview. In: Varki, A., Cummings, R.D., Esko, J.D., Stanley, P., Hart, G.W., Aebi, M., Darvill, A.G., Kinoshita, T., Packer, N.H., Prestegard, J.H., Schnaar, R.L., Seeberger, P.H. (Eds.), Essentials of glycobiology. Cold Spring Harbor Laboratory Press, New York, pp. 1–18.

Vazquez-Guillamet, C., Kollef, M.H., 2014. Treatment of gram - positive infections in critically ill patients. Bmc Infect Dis 14, 92.

Wiesner, J., Vilcinskas, A., 2010. Antimicrobial peptides: The ancient arm of the human immune system. Virulence 1, 440–464.

Wu, Y., Liu, Y., Li, X., Kebebe, D., Zhang, B., Ren, J., Lu, J., Li, J., Du, S., Liu, Z., 2018. Research progress in in-situ gelling ophthalmic drug delivery system. Asian J Pharm Sci 14, 1–15.

Xu, Y., Wang, B., Zhao, H., Wang, X., Rao, L., Ai, W., Yu, J., Guo, Y., Wu, X., Yu, F., Chen, S., 2021. In vitro activity of vancomycin, teicoplanin, linezolid and daptomycin against methicillin-resistant Staphylococcus aureus isolates collected from Chinese hospitals in 2018–2020. Infect Drug Resist 14, 5449–5456.

Zhou, L., Zhao, S.Z., Koh, S.K., Chen, L., Vaz, C., Tanavde, V., Li, X.R., Beuerman, R.W., 2012. In-depth analysis of the human tear proteome. J Proteomics 75, 3877–3885.

Chapter 2: Hydrodynamic and microscopic methods for the evaluation of glycans.

2.1. Analytical ultracentrifugation

Analytical ultracentrifugation (AUC) is the powerful matrix-free method for the characterisation of heterogeneity/polydispersity, molar mass (molecular weight) distributions, and interactions of glycans. 'Matrix-free' means that samples are separated and analysed without the need for separation columns and membranes (Harding et al., 2017). Glycans differ from pure proteins regarding their synthesis because glycans, though also produced by enzymes, have no template for the direct synthesis of carbohydrate polymers, leading to polydisperse products (Harding et al., 2015b). A 'polydisperse' macromolecular population contains a range of molecules with different molar masses, which is reasonably represented by various types of average molar mass, such as the number-, weight-, or z-average, and distributions (Harding, 1994a). AUC techniques make samples (and reference solvent) sediment in specially constructed cells, with concentration distributions being recorded by optical instruments with Rayleigh interference or/and ultraviolet (UV) absorption (Harding et al., 2017). AUC experiments are classified as sedimentation velocity (SV-AUC) or sedimentation equilibrium (SE-AUC). In general, SV experiments track a sedimenting boundary of molecules moving in a centrifugal field, while SE experiments are focused on a steady-state concentration

distribution of the sample after equilibrium is completed (see, e.g., Cole et al., 2008).

The Lamm equation (Eq. 2-5) depicts the transport process in a centrifugal field (see, e.g., Zaccai et al., 2017). The Lamm equation is derived from Fick's Frist law of diffusion:

$$J_x = -D\left[\frac{dC}{dx}\right] \tag{2-1}$$

where J_x is the net flux in the units of mol m^{-2} s^{-1}, and D is the diffusion coefficient in the units of m^2 s^{-1}. Fick's first law states that the diffusive flux is proportional to the constant D and the solute concentration gradient dC/dx.

When all molecules in a cell move towards the direction $+x$ with a speed u, the net flux at x increases by $uC(x)$, and thus, Equation (2-1) should be:

$$J_x = -D\left[\frac{dC}{dx}\right] + uC(x) \tag{2-2}$$

where $C(x)$ is a local concentration. Since $u = s\omega^2 x$ (ω is angular velocity given by the units of s^{-1}), Equation (2-2) is changed to:

$$J_x = -D\left[\frac{dC}{dx}\right] + s\omega^2 x \cdot C(x) \tag{2-3}$$

In Equation (2-3), the first term of $D\left[\frac{dC}{dx}\right]$ corresponds to transport by diffusion while the second term of $s\omega^2 x \cdot C(x)$ corresponds to transport by sedimentation. Under conditions of the AUC experiments, the radius of a finite cell with walls is described as r, and therefore, the adequate continuity equation is defined as:

$$\left(\frac{dC}{dt}\right) = -\frac{1}{r}\left(\frac{d}{dr}(J_r)\right) \quad (2\text{-}4)$$

Equation (2-3) and Equation (2-4) are combined to formulate the partial differential equation called 'the Lamm equation' (Zaccai et al., 2017):

$$\left(\frac{dC}{dt}\right) r = -\frac{1}{r}\left(\frac{d}{dr}\left[\omega^2 r^2 sC - Dr\left(\frac{dC}{dr}\right)t\right]\right)t \quad (2\text{-}5)$$

2.1.1. Sedimentation velocity in the analytical ultracentrifuge (SV-AUC)

The sedimenting boundary emerges between solution and solvent when samples are centrifuged at very high rotor speed, for example, 45,000 rpm (Harding et al., 2017). The optical detection and recording of this moving boundary provide the sedimentation coefficient, *s*. When samples (a molecule of mass *m* and density ρ dissolved in a solvent of mass m_0 and density ρ_0) are centrifuged, the molecule is affected by three forces: centrifugal, F_c, buoyant, F_b, and frictional drag forces, F_d (Zaccai et al., 2017). When these three forces are balanced, the equations are:

$$F_c + F_b + F_d = 0 \quad (2\text{-}6)$$

$$F_c = m\omega^2 r \quad (2\text{-}7)$$

$$F_b = -m_0\omega^2 r \quad (2\text{-}8)$$

$$F_d = -fu \quad (2\text{-}9)$$

where *f* is frictional coefficient. Equation (2-6) is changed to:

$$m\omega^2 r(1-\bar{v}\rho_0) = fu \qquad (2\text{-}10)$$

where $\bar{v}$ is a reciprocal of density ρ, also called as a partial specific volume, and $m_0 = m\frac{\rho_0}{\rho}$. Substituting a molar mass, M, and Avogadro's number, N_A, for a mass ($m = \frac{M}{N_A}$), we can change from Equation (2-10) to:

$$s \equiv \frac{u}{\omega^2 r} = \frac{M(1-\bar{v}\rho_0)}{N_A f} \qquad (2\text{-}11)$$

where s represents the sedimentation coefficient, the ratio of the velocity of the molecule, u, to its centrifugal acceleration, $\omega^2 r$ (Zaccai et al., 2017). The s value is given by the unit of 10^{-13} s, called 1 Svedberg (S).

The computer programme SEDFIT (Dam and Schuck, 2004) is well-used for obtaining sedimentation coefficient distributions. In this programme, the Lamm equation, Equation (2-5), is solved in order to provide the change of concentration distributions at radial positions over time, resulting in a sedimentation coefficient distribution, $g(s)$ versus s plot (Harding et al., 2015b). In this plot, an area under a curve represents a concentration, and a peak is a Gaussian whose position and width indicate sedimentation and diffusion coefficients, respectively (Zaccai et al., 2017). Corrections of this plot for diffusion produce a $c(s)$ versus s plot, and further corrections of the $c(s)$ versus s plot generate a molar mass distribution plot, $c(M)$ versus M (Harding et al., 2015a). For polysaccharides, the $g(s)$ versus s plot is

suitable due to their large molar masses and slow diffusion, while for proteins, the $c(s)$ versus s plot is more appropriate (Harding et al., 2015b). These plots are used for a measure of heterogeneity/polydispersity of samples (Harding et al., 2017).

Sedimentation coefficients of a molecule are usually determined using a particular buffer, b, with viscosity, $\eta_{T,b}$, and density, $\rho_{T,b}$, at a temperature, T, and thus, these s values should be normalised to the density and viscosity of water at 20 °C:

$$s_{20,w} = \frac{1-\bar{\upsilon}\cdot\rho_{20,w}}{1-\bar{\upsilon}\cdot\rho_{T,b}} \cdot \frac{\eta_{T,b}}{\eta_{20,w}} \cdot s_{T,b} \qquad (2\text{-}11)$$

where $s_{20,w}$ is the sedimentation coefficient of the molecule in water at 20 °C (Zaccai et al., 2017).

To eliminate thermodynamic non-ideality (co-exclusion and polyelectrolyte effects) due to excluded volumes and high charge of glycans (Harding et al., 1991), low concentrations of samples should be used (Harding et al., 2015b). The other way is extrapolating $1/s_{20,w}$ to zero concentration to produce $1/s^0_{20,w}$ as a y-axis and the Gralen coefficient k_s (ml/g) from a slope (Harding et al., 2015a).

$$\frac{1}{s_{20,w}} = \frac{1}{s^0_{20,w}}(1 + k_s C) \qquad (2\text{-}12)$$

Both $s^0_{20,w}$ and k_s are related to conformation. A sedimentation coefficient

(s, $s_{20,w}$) value usually decreases with an increase in concentration while an increase in *s* with rising concentration is evidence for self-association or weakly interaction (Zaccai et al., 2017).

2.1.2. Sedimentation equilibrium in the analytical ultracentrifuge (SE-AUC)

In SE experiments, sufficiently low rotor speeds are chosen so that the centrifugal force is equal to the back diffusion force (Harding et al., 2017). At equilibrium, changes in concentration of a sample with time should be zero (Zaccai et al., 2017), and thus, the Lamm equation is:

$$\left(\frac{dC}{dt}\right) r = -\frac{1}{r}\left(\frac{d}{dr}\left[\omega^2 r^2 sC - Dr\left(\frac{dC}{dr}\right) t\right]\right) t = 0 \qquad (2\text{-}13)$$

Therefore:

$$\omega^2 r^2 sC - Dr\left(\frac{dc}{dr}\right) t = 0 \qquad (2\text{-}14)$$

Substituting the Svedberg equation $\frac{s}{D} = \frac{M(1-\overline{v}\rho)}{RT}$ for $\frac{s}{D}$ where *R* is the gas constant, we rearrange and obtain:

$$\frac{dc}{dr} = C \cdot r \cdot \frac{\omega^2 M(1-\overline{v}\rho_0)}{RT} \qquad (2\text{-}15)$$

The second Svedberg equation states that the concentration distribution between the meniscus at *a* and point *r* follows an exponential law:

$$C(r) = C(a) \cdot e^{\left[\frac{\omega^2 M(1-\overline{v}\rho_0)}{RT} \cdot \left(\frac{r^2}{2} - \frac{a^2}{2}\right)\right]} \qquad (2\text{-}16)$$

Since Equation (2-16) does not contain a parameter of the molecular shape,

the molecular masses obtained are unrelated to conformation (Zaccai et al., 2017). The steady state profile, $c(r)$ versus r, can be transformed into the $M^*(r)$ versus r plot (Creeth and Harding, 1982a, 1982b):

$$M*(r) = \frac{[c(r)-c_m]}{\left[kc_m(r^2-r_m^2)+2k\int_{r_m}^{r}(c(r)-c_m)rdr\right]} \quad (2\text{-}17)$$

where k is a constant related to the rotor speed, and m represents the meniscus (Harding et al., 2015b).

The computer programme SEDFIT-MSTAR (Schuck et al., 2014) is used for the analysis of the M^* function. There are estimated to be $M^*(r) = M_{w,app}$ over a whole solution when $M^*(r)$ is extrapolated to $r = r_b$ at the base of a cell (Harding et al., 2015b). The alternative analysis is the 'hinge-point' method. SEDFIT-MSTAR also gives a plot of $M_{w,app}(r)$ versus $c(r)$, which means a point average molar masses as a function of local concentration. At the hinge point, namely, when $c(r)$ = the initial concentration c^0, $M_{w,app}(r)$ is estimated to be $M_{w,app}$ (Harding et al., 2015a). $M_{w,app}$ is the apparent weight average molar mass (over the whole solution), and consequently, this value has not been adjusted for nonideality. In some cases, $M_{w,app} \sim M_w$ is a reasonable approximation when a low concentration (~0.3 mg/mL) is loaded (Harding et al., 2017). For some polysaccharides, such as xanthan and alginate, $1/M_{w,app}$ needs to be extrapolated to $c = 0$ so that M_w is

estimated (Harding et al., 2015b):

$$\frac{1}{M_{w,app}} = \left(\frac{1}{M_w}\right)(1 + 2BM_w c) \quad (2\text{-}18)$$

where B is the second virial coefficient. However, Equation (2-18) is not a universal application for all cases, especially if samples are strongly charged polysaccharides. SEC-MALS can be complementary to SE-AUC in terms of this drawback, because SEC-columns dilute samples so that nonideality becomes sufficiently small (Harding et al., 2015b).

Finally, the 'average' molar mass is defined for three ways; the number- (M_n), weight- (M_w), or z-average (M_z):

$$M_n = \frac{\sum N_i \cdot M_i}{\sum N_i} \quad (2\text{-}19)$$

$$M_w = \frac{\sum N_i \cdot M_i^2}{\sum N_i \cdot M_i} \quad (2\text{-}20)$$

$$M_z = \frac{\sum N_i \cdot M_i^3}{\sum N_i \cdot M_i^2} \quad (2\text{-}21)$$

where n_i is the number of molecules of each group i whose molar mass is M_i (Harding et al., 2017). $M_z = M_w = M_n$ for perfectly monodisperse samples, though $M_z > M_w > M_n$ for most of glycans. The ratios of $I_w = \frac{M_z}{M_w}$ and $I_n = \frac{M_w}{M_n}$ indicate polydispersity (Harding et al., 2017).

2.2. Dynamic light scattering (DLS)

DLS is a complementary method for the characterisation of macromolecules,

working together with other hydrodynamic techniques, such as AUC. When light transits a solution in which glycans are dissolved, some of the light is scattered. The intensity of that scattered light rapidly fluctuates because of the Brownian motion of the molecules (Harding, 1994b). In general, small and compact molecules move faster and thus, greater fluctuation occurs (Harding et al., 2015a). An autocorrelator detects and correlates such fluctuations of intensities, I(*t*), at time *t* and following time $t + \tau$ where τ is the delay time (Harding, 1994b). The correlation function $G(\tau)$ is then calculated (see, e.g., Nobbmann et al., 2007):

$$G(\tau) = \int \frac{I(t) \cdot I(t+\tau)}{\langle I(t) \rangle^2} dt \qquad (2\text{-}22)$$

where the angular bracket represents an average of the product calculated over the long period of a measurement compared with τ (Harding, 1994b).

For dilute Brownian solutions, Equation (2-22) is associated with the translational diffusion coefficient *D*:

$$G(\tau) = 1 + \beta \cdot e^{-Dq^2\tau} \qquad (2\text{-}23)$$

where β is the fitting parameter and q is the Bragg wave vector whose intensity is determined by:

$$q = 2\pi n \cdot \frac{\sin\left(\frac{\theta}{2}\right)}{\lambda} \qquad (2\text{-}24)$$

where n is the refractive index of the buffer, λ is the wavelength of the light, and θ is the scattering angle. Consequently, from Equation (2-23), a plot of $\ln G(\tau)$

versus τ provides the translational diffusion coefficient *D*. Then the Stoke-Einstein relation converts from *D* to a hydrodynamic radius, r_h:

$$r_h = \frac{kT}{6\pi\eta_0 D} \quad (2\text{-}25)$$

where η_0 is the viscosity of the buffer and *k* is the Boltzmann constant, 1.3806452 x 10^{-23} J/K (Harding et al., 2015a). The CONTIN (Provencher, 1992) programme, combined with the 'Zetasizer software' of Malvern Instrument Ltd., gives a size distribution plot of f(r_h) versus r_h, the z-average particle radius.

The translational diffusion coefficient, D, is a function of buffer conditions (η_0 and *T*), and therefore, it can be normalised to the standard conditions – water at 20.0 °C, providing $D_{20,w}$ (Harding, 1994b). This standardization is usually automated by the software. A value of $D_{20,w}$ is an apparent one, though, since nonideality effects are much smaller for this value than the sedimentation coefficient, extrapolation to zero concentration is not necessary; $D_{20,w} \approx D^0_{20,w}$ (Harding et al., 2015a). Therefore, in most cases, measurements at a single, dilute concentration should be sufficient to give $D^0_{20,w}$ (Harding, 1994b). A value of $D^0_{20,w}$ is used in the Svedberg equation $\frac{s}{D} = \frac{M(1-\bar{v}\rho)}{RT}$ to determine an absolute value of a molar mass, together with $s^0_{20,w}$ obtained from AUC experiments.

Finally, although DLS is very rapid method taking just minutes to measure, this method has relatively low resolution (Nobbmann et al., 2007), and any separation

is not physical but mathematical. Consequently, it is complementary to more resolving methods including AUC. As well as AUC, DLS does not require a separation matrix, though this can be coupled to a SEC-MALS (Harding et al., 2015a).

2.3. Size exclusion chromatography coupled to muti-angle light scattering (SEC-MALS)

SEC-MALS, as well as SE-AUC, can determine the weight-average molar mass of glycans. Initially, single, fixed low angle light scattering (LALS) photometer was coupled on-line to a size exclusion column (a SEC column), though later a multi-angle light scattering (MALS) photometer replaced it (Wyatt, 2013). The first paper on the determination of M_w of a polysaccharide was published on sodium alginate using this novel technology (Horton et al., 1991). The values of M_w obtained by SEC-MALS were consistent with that of SE-AUC, which was the encouraging result (Harding et al., 2015a). This method has also been applied for mucin glycoproteins (Jumel et al., 1996). Although SEC is not an absolute method, and thus, needs calibration standards of known molar mass (Jumel et al., 1996), in combination with the MALS, SEC-MALS can provide absolute molar mass distributions without calibration by standards of known M_w (Harding et al., 2017).

In general, the SEC separates molar mass distributions of molecules into 'volume slices' and the MALS simultaneously conducts angular extrapolation in the 'Zimm' plot (a linear fit to the Zimm model) to provide the molar mass of each infinitesimal 'slice' which moves through a cell (Harding et al., 2017).

In the SEC, molecules of a sample are firstly separated where large molecules are excluded from the pores in the column material and smaller molecules are included in the column and subsequently the MALS collects the light scattering signals from that column at ~15 angles (Wyatt, 1993). Then concentrations are calculated from a refractive index detector and values of M_w for each slice is obtained from the equation (Zimm, 1948):

$$\frac{Kc}{R_\theta} = \left(\frac{1}{M_w} + 2Bc\right)\left[1 + \frac{16\pi^2\overline{R_g^2}}{3\lambda^2}\sin^2\frac{\theta}{2}\right] \quad (2\text{-}26)$$

where K is the polymer constant depending on the wavelength of the light and the refractive index increment dn/dc, R_θ is the Rayleigh ratio, B is the second virial coefficient given by the units of mL mol g^{-2}, and R_g is the radius of gyration given by the unit of cm (Harding et al., 2017). When the concentration is very small (<0.2 mg/mL) after separation and dilution of samples on the SEC column, $2Bc \approx 0$ is a valid assumption (Jumel et al., 1996). Nonideality effects are also negligible due to low concentrations. Consequently, a plot of $\frac{Kc}{R_\theta}$ versus $\sin^2\frac{\theta}{2}$ provides the value of M_w at the intercept. R_θ is recorded as the ratio of the intensity of the light

scattered from a molecule at an angle θ to that of the incident light (Harding et al., 2017).

SEC-MALS, although innovative technology, has some limitations. Compared to AUC, which is 'matrix-free', SEC-MALS requires a separation matrix, and as a result, some experiments are restricted by the separation range of columns, depending on shape and hydrodynamic radii, because the columns cannot adequately separate very large polymers (Harding et al., 2015a).

2.4. Capillary viscometry

Intrinsic viscosity measurement is simpler and less expensive than other hydrodynamic measurements, but it provides valuable complementary information. Three types of capillary viscometer can be used to measure the intrinsic viscosity. The simplest is the Ostwald instrument. This instrument involves comparison of flow times between solutions and solvent across a capillary under gravity (Harding et al., 2015a). A newer one is the Rolling Ball viscometer. This device uses a steel ball rolling through a capillary at a rate dependent on the viscosity of the solution or solvent (Harding et al., 2015a). Compared with the two viscometer instruments, the differential pressure viscometer is based on a different principle; detecting the pressure difference between the solution and solvent flowing along a capillary

(Harding et al., 2015a). This viscometer can be coupled to a SEC-MALS device.

The 'viscosity' is defined as a fluid's measure of its resistance to flow (Harding, 1997). The (shear) viscosity coefficient, η, of a fluid is described as:

$$\eta = \frac{\tau}{g} \tag{2-27}$$

where τ is the shearing stress and g is the rate of shear. The viscosity of a solvent is notated as η_0 and, since adding macromolecules increase the viscosity, that of a solution becomes a new value, η (Zaccai et al., 2017). In practice, both values are compared in this equation:

$$\eta_{rel} = \frac{\eta}{\eta_0} = \eta_{sp} + 1 \tag{2-28}$$

where η_{rel} is the relative viscosity and η_{sp} is the specific viscosity (Harding, 1997). The experimental values of the relative viscosity are measured by:

$$\eta_{rel} = \frac{t\rho}{t_0\rho_0} \tag{2-29}$$

where t and t_0 are flow times for a macromolecular solution (at a concentration) and solvent. The relative viscosity can be determined without the density correction (ρ: solution density and ρ_0: the solvent density) for concentrations < 1 mg/mL:

$$\eta'_{rel} = \frac{t}{t_0} \sim \eta_{rel} \tag{2-30}$$

where η'_{rel} is the 'kinematic' relative viscosity (Harding, 1997). The alternative correction can be also applied (Tanford, 1955):

$$\eta_{rel} = \eta'_{rel} + \frac{1-\bar{v}\rho_0}{\rho_0} \tag{2-31}$$

where $\bar{v}$ is the partial specific volume of a macromolecule. The reduced viscosity, η_{red}, is then determined in the equation:

$$\eta_{red} = \frac{\eta_{rel}-1}{c} \tag{2-32}$$

at a single concentration. The intrinsic viscosity, $[\eta]$, is obtained from a plot of η_{red} versus c and calculated as the intercept of this plot (Harding et al., 2017). The concentration extrapolation is conducted as the two equations, namely, the Huggins equation (Huggins, 1942) and the Kraemer equation (Kraemer, 1938):

$$\eta_{red} = [\eta](1 + K_H[\eta]c) \tag{2-33}$$

$$\frac{\ln \eta_{rel}}{c} = \eta_{inh} = [\eta](1 - K_K[\eta]c) \tag{2-34}$$

where K_H is the Huggins constant and K_K is the Kraemer constant. Alternatively, these two equations, Equation (2-33) and Equation (2-34), are combined to produce the new approximation (Solomon and Ciută, 1962):

$$[\eta] \approx \frac{1}{c} \cdot \left[2\eta_{sp} - 2\ln(\eta_{rel})\right]^{\frac{1}{2}} \tag{2-35}$$

at a single concentration (although this should be quite low).

Once determined, the intrinsic viscosity is used in conformation analysis of glycans, together with other hydrodynamic parameters, such as the sedimentation coefficient. The simplest property for conformation is the Wales-van Holde ratio (Wales and Holde, 1954). This parameter is the ratio of the Gralen coefficient k_s from Equation (2-12) to the intrinsic viscosity $[\eta]$. The values of $\frac{k_s}{[\eta]}$ ~1.6

represent a compact sphere or a random coil (Creeth and Knight, 1967, 1965), while those of $\frac{k_S}{[\eta]} \sim 0.2 - 0.5$ represent a stiff rod (Harding et al., 2017). Another property for conformational assessment is the 'Mark-Houwink-Kuhn-Sakurada (MHKS)' coefficient (a, b, c, or ε) calculated from these relations (Harding et al., 2017):

$$[\eta] = K'M^a \quad (2\text{-}36)$$

$$s = K''M^b \quad (2\text{-}37)$$

$$R_g = K'''M^c \quad (2\text{-}38)$$

$$D = K''''M^{-\varepsilon} \quad (2\text{-}39)$$

These MHKS coefficients can be obtained from simple double-logarithmic plots (Harding, 1997). For Equation (2-36), the SEC-MALS-DPV (differential pressure viscometer) system can record $[\eta](V_e)$ and $M_w(V_e)$ as a function of elution volume V_e (Harding et al., 2015a). This relation provides the limits $a = 0$ for a compact sphere, $a = 0.5 - 0.8$ for a random coil, and $a = 1.8$ for a rigid rod (Harding, 1997).

The 'ELLIPS' programme (Harding et al., 1997) is the software for simple shape modelling of glycans in terms of ellipsoid axial ratios for quasi-rigid particles. The intrinsic viscosity is affected by two factors – shape and volume (size and hydration), represented by the equation (Harding, 1997):

$$[\eta] = \nu \cdot v_s \tag{2-40}$$

where ν is called as the viscosity increment, a universal shape function or the Einstein-Simha shape factor, and v_s is the swollen specific volume, compared with the partial specific volume ($\bar{v}$). A value of ν can be obtained from the Simha-Saito formula (see Harding, 1997) and a simple approximation specifies axial ratio (a/b) for prolate and oblate ellipsoids (Figure 2-1). The designated value of a/b leads to the representation of macromolecules in the routine ELLIPS1 (Figure 2-2).

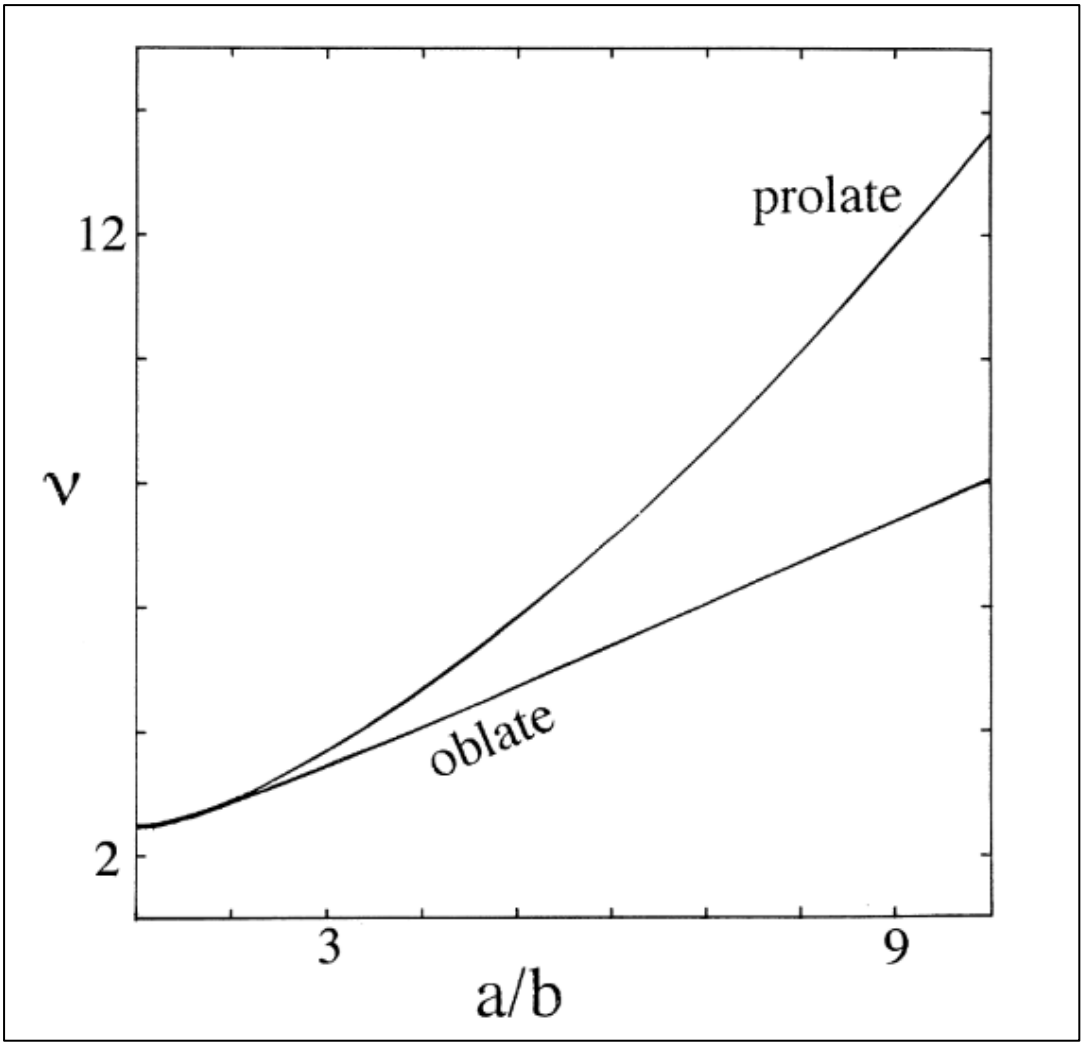

Figure 2-1: The plot of ν versus a/b (Harding, 1997)

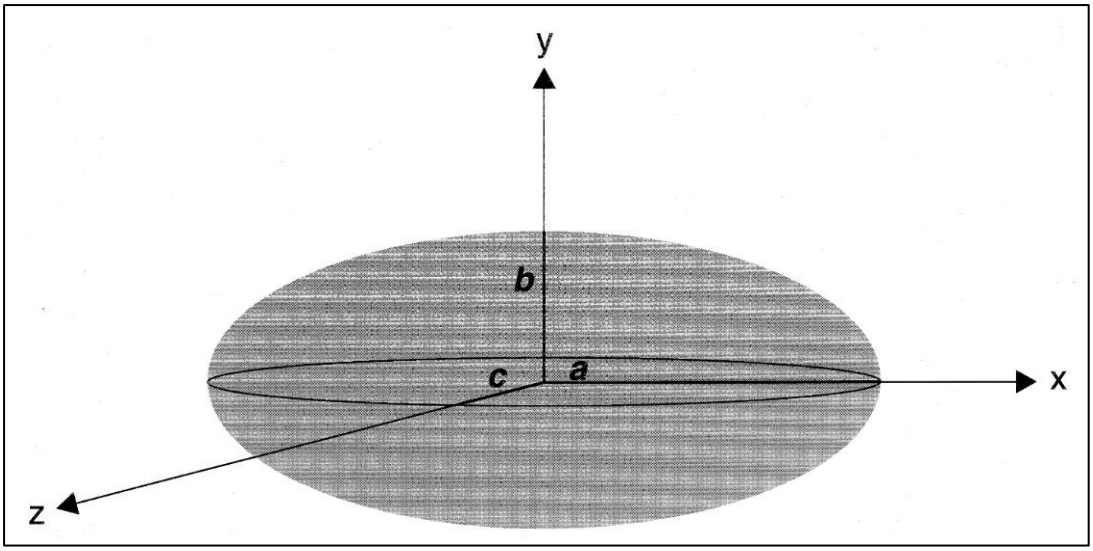

Figure 2-2: The diagram of a general triaxial ellipsoid of axe, a ≥ b ≥ c. A prolate ellipsoid corresponds to b/c=1, oblate ellipsoid for a/b=1 and a sphere a = b = c (Harding, 1997).

2.5. Scanning electron microscopy (SEM)

Electron microscopy provides information complementary to interaction studies conducted by SV-AUC. This method describes macromolecules at a scale of nanometre. In principle, electron microscopy can visualise biological molecules down to a lower limit of ~60 kDa (Zaccai et al., 2017). An illumination source of light microscopy is visible light with its wavelength λ = 400-700 nm while electron microscopy uses an electron beam with its much shorter wavelength (Flegler et al., 1993). The wavelength of an electron λ_e is defined as:

$$\lambda_e = \frac{h}{p} \tag{2-41}$$

where h is Planck's constant and p is the momentum of an electron (Zaccai et al., 2017). The momentum is the product of the mass and the velocity of an electron, and consequently, Equation (2-41) is transformed to:

$$\lambda_e = \frac{h}{m_e \cdot v} \tag{2-42}$$

An electron has its own charge ($q = |-e|$), and as a result, experiences a force qE ($E = \frac{d\Phi}{dx}$ is an electrical potential difference of Φ in volts) in an electrical field:

$$q\Phi = \frac{1}{2} m_e v^2 \tag{2-43}$$

Therefore, Equation (2-42) and Equation (2-43) are combined:

$$\lambda_e = \frac{h}{\sqrt{2 m_e e \Phi}} \approx \frac{12}{\sqrt{\Phi}} \tag{2-44}$$

where $m_e = 9.1 \times 10^{-28}\ g$ (Zaccai et al., 2017). Hence, an electron microscope

of an accelerating voltage of 15 kV generates electrons of 1.44 Å (0.144 nm). Electron microscopy is subclassified as either the transmission or scanning electron microscopy (TEM and SEM). TEM forms a phase contrast image of samples by using transmitted electrons, which have passed through and interacted with the samples, while in SEM an electron beam scans the samples and thus, secondary electrons are released, leading to signals creating an image (Zaccai et al., 2017).

2.5.1. Environmental scanning electron microscopy (ESEM)

Environmental scanning electron microscopy (ESEM) is further invented based on conventional SEM (CSEM). One of the drawbacks of CSEM is that samples should be stable and conductive in favour of high vacuum and electron beam and thus, complicated and multi-step preparation is required (Stabentheiner et al., 2010). ESEM enables the use of nonconductive and hydrated samples, being closer to their native environmental states, without such complex steps (Danilatos, 1993). The difference between ESEM and CSEM is that ESEM uses a gas, more frequently water vapour, instead of high vacuum, in a microscopic chamber (Donald, 2003). ESEM and CSEM has a similar process in which primary electrons interact with samples. In contrast, secondary electrons collide with gas atoms and generate further

electrons, amplifying signals in a cascade manner (Stabentheiner et al., 2010). In additional to daughter electrons from gas atoms, positive ions are produced and compensate for negatively charged surfaces of nonconductive samples (Stokes, 2003). This is the reason why ESEM does not require insulators to be coated with a metallic layer prior to imaging (Donald, 2003). Thus, ESEM provides useful information for naturally hydrated samples rather than CSEM, i.e., in food science (James, 2009) and microbiology (Fedel et al., 2007).

ESEM has been used for investigations of an antibiotic interaction with glycans. For example, Dinu (2020) published the report on mucin-antibiotic complexation using ESEM as a complementary tool to hydrodynamic tools (SV-AUC and DLS). This paper was the first publication for the novel combination of hydrodynamic and microscopic methods to evaluate the interactions of mucins with antibiotics. As well as this study, the current thesis will use ESEM for visualization of mucin-antibiotic aggregates.

2.6. References

Cole, J.L., Lary, J.W., Moody, T.P., Laue, T.M., 2008. Analytical ultracentrifugation: sedimentation velocity and sedimentation equilibrium. Methods Cell Biol 84, 143–179.

Creeth, J.M., Harding, S.E., 1982a. A simple test for macromolecular heterogeneity in the analytical ultracentrifuge. Biochem J 205, 639–641.

Creeth, J.M., Harding, S.E., 1982b. Some observations on a new type of point average molecular weight. Journal of Biochemical and Biophysical Methods 1, 25–34.

Creeth, J.M., Knight, C.G., 1965. On the estimation of the shape of macromolecules from sedimentation and viscosity measurements. Biochimica et Biophysica Acta (BBA) - Biophysics including Photosynthesis 102, 549–558.

Creeth, J.M., Knight, C.G., 1967. The macromolecular properties of blood-group substances. Sedimentation-velocity and viscosity measurements. Biochem J 105, 1135–1145.

Dam, J., Schuck, P., 2004. Calculating sedimentation coefficient distributions by direct modeling of sedimentation velocity concentration profiles. Methods Enzymol 384, 185–212.

Danilatos, G. D., 1993. Introduction to the ESEM instrument. Microsc Res Tech 25, 354-361.

Dinu, V., Lu, Y., Weston, N., Lithgo, R., Coupe, H., Channell, G., Adams, G.G., Gómez, A.T., Sabater, C., Mackie, A., Parmenter, C., Fisk, I., Phillips-Jones, M.K., Harding, S.E., 2020. The antibiotic vancomycin induces complexation and aggregation of gastrointestinal and submaxillary mucins. Sci Rep-uk 10, 960.

Donald, A. M., 2003. The use of environmental scanning electron microscopy for imaging wet and insulating materials. Nature materials 2, 511-516.

Fedel, M, Caciagli, P., Christé, V., Caola, I., Tessarolo, F., 2007. Microbial biofilm imaging ESEM vs HVSEM. GIT imag Microsc 2, 44-47.

Flegler, S.L., Jr., J.W.H., Klomparens, K.L., 1993. Scanning and transmission electron microscopy: an introduction. W. H. Freeman and Company, New York.

Harding, S.E., 1994a. Chapter 6 Determination of absolute molecular weights using sedimentation equilibrium analytical ultracentrifugation. In: Jones, C., Mulloy, B., Thomas, A.H. (Eds.), Methods in molecular biology (22) microscopy, optical spectroscopy, and macroscopic techniques. Humana Press, Totowa, New Jersey, pp. 75–84.

Harding, S.E., 1994b. Chapter 8 Determination of diffusion coefficients of biological macromolecules by dynamic light scattering. In: Jones, C., Mulloy, B., Thomas, A.H. (Eds.), Methods in molecular biology (22) microscopy, optical spectroscopy, and macroscopic techniques. Humana Press, Totowa, New Jersey, pp. 97–108.

Harding, S.E., 1997. The intrinsic viscosity of biological macromolecules. Progress in measurement, interpretation and application to structure in dilute solution. Prog Biophysics Mol Biology 68, 207–262.

Harding, S.E., Abdelhameed, A.S., Gillis, R.B., Morris, G.A., Adams, G.G., 2015a. Chapter 13 Characterization of capsular polysaccharides and their glycoconjugates by hydrodynamic methods. In: Lepenies, B. (Ed.), Carbohydrate-based vaccines: methods and protocols, methods in molecular biology 1331. Springer Science+Business Media, New York, pp. 211–227.

Harding, S.E., Adams, G.G., Almutairi, F., Alzahrani, Q., Erten, T., Kök, M.S., Gillis, R.B., 2015b. Chapter eighteen ultracentrifuge methods for the analysis of polysaccharides, glycoconjugates, and lignins. Methods Enzymol 562, 391–439.

Harding, S.E., Horton, J.C., Cölfen, H., 1997. The ELLIPS suite of macromolecular conformation algorithms. Eur Biophys J 25, 347–359.

Harding, S.E., Tomb, M.P., Adams, G.G., Paulsen, B.S., Inngjerdingen, K.T., Barsett, H., 2017. An introduction to polysaccharide biotechnology, Second. ed. CRC Press, Boca Raton.

Harding, S.E., Virum, K.M., Stokkeand, B.T., Smidsro, O., 1991. Molecular weight determination of polysaccharide. Advances in Cerbohydrate Anelysis 1, 6Yl4,4.

Horton, J.C., Harding, S.E., Mitchell, J.R., 1991. Gel permeation chromatography-multi-angle laser light scattering characterization of the molecular mass distribution of ‘Pronova’ sodium alginate. Biochem Soc T 19, 510–511.

Huggins, M.L., 1942. The viscosity of dilute solutions of long-chain molecules. IV. dependence on concentration. Journal of the American Chemical Society 11, 2716–2718.

James, B., 2009. Advances in “wet” electron microscopy techniques and their application to the study of food structure. Trends Food Sci Tech 20, 114-124.

Jumel, K., Fiebrig, I., Harding, S.E., 1996. Rapid size distribution and purity analysis of gastric mucus glycoproteins by size exclusion chromatography/multi angle laser light scattering. International Journal of Biological Macromolecules 18, 133–139.

Kraemer, E.O., 1938. Molecular weights of celluloses and cellulose derivates. Industrial & Engineering Chemistry Research 10, 1200–1203.

Nobbmann, U., Connah, M., Fish, B., Varley, P., Gee, C., Mulot, S., Chen, J., Zhou, L., Lu, Y., Sheng, F., Yi, J., Harding, S.E., 2007. Dynamic light scattering as a relative tool for assessing the molecular integrity and stability of monoclonal antibodies. Biotechnology Genetic Eng Rev 24, 117–128.

Provencher, S.W., 1992. Low-bias macroscopic analysis of polydispersity. In: Harding, S.E., Sattelle, D.B., Bloomfield, V.A. (Eds.), Laser Light Scattering in Biochemistry. Royal Society of Chemistry, Cambridge, UK, pp. 92–111.

Schuck, P., Gillis, R.B., Besong, T.M.D., Almutairi, F., Adams, G.G., Rowe, A.J., Harding, S.E., 2014. SEDFIT–MSTAR: molecular weight and molecular weight distribution analysis of polymers by sedimentation equilibrium in the ultracentrifuge. Analyst 139, 79–92.

Solomon, O.F., Ciută, I.Z., 1962. Détermination de la viscosité intrinsèque de solutions de polymères par une simple détermination de la viscosité. Journal of Applied Polymer Science 6, 683–686.

Stabentheiner, E., Zankel, A., Pölt, P., 2010. Environmental scanning electron microscopy (ESEM) – a versatile tool in studying plants. Protoplasma 246, 89-99.

Stokes, D. J., 2003. Recent advances in electron imaging, image interpretation and applications: environmental scanning electron microscopy. Philos Trans R Soc Lond A 316, 2771-2787.

Tanford, C., 1955. Intrinsic viscosity and kinematic viscosity. The Journal of Physical Chemistry A 8, 798–799.

Wales, M., Holde, K.E.V., 1954. The concentration dependence of the sedimentation constants of flexible macromolecules. J Polym Sci 14, 81–86.

Wyatt, P.J., 1993. Light scattering and the absolute characterization of macromolecules. Analytica Chimica Acta 272, 1–40.

Wyatt, P.J., 2013. Multiangle light scattering from separated samples (MALS with SEC or FFF). In: Roberts, G.C.K. (Ed.), Encyclopedia of biophysics. Springer, Berlin, Heidelberg.

Zaccai, N.R., Serdyuk, I.N., Zaccai, J., 2017. Methods in molecular biophysics, Second. ed. Cambridge University Press, Cambridge.

Zimm, B.H., 1948. The scattering of light and the radial distribution function of high polymer solutions. J Chem Phys 16, 1093–1099.

Chapter 3: Hydrodynamic compatibility of hyaluronic acid and tamarind seed polysaccharide as ocular mucin supplements.

3.1. Introduction

As people age, their production of ocular mucin containing lachrymal fluid—with its natural protective and lubricating properties for the surface of the eye—diminishes, a term known medically as *Keratoconjunctivitis sicca* or "dry eye" (Forrester et al, 2016). Solutions of polysaccharides in artificial tear drop formulations are popularly used to consolidate the mucin (of primarily type MUC5AC, also MUC2) which alleviates these symptoms. A problem with such formulations is how to prolong their residence time on the eye surface. The main reason for this problem is that ocular protective mechanisms (involving blinking, both basal and reflex lachrymation, and drainage through nasolacrimal ducts) quickly eliminate these eye drops from the precorneal region, where such drugs are absorbed and work (Uccello-Barretta et al., 2010). As a result, and depending on the severity, this can lead to the need for repeated administration (Lee et al., 2017). Therefore, various studies have investigated novel preparations to overcome such disadvantages of currently available formulations. For example, based on the viscosity-enhancing effects of gelatin, the grafting of thermoresponsive polymer segments onto proteinaceous networks has led to promising results (Luo and Lai,

2017) and, more recently, the lectin *Helix pomatia* agglutinin has been considered as an ocular mucoadhesive component (Luo et al., 2020). The properties of a promising new glutathione-dependent polymeric hydrogel with good eye drop mucoadhesive properties has also been explored (Lai et al., 2020).

Another highly significant development has been the combination of hyaluronic acid (HA) and tamarind seed gum polysaccharide (TSP), whose medical benefits were first reported by Barabino et al. (2013). Of the two components, both natural polysaccharides, HA is a linear polyanionic molecule chemically grouped in a glycosaminoglycan and has the repeating dimer {→4)-β-D-glucopyranosyluronic acid-(1→3)-*N*-acetyl-2-amino-2-deoxy-β-D-glucopyranosyl-(1→} (Hokputsa et al., 2003a, 2003b). When it comes to the current market situation, it has been reported (Lee et al., 2017) that 0.1–0.5% (*w/v*) HA solutions are available commercially as either active or inactive ingredients to supplement ocular fluid (see also refs (Johnson et al., 2006; Rah, 2011)). Hammer and Burch (1984) have suggested that 0.17% HA showed more protective effects as a coating on the eye compared to the highly viscous, more concentrated applications (1%, equivalent to 10 mg/mL) which transmit excessive shear force to endothelial cells. An alternative approach that can also help with product stability issues is using HA in a binary mixture with another polysaccharide. The second polysaccharide, TSP (Figure 3-

1) is a non-ionic, neutral and branched xyloglycan, which is comprised of a cellulose-like backbone, partially replaced at the O-6 position of its glucopyranosyl units with α-D-xylopyranose (Barabino et al., 2013; Semenzato et al., 2014).

A comparative study by Rolando and Valente (2007) indicated that both 0.5% and 1% solutions of TSP are comparable to 0.2% HA in removing dry eye syndrome symptoms. Later, Barabino et al. (2013) published their results with mixtures of HA and TSP, showing that this combination is effective in fixing the tear film on the cornea and repairing endothelial damage in dry eye patients. One principal reason for these outcomes is that the structural similarity of TSP to transmembrane mucins (MUC1) on the eye surface could lead to its longer retention time (Rolando and Valente, 2007).

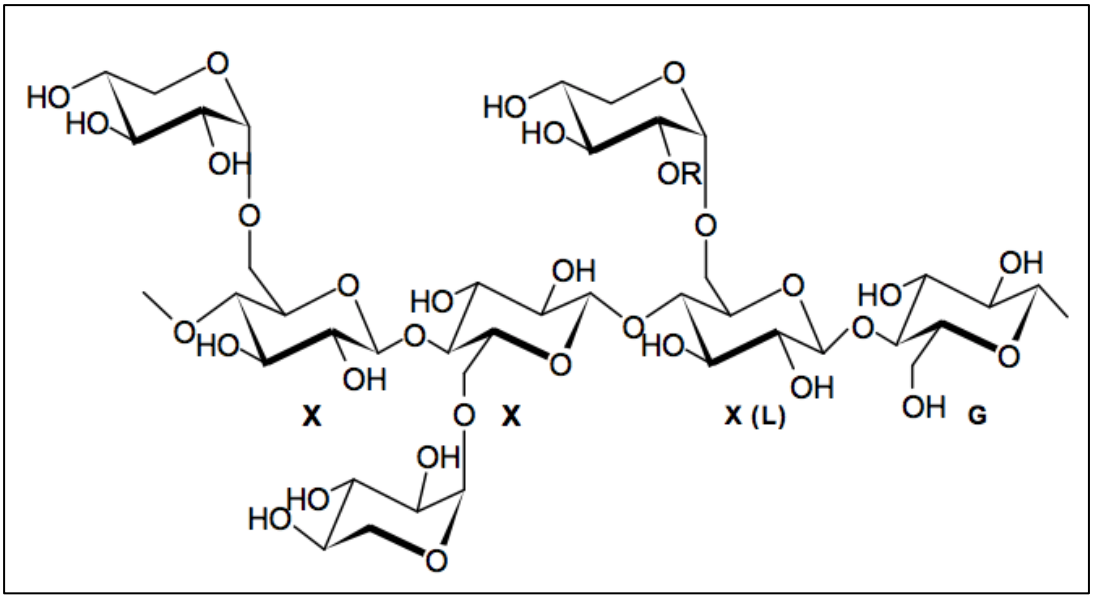

Figure 3-1: Chemical structure of tamarind seed xyloglucan (motif XXXG) or β-D-galactopyranose (motif XXLG). Adapted from Patel et al. (2008).

In addition, recent evidence using nuclear magnetic resonance spectroscopy (NMR)—a powerful method for investigating macromolecular-ligand interactions (Lian, 2001)—has suggested that there is an interaction between these two polysaccharides (Uccello-Barretta et al., 2013). We now seek to reinforce those observations by exploring the hydrodynamic compatibility and stability of these mixtures. Specifically, we examine key hydrodynamic parameters such as the molar mass and intrinsic viscosity by size exclusion chromatography coupled to multi-angle (laser) light scattering SEC-MALS and capillary / differential pressure viscometers, together with sedimentation velocity in the analytical ultracentrifuge, SV-AUC to assess the heterogeneity and interaction strength. The matrix-free method of analytical ultracentrifugation—with its huge dynamic range (molar masses from $10^2 – 10^8$ g/mol) is a key or "gold standard" method used to assess the molecular integrity of other biotherapeutic systems such as monoclonal antibodies (in terms of disassembly, denaturation of aggregation effects) and this is the first time that this method has been used to assess a dry-eye formulation. It has both a high separation and analysis ability without the need for columns or membranes (Harding, 2018; Harding et al., 2015). We assess the change in the intrinsic viscosity with molar mass in order to estimate conformations of HA and TSP by SEC-MALS and viscometry, assess the state of self-association/aggregation of the

individual components and for interaction/aggregation phenomena of the mixtures using SV-AUC, and finally investigate the stability of HA, TSP, and their mixtures. Although polysaccharides such as cellulose acetate (Yang et al., 2020), proteins (Wang et al., 2019) and other natural polymers (Wang et al., 2018) are commonly used singly in biomedical applications, examples of the combined use of natural polymers for medicinal purposes are not so frequent but are increasing in importance. The HA-TSP system has provided a further good example (Barabino et al., 2013; Uccello-Barretta et al., 2013, 2010; Yoon and Lee, 2019), now reinforced by the present analytical ultracentrifuge-based study.

3.2. Materials and methods

3.2.1. Materials

Hyaluronic acid and tamarind seed polysaccharide were supplied by Farmigea S.p.A., Pisa, Italy. HA or TSP samples were dissolved in a phosphate-chloride buffered saline solution (PBS, or “Paley buffer”) at pH ~6.8 adjusted to an ionic strength of I = 0.1 mol/L by the addition of NaCl (Green, 1933).

Stock solutions of HA and TSP were prepared by stirring gently for 30 min followed by overnight dialysis at room temperature against a two-litre

volume of PBS. The concentration, c (g/mL) of the stock solution (either HA or TSP) was then measured using a differential refractometer (Atago DD7, Tokyo, Japan) set to zero with PBS, and using a refractive increment dn/dc of 0.167 mL/g for HA (Hokputsa et al., 2003a), and 0.152 mL/g for TSP (Wang et al., 1997). HA/TSP was prepared by adding equal volumes with various concentrations, resulting in a range of ratios (HA:TSP = 1:3, 1:1 and 3:1) and final concentrations (4.0 mg/mL, 2.0 mg/mL and 1.0 mg/mL commensurate with concentrations used in formulations, and with materials remaining in solution (on the premise there are no significant irreversible aggregation/ complex formation interactions).

3.2.2. Sedimentation velocity in the analytical ultracentrifuge

Sedimentation coefficients and sedimentation coefficient distributions were determined using the optimal XL-I analytical ultracentrifuge (Beckman Instruments, Palo Alto, CA, USA) with Rayleigh interference optics. Reference solvent or dialysate (420 μL) and HA, TSP or HA/TSP samples (400 μL) with different concentrations were injected into channels of 12 mm, double-sectored cells with sapphire windows. Then these cells were loaded into an eight-hole rotor and centrifuged at a rotor speed of 45,000

rpm at a temperature of 20.0 °C for a run time of ~24 h. The data was analysed using the SEDFIT algorithm (Dam and Schuck, 2004), which gives the sedimentation coefficient distribution, $g^*(s)$ versus $s_{T,b}$, where s is the sedimentation coefficient. The s value was then corrected to standard solvent conditions (density and viscosity of water at 20.0 °C) to produce $s_{20,w}$ using the equation (Schachman, 1950):

$$s_{20,w} = \{(1 - \bar{v}\rho_{20,w})/(1 - \bar{v}\rho_{T,b})\}\{\eta_{T,b}/\eta_{20,w}\} \cdot s_{T,b} \quad (2\text{-}11)$$

where $\bar{v}$ was the partial volume of each sample. To eliminate the effect of nonideality, the equation was used for the extrapolation (Gralén, 1994):

$$\frac{1}{s_{20,w}} = \frac{1}{s^0_{20,w}}(1 + k_s c) \quad (2\text{-}12)$$

where k_s is the Gralén coefficient (mL/g).

3.2.3. Size exclusion chromatography coupled to multi-angle laser light scattering (SEC-MALS)

Weight average molar masses (M_w) of HA, TSP and HA/TSP were estimated by SEC-MALS (Hokputsa et al., 2003a; Patel et al., 2008; Picout et al., 2003; Wyatt, 1992). The solvent/ buffer was pumped at a steady flow rate of 0.5 mL/min through a column (Shodex LB-805), which was protected by a guard column (Shodex LB-G6B), coupled on-line to MALS (Dawn Heleos-II), a

differential pressure viscometer (ViscoStar-II) and refractive index (Optilab rEX) detectors (Wyatt Technology, Santa Barbara, CA, USA). After being filtered through a 0.2 μm syringe filter (Whatman, Maidstone, England), the solutions of the HA, TSP, and HA/TSP sample prepared at HA:TSP = 1:1 respectively, were injected into the size exclusion system using the Spark-Holland Marathon Basic autosampler. ASTRA^{TM} (Version 6.2) software (Wyatt Technology, Santa Barbara, CA, USA) was used to analyse the data. As concentrations are low, there is no need to extrapolated to infinite dilution. Therefore, apparent weight average molar mass ($M_{w,app}$) was calculated by using a linear fit to the Zimm model (Zimm, 1948):

$$\frac{Kc}{R_\theta} = \left(\frac{1}{M_w} + 2Bc\right)[1 + \frac{16\pi^2\overline{R_g^2}}{3\lambda^2}\sin^2\frac{\theta}{2}] \quad (2\text{-}26)$$

where K is an experimental constant dependent on the wavelength of the light and the refractive increment of the polysaccharide, R_θ is the Rayleigh ratio used to determine the ratio of the integrity of light scattered by a macromolecule at an angle θ to that of the incident radiation, B is the second virial coefficient (mL·mol·g^{-2}), R_g is the radius of gyration (cm) (Harding et al., 2017).

$M_{w,app}$ is obtained from the intercept (Picout et al., 2003). We make the reasonable assumption that correction for thermodynamic nonideality was

assumed to be unnecessary due to the high dilutions on the SEC columns (see, for example, Almutairi et al. (2015)) and hence M_w the "ideal" molar mass ~ $M_{w,app}$.

3.2.4. Capillary viscometry

HA solutions ranging either from 0.03 to 1 mg/mL, TSP solutions (from 0.03 to 1.91 mg/mL), and HA/TSP solutions (1 to 4 mg/mL as total concentrations) were analysed using a semiautomated viscosity measuring system (AVS 400, Schott Geräte, Hofheim, Germany) at a temperature of 20.00 °C in a 2 mL Ostwald viscometer (Table 3-1). Considering that a density correction is redundant due to low concentration (<2 mg/mL) (Patel et al., 2008), the relative viscosity, η_{rel}, was estimated to be the ratio of the flow time of the solution t (sec) to that of solvent t_0:

$$\eta_{rel} \approx \frac{t}{t_0} = \eta_{sp} + 1 \tag{3-1}$$

where η_{sp} is the specific viscosity (Harding, 1997). Then the reduced specific viscosity, η_{red}, (mL/g) and the inherent viscosity, η_{inh}, (mL/g) were obtained from:

$$\eta_{red} = (\eta_{rel} - 1)/c \tag{2-32}$$

$$\eta_{\text{inh}} = (\ln \eta_{\text{rel}})/c \tag{3-2}$$

where c (g/mL) is the solute concentration (Harding, 1997).

These η_{red} and η_{inh} can be extrapolated to zero concentration in order to eliminate nonideality effect, leading to the intrinsic viscosity $[\eta]$:

$$\eta_{\text{red}} = [\eta]\,(1 + K_{\text{H}} \cdot [\eta] \cdot c) \tag{3-3}$$

$$\eta_{\text{inh}} = [\eta]\,(1 - K_{\text{K}} \cdot [\eta] \cdot c) \tag{3-4}$$

where K_{H} is the Huggins constant (Huggins, 1942) and K_{K} is the Kraemer constant (Kraemer, 1938). Additionally, a combination of equations (3-7) and (3-8) was used (Solomon and Ciută, 1962):

$$[\eta] \simeq \frac{1}{c} \cdot [2\eta_{\text{sp}} - 2\ln(\eta_{\text{rel}})]^{1/2} \tag{3-5}$$

3.3. Results and discussion

3.3.1. Comparison of hydrodynamic properties of HA and TSP of the preparations

Table 3-1 summarizes the hydrodynamic properties of the hyaluronic acid and tamarind seed gum preparations (supplied by Farmigea AG) in the phosphate-chloride buffer. Sedimentation velocity (Figure 3-2a,b) and the elution profiles from SEC-MALS (Figure 3-3a,b) show unimodal behaviour for both HA and TSP. Extrapolation of the sedimentation coefficients to zero concentration (Figure 3-2c,d) yield $s_{20,w}$ values of (4.7

± 0.2)S and (5.4 ± 0.2)S, with concentration dependence or Gralén "k_s" parameter values, respectively of (1171 ± 20) ml/g and (240 ± 30) ml/g. The lower value for k_s for TSP is commensurate with the presence of weak self-associative effects previously reported (Patel et al., 2008), due to a gentle slope compared to HA, which has an opposing effect on the concentration dependence to hydrodynamic nonideality.

Table 3-1: Hydrodynamic properties of hyaluronic acid (HA) and tamarind seed gum polysaccharide (TSP) in PBS "Paley" buffer.

Sample	HA	TSP
$[\eta]$ (ml/g)	1475 ± 30*	675 ± 20*
$s^0_{20,w}$ (S)	4.7 ± 0.2*	5.4 ± 0.2*
a	0.86	0.63
$10^{-3} \times M_w$ (g/mol)	680 ± 30*	830 ± 30*
M_z/M_w	1.1	1.1
M_w/M_n	1.1	1.2

*These figures are within 2 SDs (Standard Deviation).

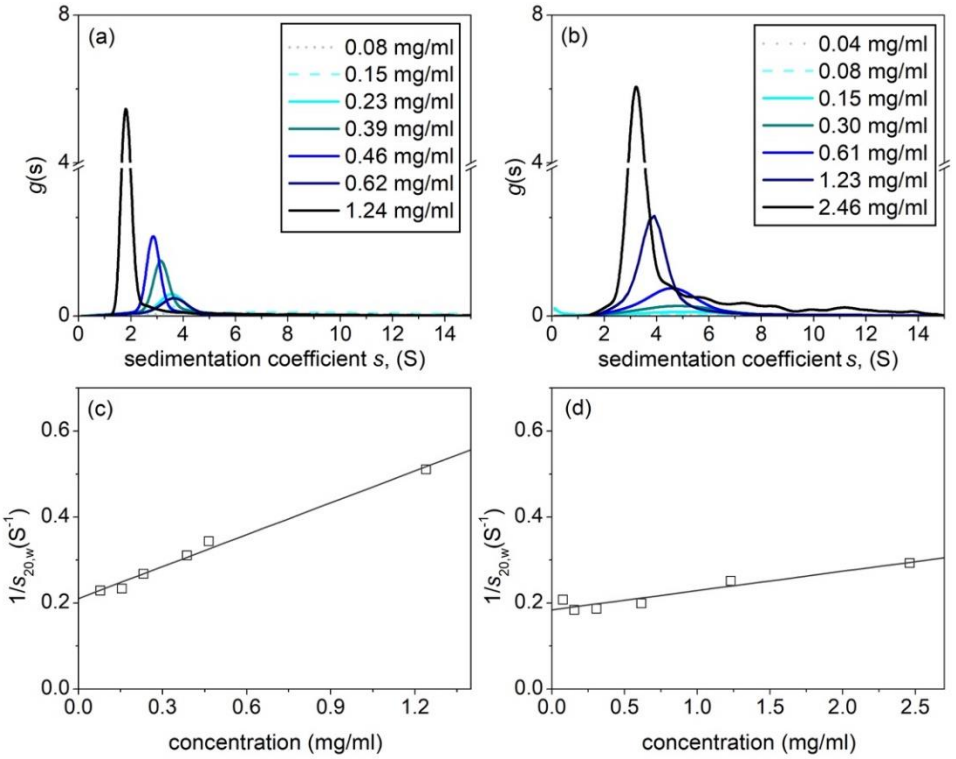

Figure 3-2. Sedimentation coefficient distributions. (**a**) Hyaluronic acid, HA. (**b**) Tamarind seed polysaccharide, TSP. (**c**) Corresponding concentration extrapolation to zero concentration to eliminate nonideality effects for HA (**d**) Corresponding plot for TSP. Solution pH = 6.8, I = 0.1, temperature = 20.0 °C.

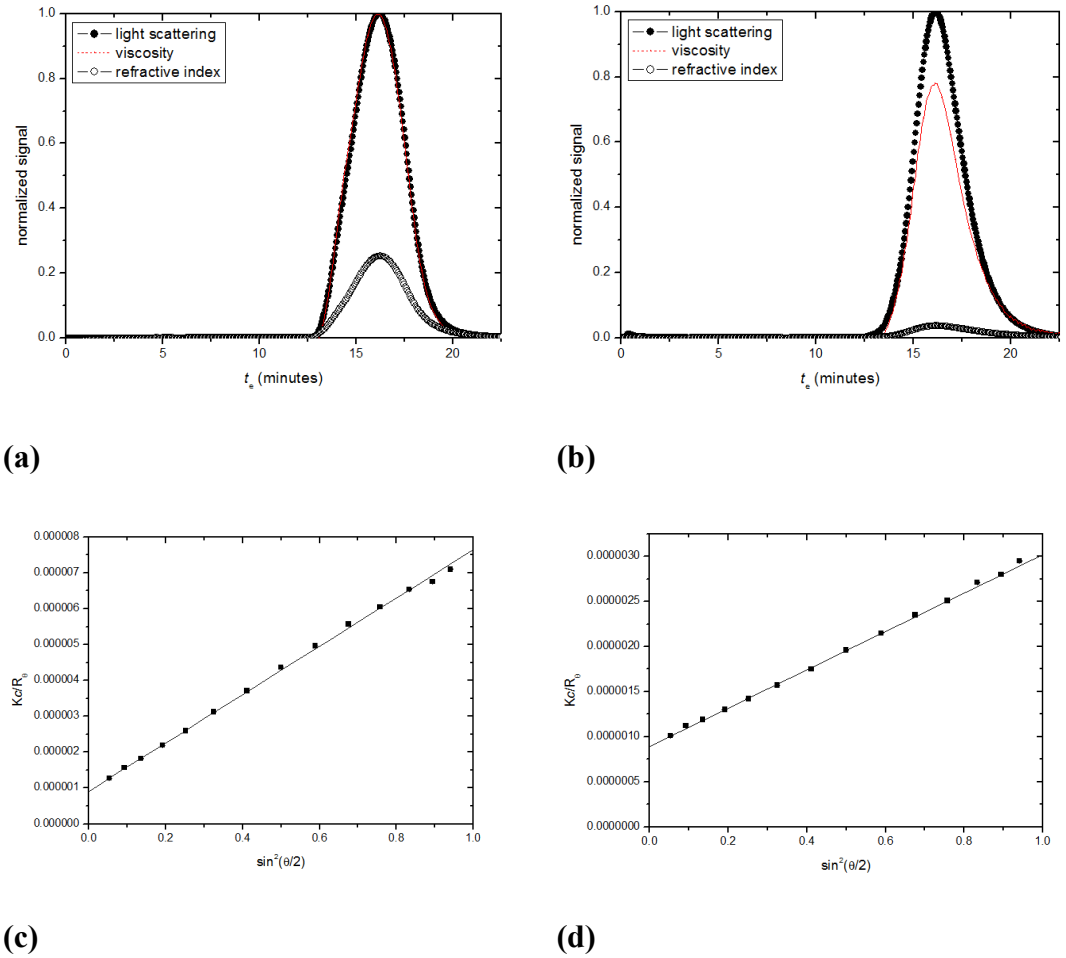

Figure 3-3. Size exclusion chromatography—multiangle light scattering (SEC-MALS) elution profiles for (**a**) hyaluronic acid, HA and (**b**) tamarind seed polysaccharide, TSP. Solid black circles: light scattering signal at a scattering angle θ = 90°. Open circles: concentration (refractive index) signal; dashed line: differential pressure (viscosity) signal; t_e = elution time. (**c**) Zimm fit of Kc/R_θ (see text for definitions) vs $\sin^2(\theta/2)$ for HA, at a single elution time t_e. (**d**) Corresponding plot for TSP. Solution pH = 6.8, I = 0.1, temperature = 20.0 °C.

SEC-MALS elution profiles for HA and TSP respectively are given in Figure 3-3a,b, and corresponding typical Zimm extrapolations for specific elution volumes are given in Figure 3-3c,d. Weight average molar masses M_w of (680 ± 30) kDa and (830 ± 30) kDa for the HA and TSP preparations are obtained, with low polydispersities commensurate for an optical formulation.

Corresponding viscosity plots obtained with the Ostwald capillary viscometer are shown in Figure 3-4 for HA (Figure 3-4a) and TSP (Figure 3-4b) respectively, yielding values of (1475 ± 30) ml/g and (675 ± 20) ml/g, which were the mean values of the Huggins/Kraemer intercepts. There was no difference between capillary and DPV viscometers.

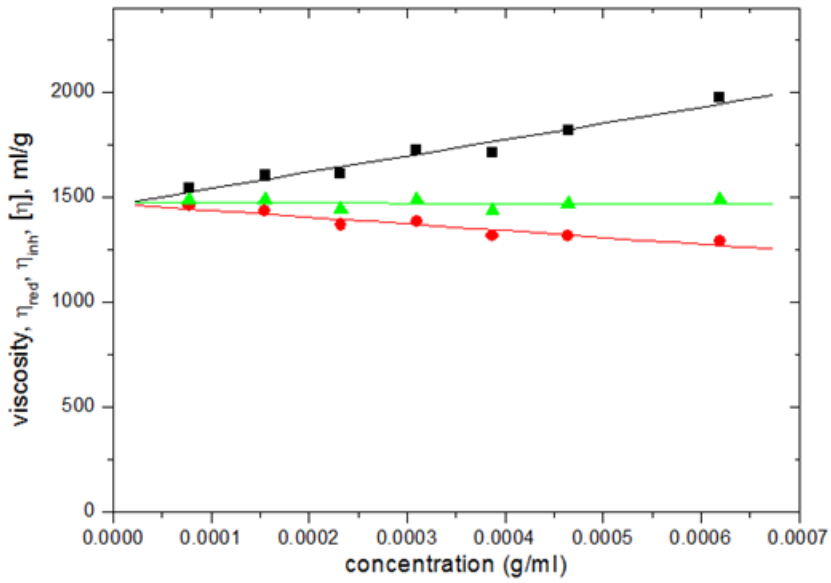

(a)

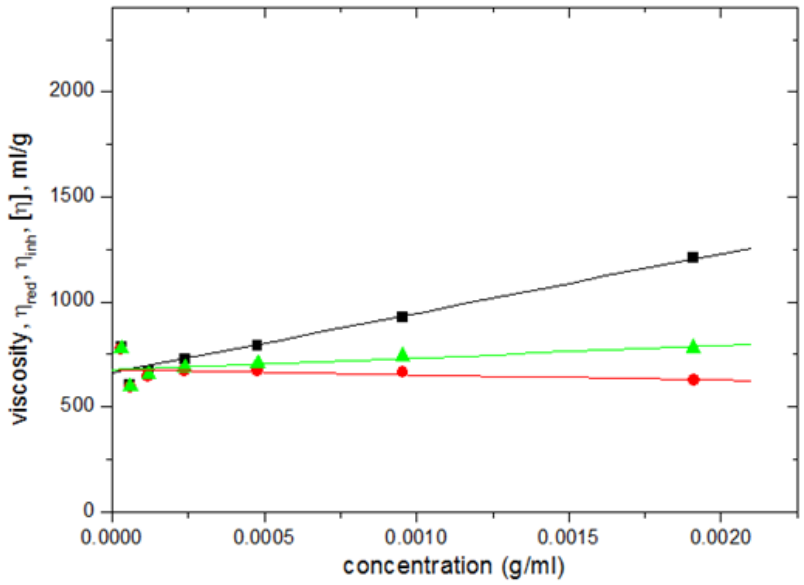

(b)

Figure 3-4. Evaluation of the intrinsic viscosity [η] from Ostwald viscometry: (a) HA and (b) TSP. Squares: Huggins' extrapolation; triangles: Solomon–Ciuta; circles: Kraemer extrapolation. Solution pH = 6.8, I = 0.1, temperature = (20.00 ± 0.05) °C.

Values for the molar mass and intrinsic viscosity for the Farmigea hyaluronic acid preparations (Table 3-1) are somewhat lower than we analysed previously from a different source (Hokputsa et al., 2003a, 2003b). By contrast the tamarind seed gum preparations gave similar results to those found previously in our research group (Patel et al., 2008; Picout et al., 2003). The differential pressure Viscostar (Wyatt Technology, Santa Barbara USA) viscometer attached on-line to SEC allows relative viscosities $\eta_{rel}(t_e)$ to be recorded as a function of elution volume (or elution time t_e), and the corresponding molar masses $M_w(t_e)$.

Since the concentration is known also for each value of t_e from the refractive index detection, this enables an estimate for $[\eta](t_e)$ to be obtained from equation (3-9). Mark–Houwink–Kuhn–Sakurada (MHKS) plots of log $[\eta](t_e)$ vs log $M_w(t_e)$ for HA and TSP respectively are given in (Figure 3-4a,b), enabling evaluation of the MHKS conformation parameter a:

$$[\eta](t_e) = M_w(t_e)^a \qquad (3\text{-}6)$$

From Figure 3-5a (HA) a value of a of 1.1 is obtained, corresponding to a stiff extended conformation, although $>M$ = 800 kDa a lower value is obtained ($a \sim 0.55$) corresponding to a flexible random coil conformation. However, the MHKS coefficient of HA is $a = 0.86$ without consideration of

this transition. Figure 3-5b we obtain $a = 0.63$ for TSP, also corresponding to a flexible random coil.

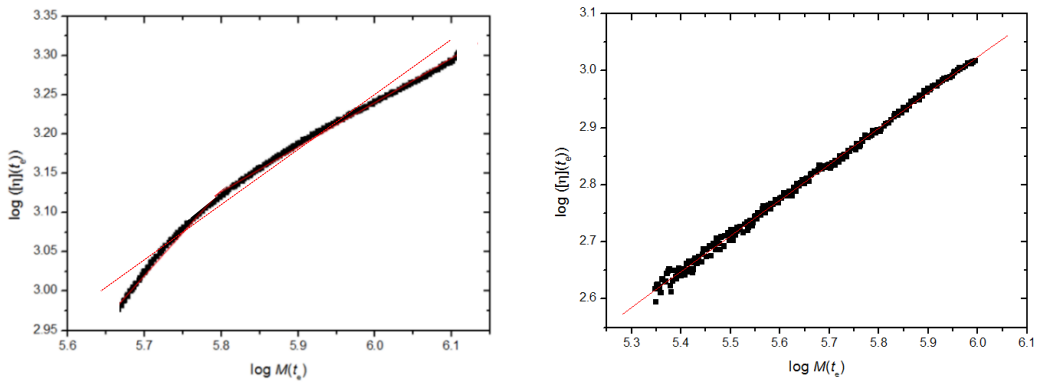

(a) **(b)**

Figure 3-5. Mark–Houwink–Kuhn–Sakurada plots of log intrinsic viscosity vs log molecular weight $M(t_e)$ at corresponding elution times t_e: (a) HA and (b) TSP. Solution pH = 6.8, I = 0.1, temperature = (20.0 ± 0.1) °C.

3.3.2 Hydrodynamic behaviour of mixtures of HA and TSP

Figure 3-6a shows the SEC-MALS profile for a mixture of HA with TSP. One can see a slight shift to lower elution times (higher molar masses) relative to HA and TSP by themselves (Figure 3-3a,b with a shoulder at lower elution time suggestive of some degree of complexation. Analysis using ASTRA software shows a small decrease in the measured M_w (= 720 ± 30) kg/mol compared with the predicted value of 755 kg/mol.

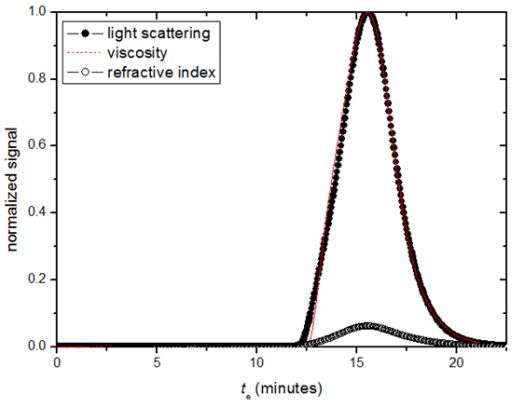

(a)

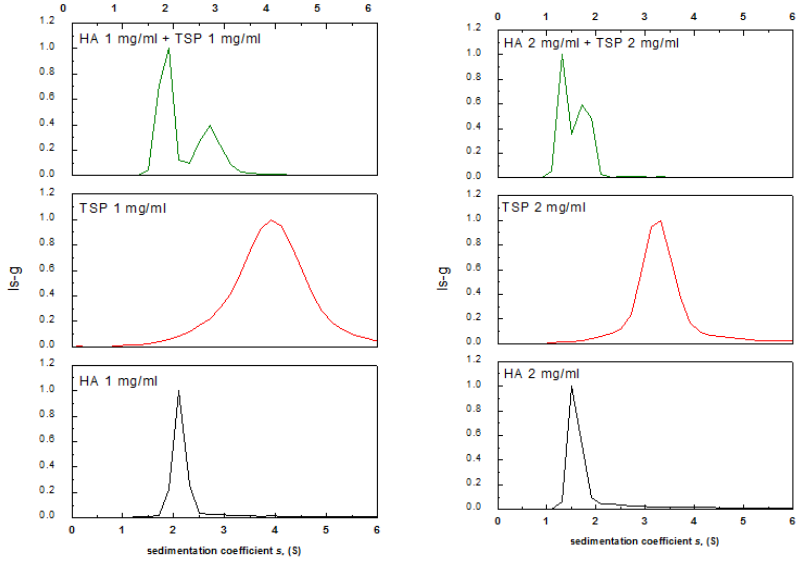

(b) **(c)**

Figure 3-6. (a) Elution profiles for a 1:1 mixture of HA to TSP in 0.1M, pH 6.8 PBS buffer. Solid circles—light scattering 90° signal. Open circles—concentration (refractive index) signal. Dashed line—relative viscosity signal. The concentration of HA = 1 mg/mL, and TSP= 1 mg/mL. (b) Sedimentation coefficient distributions for HA (black), TSP (red) and HA-TSP mixture (green). Concentrations of HA, TSP 1 mg/mL. (c) As (b) but concentrations of HA, TSP = 2.0 mg/mL.

These observations are reinforced by the results from intrinsic viscosity. Table 3-2 shows the comparison of the theoretical intrinsic viscosity calculated from the ratio of HA to TSP in each mixture with varying ratios (the HA:TSP ratios = 3:1, 1:1 and 3:1), and the actual intrinsic viscosity obtained experimentally from the capillary viscometry. It is clear that there is no significant increase (HA:TSP = 1:1 and 1:3).

Table 3-2: Measured intrinsic viscosities for HA:TSP mixtures compared with the theoretically predicted (based on values from Table 3-1) if there was no interaction. The experimental value of HA:TSP = 1:3 was lower than the theoretical one because the portion of HA was smaller than TSP, which was less viscous than HA.

HA:TSP ratio	**[η]**	**[η] (theoretical)**
1:3	780 mL/g	940 mL/g
1:1	1100 mL/g	1075 mL/g
3:1	1180 mL/g	1200 mL/g

3.4. Conclusions

The present findings of this interaction study using mixtures of hyaluronic acid and tamarind seed polysaccharides implies there is no incompatibility in solutions of the two, at concentrations used in popular formulations to help supplement reduced lachrymal fluid/ ocular mucin in an aging population. Earlier observations with similar concentrations using NMR spectroscopy (Uccello-Barretta et al., 2010) have demonstrated a synergistic interaction between the two polysaccharides. The present study complements those observations by showing that no large aggregate or supramolecular formation was evident, reassuring for formulations involving the two polymers.

In the following chapter, we consider the hydrodynamic properties of another important glycan – teicoplanin – considered for use as an antibiotic in the treatment of ocular and other diseases.

3.5. References

Almutairi, F.M., Erten, T., Adams, G.G., Hayes, M., McLoughlin, P., Kök, M.Ş., Mackie, A.R., Rowe, A.J., Harding, S.E., 2015. Hydrodynamic characterisation of chitosan and its interaction with two polyanions: DNA and xanthan. Carbohyd Polym 122, 359–366.

Barabino, S., Rolando, M., Nardi, M., Bonini, S., Aragona, P., Traverso, C.E., 2013. The effect of an artificial tear combining hyaluronic acid and tamarind seeds polysaccharide in patients with moderate dry eye syndrome: A new treatment for dry eye. Eur J Ophthalmol 24, 173–178.

Dam, J., Schuck, P., 2004. Calculating sedimentation coefficient distributions by direct modeling of sedimentation velocity concentration profiles. Methods Enzymol 384, 185–212.

Forrester, J.V., Dick, A.D., McMenamin, P.G., Roberts, F., Pearlman, E., 2016. The eye basic sciences in practice, Fourth. ed. Elsevier, London.

Gralén, N., 1994. Sedimentation and diffusion measurements on cellulose and cellulose derivatives. University of Uppsala.

Green, A.A., 1933. The preparation of acetate and phosphate buffer solutions of known pH and ionic strength. Journal of the American Chemical Society 55, 2331–2336.

Hammer, M.E., Burch, T.G., 1984. Viscous corneal protection by sodium hyaluronate, chondroitin sulfate, and methylcellulose. Investigative ophthalmology & visual science 25, 1329–1332.

Harding, S.E., 1997. The intrinsic viscosity of biological macromolecules. Progress in measurement, interpretation and application to structure in dilute solution. Prog Biophysics Mol Biology 68, 207–262.

Harding, S.E., 2018. The Svedberg Lecture 2017. From nano to micro: the huge dynamic range of the analytical ultracentrifuge for characterising the sizes, shapes

and interactions of molecules and assemblies in Biochemistry and Polymer Science. Eur Biophys J 47, 697–707.

Harding, S.E., Adams, G.G., Almutairi, F., Alzahrani, Q., Erten, T., Kök, M.S., Gillis, R.B., 2015. Chapter 18 Ultracentrifuge methods for the analysis of polysaccharides, glycoconjugates, and lignins. Methods Enzymol 562, 391–439.

Harding, S.E., Tomb, M.P., Adams, G.G., Paulsen, B.S., Inngjerdingen, K.T., Barsett, H., 2017. An Introduction to Polysaccharide Biotechnology, Second. ed. CRC Press, Boca Raton.

Hokputsa, S., Jumel, K., Alexander, C., Harding, S.E., 2003a. A comparison of molecular mass determination of hyaluronic acid using SEC/MALLS and sedimentation equilibrium. Eur Biophys J 32, 450–456.

Hokputsa, S., Jumel, K., Alexander, C., Harding, S.E., 2003b. Hydrodynamic characterisation of chemically degraded hyaluronic acid. Carbohyd Polym 52, 111–117.

Huggins, M.L., 1942. The viscosity of dilute solutions of long-chain molecules. IV. Dependence on concentration. Journal of the American Chemical Society 11, 2716–2718.

Johnson, M.E., Murphy, P.J., Boulton, M., 2006. Effectiveness of sodium hyaluronate eyedrops in the treatment of dry eye. Graefe's Archive Clin Exp Ophthalmol 244, 109–112.

Kraemer, E.O., 1938. Molecular weights of celluloses and cellulose derivates. Industrial & Engineering Chemistry Research 10, 1200–1203.

Lai, J.-Y., Luo, L.-J., Nguyen, D.D., 2020. Multifunctional glutathione-dependent hydrogel eye drops with enhanced drug bioavailability for glaucoma therapy. Chem Eng J 402, 126190.

Lee, D., Lu, Q., Sommerfeld, S.D., Chan, A., Menon, N.G., Schmidt, T.A., Elisseeff, J.H., Singh, A., 2017. Targeted delivery of hyaluronic acid to the ocular surface by a polymer-peptide conjugate system for dry eye disease. Acta Biomater 55, 163–171.

Lian, L.-Y., 2001. NMR studies of protein-ligand interactions. In: Harding, S.E., Chowdhry, B.Z. (Eds.), Protein-Ligand Interactions, Structure and Spectroscopy: A Practical Approach. Oxford University Press, Oxford, UK, pp. 383–405.

Luo, L.-J., Lai, J.-Y., 2017. Epigallocatechin gallate-loaded gelatin-g-poly(N-Isopropylacrylamide) as a new ophthalmic pharmaceutical formulation for topical use in the treatment of dry eye syndrome. Sci Rep-uk 7, 9380.

Luo, L.-J., Nguyen, D.D., Lai, J.-Y., 2020. Long-acting mucoadhesive thermogels for improving topical treatments of dry eye disease. Mater Sci Eng C 115, 111095.

Patel, T.R., Morris, G.A., Ebringerová, A., Vodeničarová, M., Velebný, V., Ortega, A., Torre, J.G. de la, Harding, S.E., 2008. Global conformation analysis of irradiated xyloglucans. Carbohyd Polym 74, 845–851.

Picout, D.R., Ross-Murphy, S.B., Errington, N., Harding, S.E., 2003. Pressure cell assisted solubilization of xyloglucans: Tamarind seed polysaccharide and detarium gum. Biomacromolecules 4, 799–807.

Rah, M.J., 2011. A review of hyaluronan and its ophthalmic applications. Optometry - J Am Optometric Assoc 82, 38–43.

Rolando, M., Valente, C., 2007. Establishing the tolerability and performance of tamarind seed polysaccharide (TSP) in treating dry eye syndrome: results of a clinical study. Bmc Ophthalmol 7, 5.

Schachman, H.K., 1950. Ultracentrifugation in Biochemistry. Academic Press, New York, NY, USA; London, UK.

Semenzato, A., Costantini, A., Baratto, G., 2014. Green polymers in personal care products: Rheological properties of tamarind seed polysaccharide. Cosmet 2, 1–10.

Solomon, O.F., Ciută, I.Z., 1962. Détermination de la viscosité intrinsèque de solutions de polymères par une simple détermination de la viscosité. Journal of Applied Polymer Science 6, 683–686.

Uccello-Barretta, G., Balzano, F., Vanni, L., Sansò, M., 2013. Mucoadhesive properties of tamarind-seed polysaccharide/hyaluronic acid mixtures: A nuclear magnetic resonance spectroscopy investigation. Carbohyd Polym 91, 568–572.

Uccello-Barretta, G., Nazzi, S., Zambito, Y., Colo, G.D., Balzano, F., Sansò, M., 2010. Synergistic interaction between TS-polysaccharide and hyaluronic acid: Implications in the formulation of eye drops. Int J Pharmaceut 395, 122–131.

Wang, K., Wen, H.-F., Yu, D.-G., Yang, Y., Zhang, D.-F., 2018. Electrosprayed hydrophilic nanocomposites coated with shellac for colon-specific delayed drug delivery. Mater Design 143, 248–255.

Wang, M., Hai, T., Feng, Z., Yu, D.-G., Yang, Y., Bligh, S.A., 2019. The relationships between the working fluids, process characteristics and products from the modified coaxial electrospinning of zein. Polymers-basel 11, 1287.

Wang, Q., Ellis, P.R., Ross-Murphy, S.B., Burchard, W., 1997. Solution characteristics of the xyloglucan extracted from Detarium senegalense Gmelin. Carbohyd Polym 33, 115–124.

Wyatt, P.J., 1992. Combined differential light scattering with various liquid chromatography separation techniques. In: Harding, S.E., Sattelle, D.B., Bloomfield, V.A. (Eds.), Laser Light Scatt Biochemistry. Royal Society of Chemistry, Cambridge, UK, pp. 35–38.

Yang, Y., Chang, S., Bai, Y., Du, Y., Yu, D.-G., 2020. Electrospun triaxial nanofibers with middle blank cellulose acetate layers for accurate dual-stage drug release. Carbohyd Polym 243, 116477.

Yoon, W.H., Lee, K.H., 2019. Rheological properties and efficacy of the formulation of hyaluronic acid with tamarind seed polysaccharide for arthritis. Biorheology 56, 31–38.

Zimm, B.H., 1948. The scattering of light and the radial distribution function of high polymer solutions. J Chem Phys 16, 1093–1099.

Chapter 4: Self-association of the glycopeptide antibiotic teicoplanin A2 in aqueous solution studied by molecular hydrodynamics.

4.1. Introduction

Teicoplanin is a member of the glycopeptide antibiotic family, such as vancomycin, to treat severe bacterial infections. This glycopeptide antibiotic was first extracted from *Actinoplanes teichomyceticus*, which was discovered in 1978 from an Indian soil sample (Parenti et al., 2006). Its main chemical structure (Figure 4-1) is a heptapeptide with three monosaccharide residues: α-D-mannose, *N*-acetyl-β-D-glucosamine, and *N*-acyl-β-D-glucosamine (Barna et al., 1984; Hunt et al., 1984). For teicoplanin, there are six major subtypes (A2-1 through A2-5, and A3-1) and four minor subtypes (from RS-1 to RS-4) (Bernareggi et al., 1992). Of these subtypes, teicoplanin is primarily formed by bacteria as a blend of A2-1 through A2-5 lipoforms which have different fatty acid chains attached to the GlcNAc (N-acetyl-β-D-glucosamine) residue (Zanol et al., 1988). The antibiotic mechanism teicoplanin is similar to another glycopeptide vancomycin (structurally similar, although not containing lipid), and both antibiotics inhibit the formation of the peptidoglycan chains of bacterial cell walls, by attaching to the D-Ala-D-Ala C-terminus of the pentapeptide substrate via hydrogen bonds (Reynolds, 1989). Moreover, teicoplanin is known to interact with this pentapeptide substrate through

its hydrophobic lipid chain, resulting in the positioning of the antibiotic being adjacent to the peptidoglycan (Vimberg et al., 2019; Zeng et al., 2016).

Teicoplanin is used in the treatment of life-threatening infectious diseases caused by multidrug-resistant Gram-positive bacteria, including methicillin-resistant *Staphylococcus aureus* (MRSA) and *Enterococci*. Teicoplanin has a proven, outstanding high efficacy in various tissue sites, such as the heart and respiratory tracts (Vimberg, 2021). Its main routes of administration are intravenous and intramuscular, although it is also given orally and is considered for topical administration, especially for treating ocular infections.

The therapeutic plasma concentration of teicoplanin ranges from 10 to 30 mg/L, depending on the severity of the disease or the range of infectious sites, for example, bone infections (Pea, 2020; Pea et al., 2003; Wilson, 2000), and has been found to bind to serum albumin in the blood (Wilson, 2000). On the other hand, oral and topical (ocular infections) administrations are limited. The oral route is used for the treatment of pseudomembranous colitis caused by *Clostridium difficile* (Wenisch et al., 1996). In terms of ocular infections, Kaye suggested synergistic benefits of teicoplanin with other antibiotics, such as meropenem, against *S. aureus* keratitis (Kaye, 2017; Sueke et al., 2015), although Kaye's research group concluded that there was little penetration of teicoplanin into human aqueous humour below the

cornea with the administration of 10 mg/mL eye drops (Kaye et al., 2009). Antoniadou et al. also reported a similar result: no penetration into the aqueous humour, with the subconjunctival injection (approximately 0.5 mL) of 25 mg teicoplanin (Antoniadou et al., 1998).

Since the beginning of the Covid-19 pandemic in December 2019, teicoplanin has been spotlighted as a potential drug candidate against severe acute respiratory syndrome coronavirus 2 (SARS-CoV-2) due to its well-known antiviral ability. Zhou and colleagues had earlier indicated that teicoplanin inhibited cell entry of the SARS-CoV virus (Zhou et al., 2016). In order to cross the cell membrane and enter a host cell, both SARS-CoV and SARS-CoV-2 viruses depend on cysteine proteinase cathepsin L (CTSL), which splits viral spike (S) glycoproteins attached to a host receptor so that viruses are released from an endosome within the host cell (Yu et al., 2022; Zhou et al., 2016). The fatty acid chain of teicoplanin interacts with CTSL, while vancomycin, without such a hydrophobic group, cannot express antiviral activity against CTSL-dependent viruses (Zhou et al., 2016). Consequently, some clinical studies were focused on the novel medical use of teicoplanin as a Covid-19 drug (Ceccarelli et al., 2021, 2020). Regardless of whether teicoplanin is used in the treatment of Covid-19 or co-infections of Gram-positive bacteria in Covid-19 patients, its use is still in demand.

However, there has been a growing concern about the resistance to teicoplanin in pathogens since its approval in Europe in 1988. In the same year, it was already shown that vancomycin- and teicoplanin-resistant *Enterococci* strains had been isolated from patients in France (Leclercq et al., 1989). Gram-positive bacteria, especially *Enterococci*, acquire resistance by modifying their D-Ala-D-Ala moiety of peptidoglycan precursors, Lipid II. This moiety is transformed to either D-Ala-D-Lac (*vanA, vanB, vanD*) or D-Ala-D-Ser (*vanC, vanE, vanG*) in resistant strains, and as a result, glycopeptides have a low affinity to these phenotypes of precursors (Blaskovich et al., 2018; Butler et al., 2014).

Although it is important to explore how teicoplanin binds to the Lipid II moiety regardless of its phenotypes, the knowledge of the biological form of teicoplanin in an aqueous solution is of importance. It is known that the minimum volume of solvent required to dissolve 400 mg of teicoplanin is 3 ml because, below that value, a gel might be formed in the solution (Wilson, 2000). This gelation/coalescence of teicoplanin was thought to be caused by micellization due to its hydrophobic tail (Armstrong and Nair, 1997; Wan and Blomberg, 1997), although a teicoplanin derivative without that tail can still aggregate in solution (Bardsley et al., 2002). This concentration-dependent aggregation might lead to poor permeability of teicoplanin across the epithelial lining by the oral and topical (ocular) routes, and

additionally, the aggregated form may be responsible for excessive exposure of teicoplanin, resulting in more bacteria acquiring resistance. Due to its importance, in this study, we perform an analysis of this associative/aggregation effect using the powerful hydrodynamic techniques of sedimentation velocity and sedimentation equilibrium in the analytical ultracentrifuge (SV-AUC, SE-AUC) taking advantage of the inherent separation and analysis facilities of the analytical ultracentrifuge (AUC). Analytical ultracentrifugation is a matrix-free method with a broad range of molar masses, 10^2-10^8 g/mol, and the key technique used to explore the molecular behaviours of proteins, polysaccharides, or other macromolecules in solution (Harding, 2018). AUC has recently been used to characterize the self-associative properties of vancomycin (Phillips-Jones et al., 2017b) and its interactions with VanS (Phillips-Jones et al., 2017a) and mucins (Dinu et al., 2020).

Then I also assess the solution conformation of the association/aggregation products using molecular viscometric analysis of the intrinsic viscosity [η], in combination with the sedimentation coefficient from sedimentation velocity. We believe this present study is the first report demonstrating the self-association of teicoplanin with hydrodynamic methods.

4.2. Materials and methods

4.2.1 Teicoplanin

Teicoplanin A2 (monomer molar mass: M_1 = 1877.6 g/mol for teicoplanin A2-1, M_1 = 1879.7 g/mol for teicoplanin A2-2 and A2-3, and M_1 = 1893.7 g/mol for teicoplanin A2-4 and A2-5) was purchased in powder form from Sigma-Aldrich, United Kingdom. Its structure is shown in Figure 4-1:

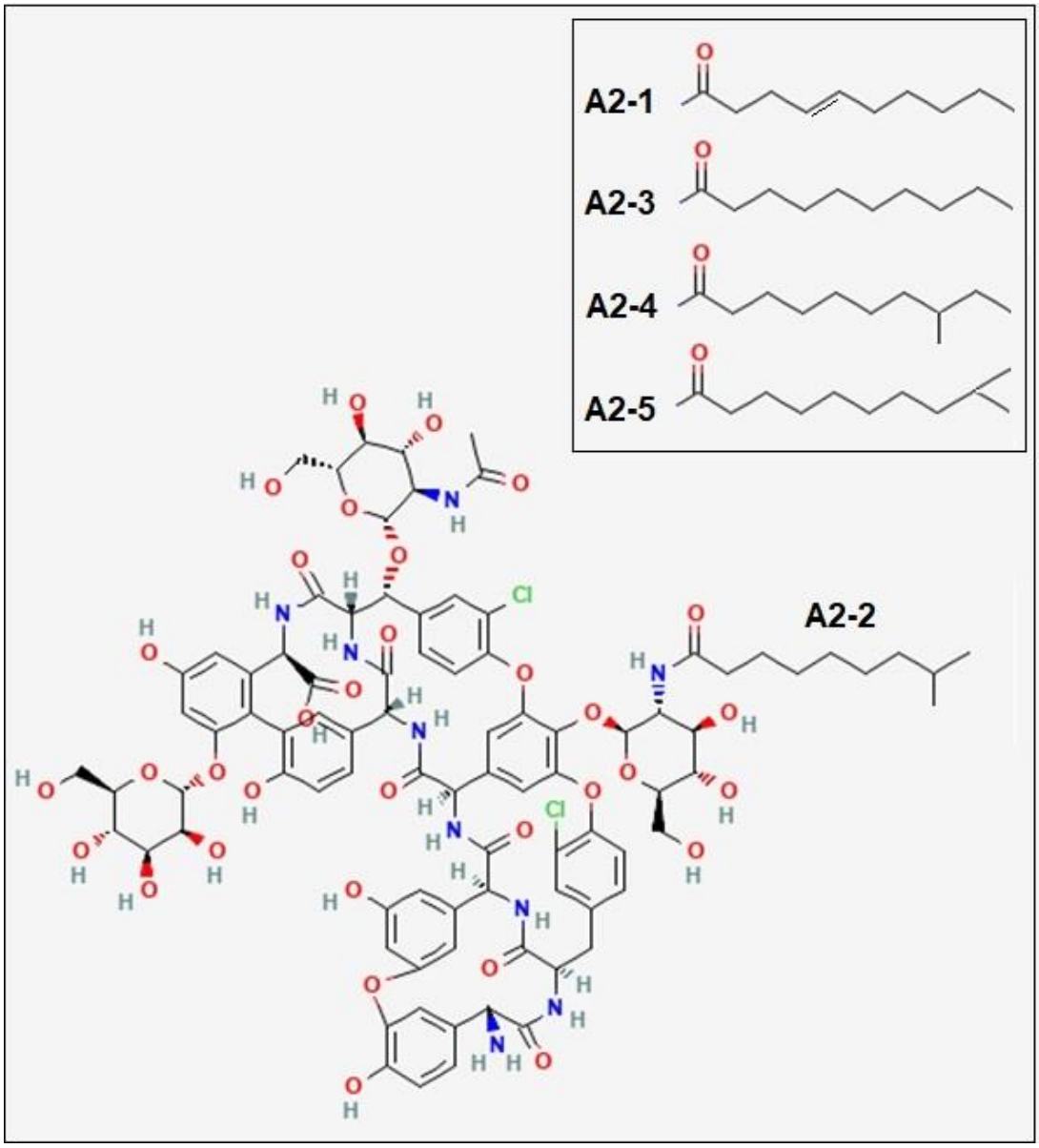

Figure 4-1: Structure of teicoplanin (adapted from the National Institute for Health/ National Center of Biotechnology Information based on an original structure given by F. Parenti(1986)). Teicoplanin lipoform A2-2 (M_1 = 1879.7 g/mol) shown: the other major lipoforms of A2 with different acyl chains are shown in the inset.

Teicoplanin samples were prepared in a phosphate-chloride buffered saline solution (PBS, or “Paley buffer”) at pH~6.8 and, by adding NaCl, adjusted to an ionic strength of I = 0.1 mol/L (Green, 1933).

The concentration, *c* (g/mL) of the stock solution was then measured using a differential refractometer (Atago DD7, Tokyo, Japan) set to zero with the reference solvent (PBS) and using a refractive increment *dn/dc* of 0.188 mL/g for teicoplanin (Tesarová et al., 2001). The measured concentration was multiplied by 0.96 for moisture content correction, being calculated from the difference in the weights of teicoplanin powder before and after the vacuum oven (Vacuum Oven 31 litres, Fistreem, Cambridge, UK) drying overnight (Taber, 1980).

The partial specific volume $\bar{v}$ from solution/ solvent densities was determined using an Anton-Paar (Graz, Austria) digital density meter (Kratky et al., 1973), and application of:

$$\bar{v} = \frac{1}{\rho_0} \cdot \left(1 - \frac{\rho - \rho_0}{c}\right) \qquad (4\text{-}1)$$

at a concentration, *c*, of 10.2 mg/mL, and where ρ and ρ_0 are the densities of the solution and solvent, respectively. A value of (0.64 ± 0.01) mL/g, was obtained, similar to that for vancomycin (Phillips-Jones et al., 2017b).

4.2.2. Sedimentation velocity in the analytical ultracentrifuge

Experiments to determine sedimentation coefficients and sedimentation coefficient distributions were performed at a temperature of 20.0 °C using an Optimal XL-I analytical ultracentrifuge (Beckman Instruments, Palo Alto, CA, USA) with Rayleigh interference optics. Teicoplanin samples (400 μL) and reference solvent (PBS, 420 μL) were injected into channels of the 12 mm double sector epoxy cells with sapphire windows. These cells were then centrifuged at 47500 rpm for a run time of ~24 h and the data obtained were analysed in SEDFIT using the least squares, ls-g*(*s*) processing method (Dam and Schuck, 2004). This generates the sedimentation coefficient distribution, g(*s*) versus $s_{\mathrm{T,b}}$, where $s_{\mathrm{T,b}}$ is the sedimentation coefficient, at temperature *T* in buffer *b*. The *s* value in Svedberg units, S = 10^{-13} seconds, was then normalised to standard conditions (density $\rho_{20,w}$ and viscosity $\eta_{20,w}$ of water at 20.0 °C) to give $s_{20,w}$ from the equation (Schachman, 1950):

$$s_{20,w} = \frac{1-\bar{v}\cdot\rho_{20,w}}{1-\bar{v}\cdot\rho_{T,b}} \cdot \frac{\eta_{T,b}}{\eta_{20,w}} \cdot s_{T,b} \qquad (4\text{-}2)$$

where $\rho_{T,b}$ and $\eta_{T,b}$ are the density and the viscosity of buffer *b* at temperature *T*, respectively.

4.2.3. Sedimentation equilibrium in the analytical ultracentrifuge

Due to the longer time required compared to sedimentation velocity, sedimentation equilibrium experiments were performed at a temperature of 7.0 °C (to stabilise teicoplanin samples) also using the Optimal XL-I analytical ultracentrifuge to obtain equilibrium concentration distribution profiles. To characterise the self-association/aggregation of teicoplanin, 12 mm double sector epoxy cells were loaded with the same volumes (100 μL) of both solution and solvent and run at 45000 rpm for a run time of ~48 h. Lower experiment temperature stabilised samples. Records of concentration distributions of teicoplanin at equilibrium were subsequently analysed using the model-independent SEDFIT-MSTAR algorithm (Schuck et al., 2014). Since the non-ideality of teicoplanin is negligible due to a low concentration, we estimated that apparent weight average molar masses $M_{w,app}$ were approximately equal to the true weight average molar masses M_w (Creeth and Harding, 1982).

4.2.3. Hydrodynamic radius determination by dynamic light scattering (DLS)

Dynamic or quasi-elastic light scattering (DLS or QLS) measurements were made on the fixed scattering angle Zetasizer Nano-S system (Malvern

instruments Ltd., Malvern UK) equipped with a 4mW He-Ne laser at a wavelength of 632.8nm (Harding et al., 1992; Nobbmann et al., 2007). Samples in solution were measured in a quartz cuvette at 20.0°C. A scattering angle of 173° was used, and collected in manual mode, requiring a measurement duration of 90 seconds. The resulting data were analysed using the "Zetasizer Software (Version 7.1)" (Malvern Instruments Ltd., Malvern, UK), providing a volume distribution of translational diffusion coefficients based on a form of the CONTIN program (Provencher, 1992). The viscosity of the buffer used was calculated using a solvent builder interface and takes the effects of buffer salts into account. The z-average hydrodynamic radii r_z (nm), were evaluated from the z-average translational diffusion coefficients D_z by the Stokes-Einstein equation (Harding et al., 1992):

$$r_z = k_B T / \{6\pi\eta D_z\} \quad (4\text{-}3)$$

where k_B is the Boltzmann constant, T is the absolute temperature and η is the viscosity of the medium. The following assumptions were made (i) the solutions were sufficiently dilute and sample sizes sufficiently small that non-ideality effects were not significant – i.e. an extrapolation to zero concentration was not necessary. This is reasonable as the non-ideality is due

to the low concentration and small size of teicoplanin, and for translational diffusion, the two main contributory factors to non-ideality – the hydrodynamic and thermodynamic terms - compensate for each other and can even cancel each other out (Harding and Johnson, 1985a, 1985b). (ii) the teicoplanin in its monomeric and multi-metric form were quasi-spheroidal and not asymmetric so there was no angular dependence of the measured D_z, values on anisotropic rotational diffusion effects – i.e. an extrapolation to zero angles was not necessary.

4.2.4. Intrinsic viscosity measurement

Teicoplanin solutions were analysed using the capillary viscometer AMVn (Anton-Paar, Graz, Austria). This measurement was conducted at a temperature of 25.0 °C based on the rolling ball viscosity method. With a 1.4mm steel ball moving in a 1.6 mm diameter glass capillary, the flow time of the solvent and solution was then determined. The relative viscosity was calculated from the equation:

$$\eta_{rel} = \frac{\rho \cdot t}{\rho_0 \cdot t_0} = \eta_{sp} + 1 \qquad (4\text{-}4)$$

where η_{sp} is the specific viscosity (Harding, 1997). Then the intrinsic viscosity $[\eta]$ was estimated from the Solomon-Ciuta relation(Solomon and

Ciută, 1962) at a concentration of 10.2 mg/ml:

$$[\eta] \approx \frac{1}{c} \cdot \left[2\eta_{sp} - 2ln(\eta_{rel})\right]^{\frac{1}{2}} \quad (5)$$

4.3. Results and discussion

4.3.1. Hydrodynamic properties of teicoplanin

Figure 4-2 shows the sedimentation coefficient distribution function g(*s*) plotted versus $s_{20,w}$, where g(*s*) is the proportion of sedimentation coefficient values lying within the range of *s* and *s*+*ds*. Sedimentation velocity plots obtained using the algorithm SEDFIT for teicoplanin (Figure 4-2) reveal unimodal behaviour at much higher *s*-values than expected for monomeric teicoplanin, for concentrations >0.5 mg/ml. Below this concentration separation occurred with bimodality. Figure 4-3 shows a plot of *s* vs *c* for those concentrations where unimodality is still clear. The extrapolated value of ~ 4.65 S is in good agreement with a spherical 18-19-mer of the molar mass of 35400, while the lower extrapolated value of ~ 0.7 S is the predicted value for a spheroidal unimer.

In order to effectively assess the 19-merisation, we sought the application of a chaotropic agent (6M GuHCl) to reduce the solvent effects of water and make teicoplanin more soluble. 6M GuHCl disrupts hydrogen bonds between

water molecules so that teicoplanin A2 is prevented from aggregating in solution. The *s*-value of teicoplanin dissolved in 6M GuHCl was ~0.7 S and $s_{20,w}$ was (1.17 ± 0.01) S. For the weight-average molar mass, M_w = (1.75 ± 0.35) kDa (see Figure 4-4), corresponding the unimer, was obtained. Since teicoplanin was dissolved in the chaotropic agent, the teicoplanin samples did not become 18-19mer over 0-10 mg/mL.

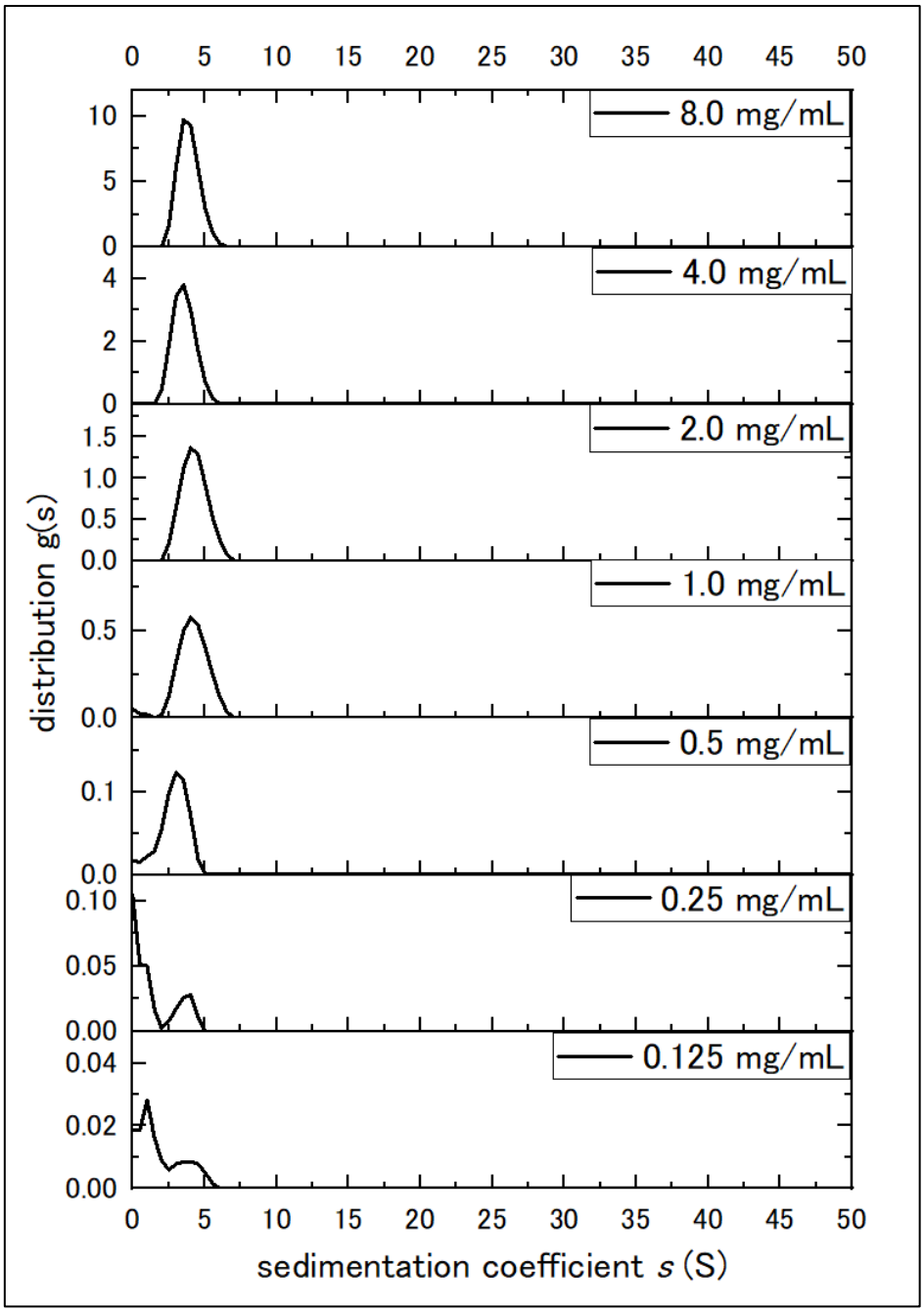

Figure 4-2: Sedimentation coefficient distribution of teicoplanin A2 at different concentrations from 0-5 mg/mL. The Y-axis ranges are different for each sample because that is clearer to see unimodality for higher concentrations (>0.5 mg/mL) and separation occurring for lower concentrations (<0.5 mg/mL). There were no aggregations between 10-50 S.

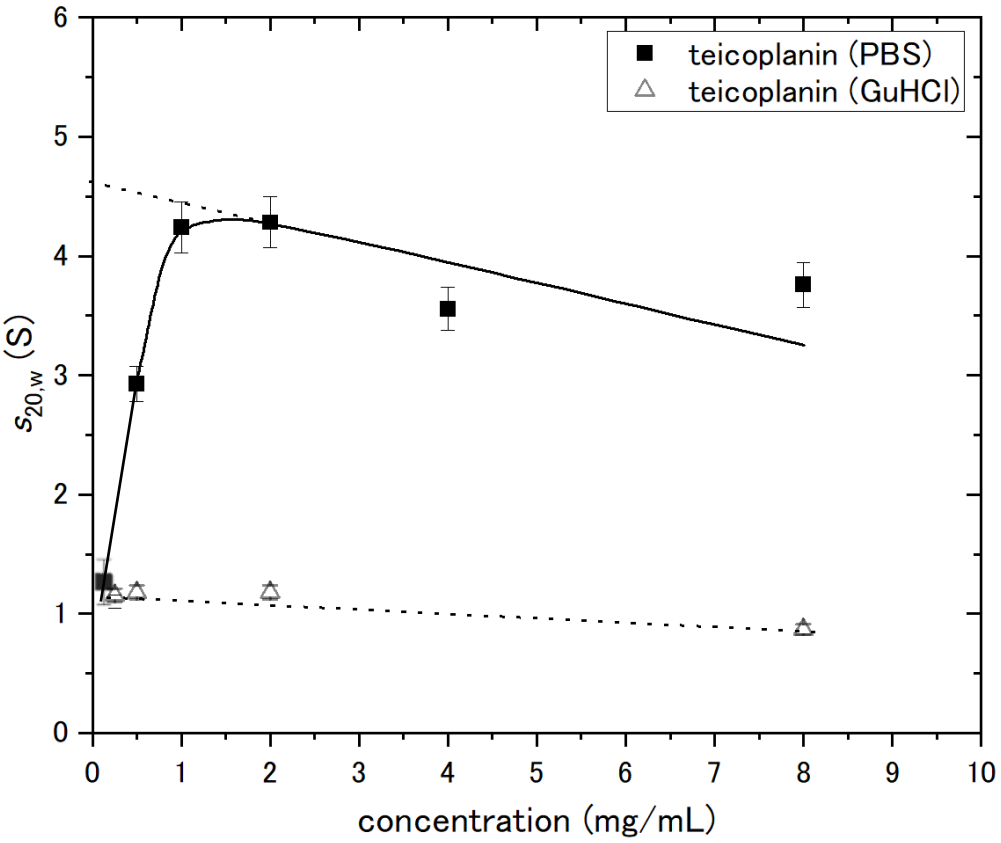

Figure 4-3: Change of apparent sedimentation coefficient ($s_{20,w}$) of teicoplanin A2 with sedimenting concentration, *c*. Concentrations were corrected for radial dilution. The extrapolated value of ~ 4.65 S is consistent with a spherical 18-19-mer of the molar mass of 35400. The lower extrapolated value of ~ 0.7 S is the predicted value for a spheroidal unimer, which is consistent with the *s*-value of teicoplanin dissolved in 6M GuHCl, $s_{20,w}$ = (1.17 ± 0.01) S. Solid line is a standard French curve fit to the data.

4.3.2. Teicoplanin self-association

To determine the weight-average molar masses M_w of teicoplanin, the *M** extrapolation method (Creeth and Harding, 1982) and hinge point analysis (Schuck et al., 2014) incorporated in the sedimentation equilibrium-based SEDFIT-MSTAR software (Schuck et al., 2014) were used. A similar approach was previously used in the analysis of vancomycin (Phillips-Jones et al., 2017b). Rayleigh interference optics provides an accurate record of a sedimentation equilibrium concentration profile *c(r)* vs *r*, which means that the local concentration *c* at the radial position *r* (cm) is from the rotation centre. *M**(r) is a useful operational point average molar mass parameter. $M^*(r \rightarrow r_b) = M_w$ is the weight average molar mass over the whole macromolecular distribution, where *r* is the radial position at the cell base. This method is particularly advantageous for polydisperse/ or self-associating systems (Creeth and Harding, 1982). As an additional check, the "hinge point method" (the value of the point weight average molar mass, $M_w(r)$ at the "hinge point" in the sedimentation equilibrium distribution, i.e. the radial position in the cell where the local concentration c(r) = the original loading concentration) provides another estimate for the whole distribution molar mass M_w (Schuck et al., 2014).

When the value of apparent weight average molar masses M_w was extrapolated to zero concentration (1.9 ± 0.1) kDa was obtained, comparable to (M_1 = 1879.7 g/mol) of teicoplanin A2-2. This function also gives an approximation of the point weight average molar mass at the hinge point r_{hinge}. At this radial position r_{hinge} the corresponding concentration $c(r)$ is equal to the initial loading concentration c, $M_w(r_{hinge}) = M_w$. The value of (2.7 ± 0.1) kDa was obtained which is greater than the monomer molar mass of teicoplanin A2-2 because of self-association.

Regardless of whether using the hinge point method or the M^* method, the change of the apparent weight average molar masses $M_{w,app}$ plateaus from c = 1 mg/mL (Figure 4-4), giving a value of (35400 ± 1000) g/mol. This corresponds to ~ 19mers in the hinge point method while (33000 ± 1000) g/mol corresponds to ~ 18mers for the M^* method.

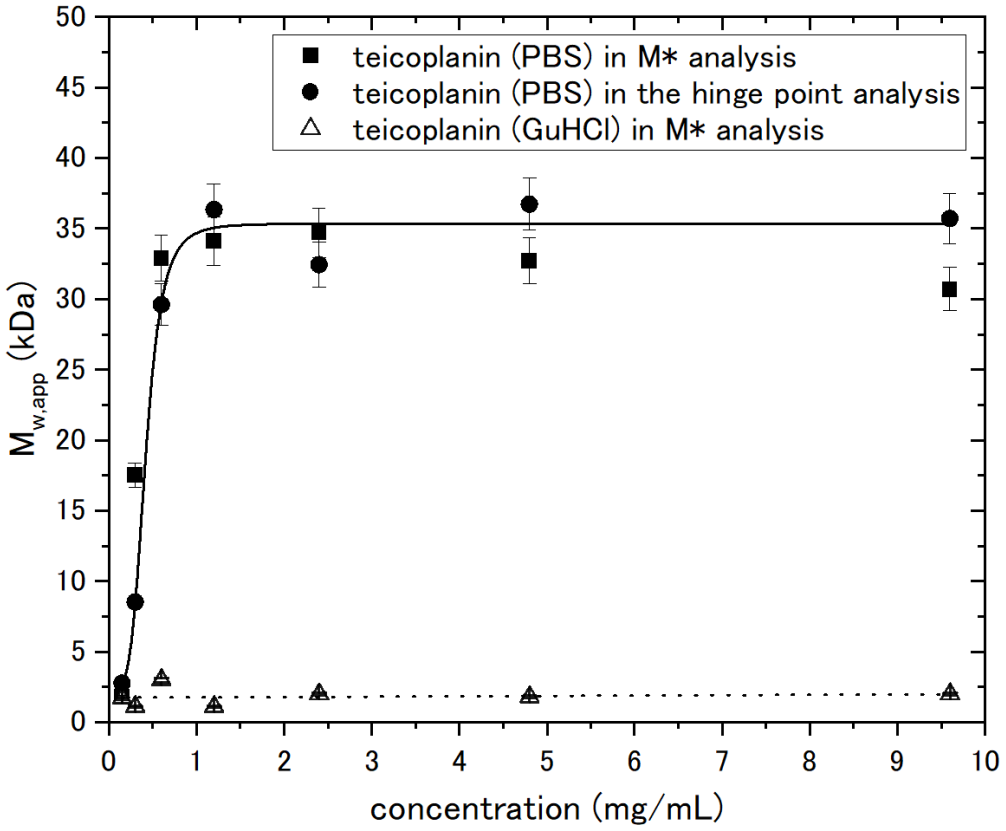

Figure 4-4: Change of weight average molar mass M_w of teicoplanin with loading concentration derived from sedimentation equilibrium analysed by SEDFIT-MSTAR. Solid square symbols are molar masses $M_{w,app}$ obtained from the M^* method. Solid round symbols are molar masses $M_{w,app}$ obtained from the hinge point method. Solid line is a standard French curve fit to the data. Open triangle symbols are molar masses $M_{w,app}$ of teicoplanin dissolved in 6M GuHCl from the M* method.

4.3.3. Dynamic light scattering analysis

The self-associative process was confirmed by DLS measurements. Three concentrations were analysed (0.125, 1.25 and 12.5 mg/mL). At 12.5 mg/mL (which corresponds from Figures 4-3 and 4-4 to the 18-19 mer species) a particle size distribution of $r_z \sim 3.2$nm is observed, and as the concentration is lower the size distribution becomes clearly smaller, indicating dis-assembly towards a smaller molecule (Figure 4-5).

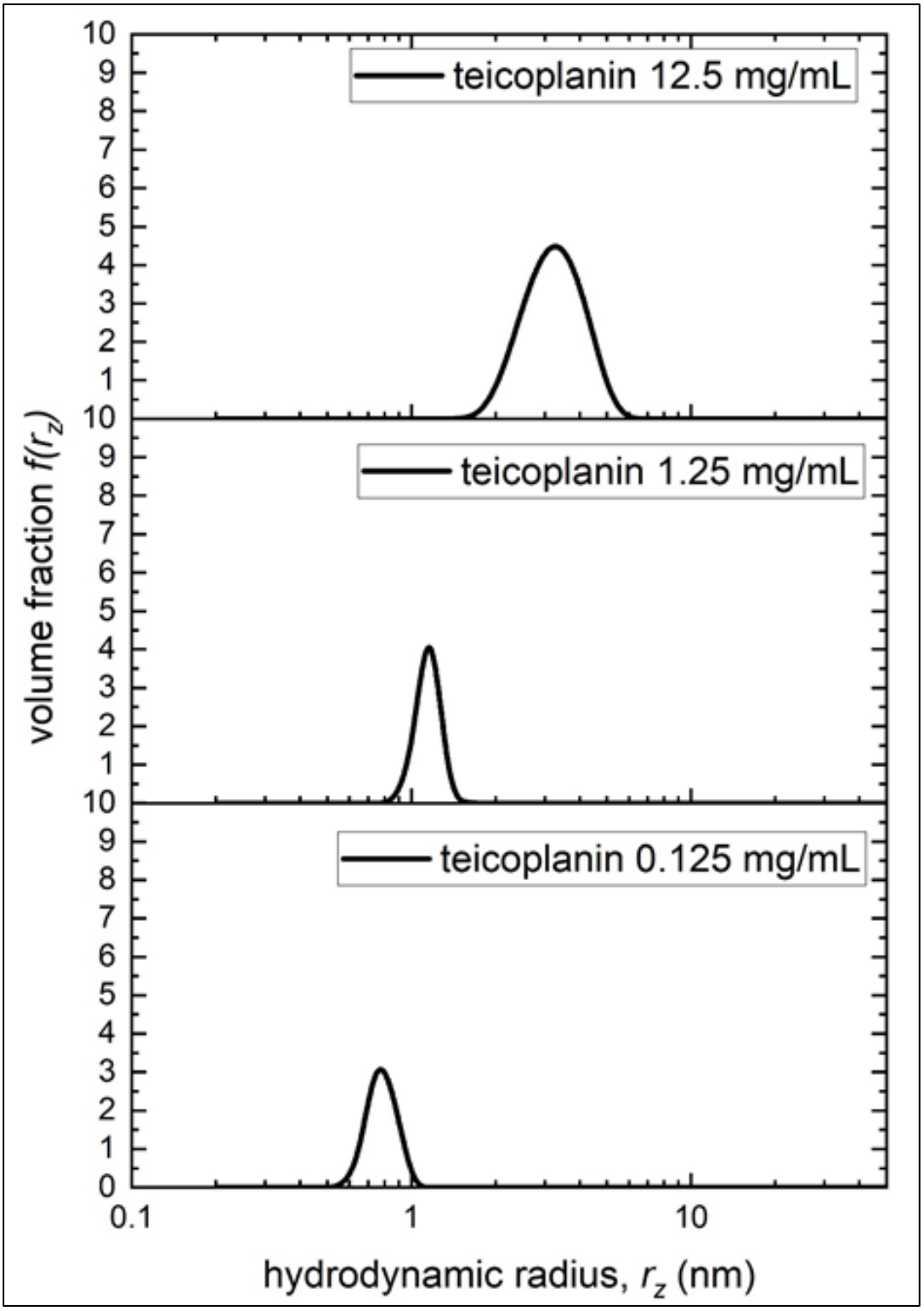

Figure 4-5: Distribution of z-average hydrodynamic radii obtained from dynamic light scattering measurements at 20.0°C for teicoplanin in solution at concentrations 12.5, 1.25 and 0.125 mg/mL.

4.3.4. Conformational analysis of teicoplanin 18-19mer assembly

The sensitive hydrodynamic conformation probe of intrinsic viscosity [η] was used to assess the conformation of the teicoplanin ~ 19mer assembly, reinforced by the sedimentation coefficient, molar mass and (z-averaged) hydrodynamic radius r_z from dynamic light scattering. To avoid possible dissociation effects and to ensure a sufficient flow-time increment, we estimate [η] using the Solomon-Ciuta equation (4-5) at a concentration of 10.2 mg/mL. A value for [η] of (3.2±0.1) mL/g.

In order to interpret this in terms of a molecular shape it is necessary to consider the contribution of the swollen specific volume of the assembly in solution v_s (which will be swollen due to a time-averaged association with the surrounding solvent through dynamic hydrogen bonding and other associative processes) (Harding et al., 1992):

$$[\eta] = \nu.v_s \qquad (4\text{-}6)$$

Equation (4-6) ν is the Einstein-Simha shape factor. v_s is likely to be higher than for proteins due to the relatively large proportion of carbohydrates which tends to have a greater affinity for solvent. In *Table 4-1* values of the shape factor ν, and their corresponding ellipsoid of revolution axial ratios *a/b* were

calculated based on either a prolate or oblate model, using the routine ELLIPS1 (Harding et al. 1997) for 3 cases of $v_s/\bar{v}$, including the (unlikely) case of no swelling $v_s/\bar{v} = 1$. The maximum value for $v_s/v = 2$, which corresponds to the minimum value of $a/b = 1$ (i.e. a sphere, Figure 6), and this seems the most likely scenario.

Table 4-1: Values of the viscosity shape function ν and axial ratio a/b for different values of v_s/v

$v_s/ \bar{\upsilon}$	**v_s (mL/g)**	**ν**	**(*a/b*)** prolate	**(*a/b*)** oblate
1 *	0.64	5.0	4.3	5.4
1.5	0.96	3.3	2.5	2.8
2	1.28 **	2.5	1	1

*no swelling through dynamic hydration effects. v_s: swollen specific volume;

**when v_s = 1.28, a/b is the smallest value (= 1).

$\bar{\upsilon}$: partial specific volume (0.64 mL/g)

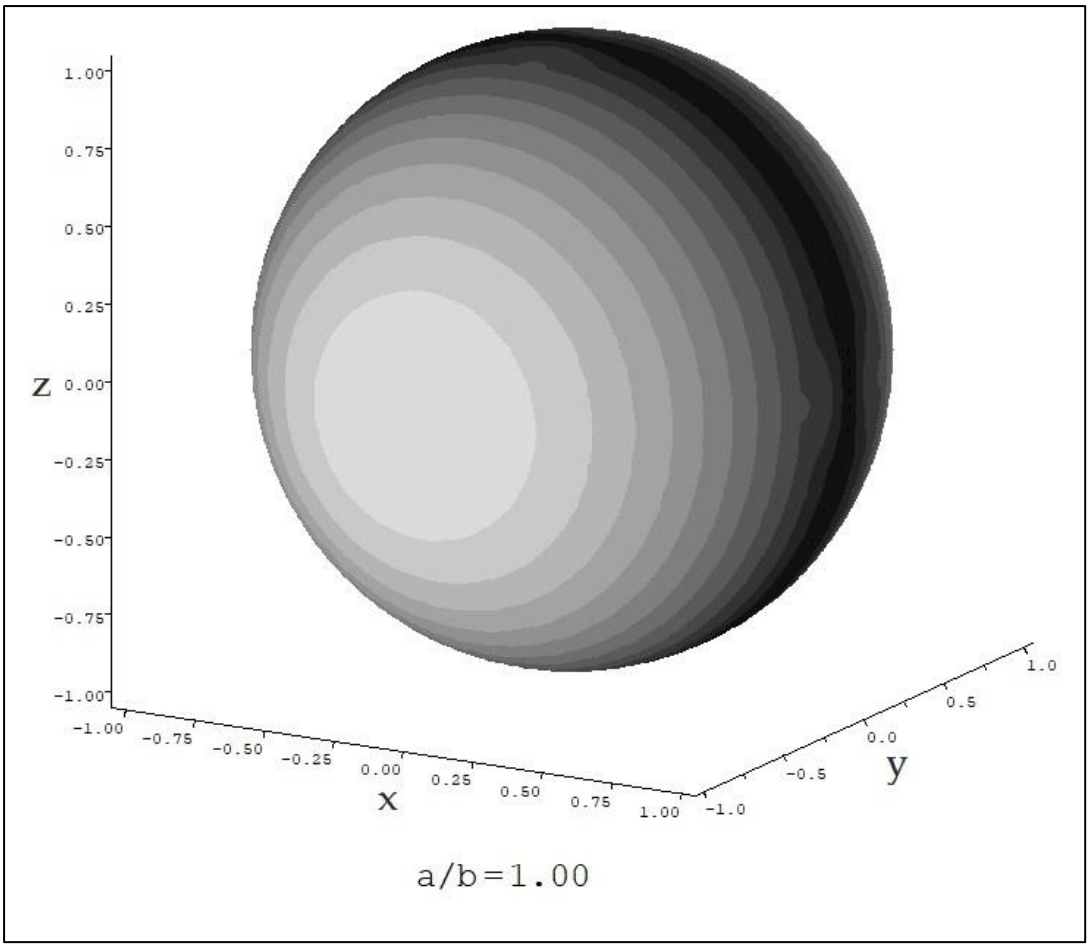

Figure 4-6: ELLIPS1 (Harding et al., 1997) representation of the conformation of teicoplanin showing an axial ratio (*a/b*) = 1: i.e. a sphere.

To check this, we use a global fitting approach known as SingleHYDFIT (Ortega and Torre, 2007) which combines intrinsic viscosity data with sedimentation coefficient and dynamic light scattering (hydrodynamic radius) data together, along with the molecular weight and partial specific volume. It involves the minimization of a global fitting function (Figure 4-7). The E2 protocol (ratio of ellipsoid) was chosen and run twice: once with an assumed molar mass equivalent of an 18-mer (33835Da) and once again with an assumed molar mass of 19-mer (35714Da). Delta (Δ) was plotted against the axial ratio, where values <1 mean oblate and >1 mean prolate (Figure 4-7).

In Figure 4-7, the plot shows the optimisation of axial ratios and provides an indication of the most likely value to occur. SingleHYDFIT yielded an axial ratio of (1.0±0.0) for both molar masses of 18- and 19-mers and suggested that the supramolecular structure was that of a sphere regardless of whether it would be an 18- or 19-mer, confirming the swelling factor of 2 through hydration.

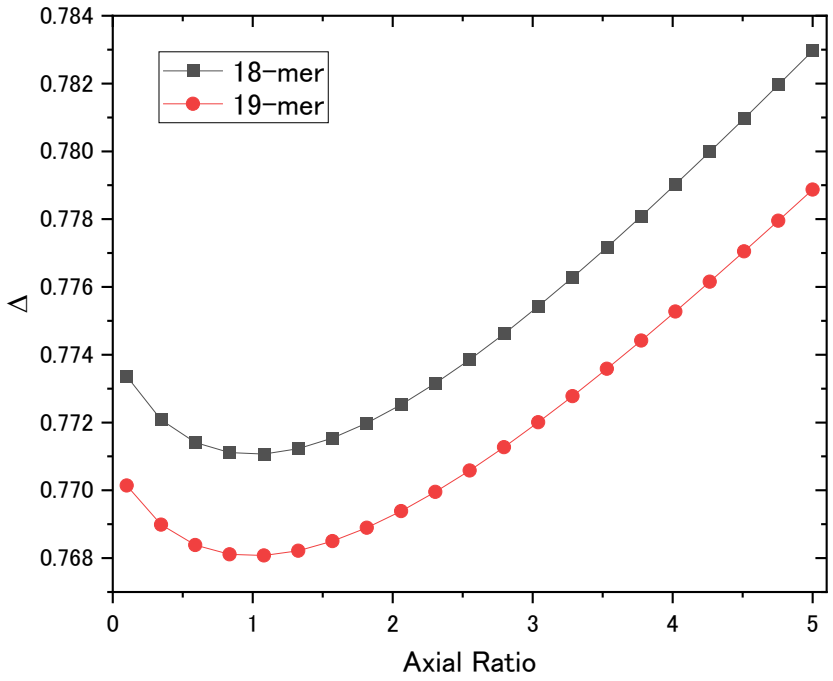

Figure 4-7. Minimisation function performed by SingleHYDFIT on teicoplanin, using the above hydrodynamic parameters and molar mass consistent with either 18-mer (black square) or 19-mer (red circle). Both plots minimise to 1.0 axial ratio.

4.4. Conclusions

In conclusion, based on the matrix-free methods of analytical ultracentrifugation and macromolecular viscometry, teicoplanin appears in phosphate-chloride buffered solution at pH6.8 and I=0.10 mol/L as a spheroidal 18-19mer assembly with a swelling ratio in a solution of ~ 2 which dissociates at concentrations < 0.5 mg/mL. This spherical conformation would be consistent with a micellar-like association with the acyl chains on the inside.

There are some similarities with another “last line of defence” glycopeptide antibiotic vancomycin (Hughes et al., 2017; Phillips-Jones et al., 2017b) On the one hand, vancomycin also shows reversible self-associative behaviour above a similar concentration, but this appears to largely truncate to a monomer-dimer only. On the other hand, teicoplanin with its higher degree of glycosylation (two residues in vancomycin versus three residues in teicoplanin) and the lipid chains attached to one of the GlcNAc residue self-associates to give a much larger 18-19mer structure in solution, a structure which is broken by the hydrogen and ionic bond disruptive agent 6M GuHCl. As to the nature of this large spherical n-mer association, it could either be due to micellization inspired by its fatty acid chain (Armstrong and Nair, 1997; Wan and Blomberg, 1997) or it could be due to the non-specific association of its other hydrophobic regions (Bardsley et al., 2002). Interestingly, *teicoplanin*

aglycon without a lipid chain had previously been found to dimerise weakly in solution (Bardsley et al., 2002). Each or both structural differences may affect the number of building blocks during polymerisation, requiring further research by sedimentation equilibrium experiments using teicoplanin derivatives without either a long acyl chain or sugar units.

In the clinical setting, serum concentrations of teicoplanin are >10 μg/mL or 10 mg/L for intravenous injection (Wilson, 2000), resulting in a unimer form of teicoplanin in blood, pH7.4 and I=0.15 mol/L (Covington and Robinson, 1975). On the other hand, 10 mg/mL of eye drops (Kaye et al., 2009) would lead to the 18-19 mers on the conjunctiva due to the difficulty of diluting quickly, which makes it harder for teicoplanin to permeate beyond the cornea. This means that any concentration >0.5 mg/mL has the potential to reduce topical penetration, while at lower concentrations (<10 mg/L or 10 μg/mL) the dose is below the therapeutic concentration and thus ineffective (Wilson, 2000). Furthermore, if the hydrophobic acyl groups are involved with the binding to the bacterial peptidoglycan, then micellization would appear to reduce the efficacy as an antibiotic at these higher doses.

Additionally, the methods we used can be applied to other members of glycan antibiotics, such as dalbavancin, a lipoglycopeptide with both a fatty acid chain and

two sugar residues. Dalbavancin is a second-generation drug developed based on both vancomycin and teicoplanin (Scheinfeld, 2006). Our combined understanding of the different hydrodynamic behaviour of vancomycin and teicoplanin will help in the development of dalbavancin and other important future-generation antibiotic drugs would result in a better understanding of the structural effects on the aggregational behaviour of some antibiotics. The presence of the third carbohydrate residue and its reinforcement of the interaction potential through hydrophobic interactions of teicoplanin also bears comparison with a new study using molecular dynamics simulations of the semisynthetic disaccharide antibiotic oritavancin which opens the door for a new generation of antibiotics in the fight against bacterial disease (Khamesipour et al., 2015) – and the increasing threat of antimicrobial resistance (Olademehin et al., 2022; Phillips-Jones and Harding, 2018).

In the next chapter, we consider the behaviour of mixtures of teicoplanin with mucins.

4.5. References

Antoniadou, A., Vougioukas, N., Kavouklis, E., Chrissouli, Z., Giamarellou, H., 1998. Penetration of teicoplanin (TEC) into human aqueous humor (AH) after subconjunctival (SCJ) and IV administration. Clinical Infectious Diseases 27, 967.

Armstrong, D.W., Nair, U.B., 1997. Capillary electrophoretic enantioseparations using macrocyclic antibiotics as chiral selectors. Electrophoresis 12–13, 2331–42.

Bardsley, B., Zerella, R., Williams, D.H., 2002. Aggregation, binding, and dimerisation studies of a teicoplanin aglycone analogue (LY154989). J Chem Soc Perkin Transactions 2 0, 598–603.

Barna, J.C.J., Williams, D.H., Stone, D.J.M., Leung, T.W.C., Doddrell, D.M., 1984. Structure elucidation of the teicoplanin antibiotics. J Am Chem Soc 106, 4895–4902.

Bernareggi, A., Borghi, A., Borgonovi, M., Cavenaghi, L., Ferrari, P., Vékey, K., Zanol, M., Zerilli, L.F., 1992. Teicoplanin metabolism in humans. Antimicrob Agents Ch 36, 1744–1749.

Blaskovich, M.A.T., Hansford, K.A., Butler, M.S., Jia, Z., Mark, A.E., Cooper, M.A., 2018. Developments in glycopeptide antibiotics. Acs Infect Dis 4, 715–735.

Butler, M.S., Hansford, K.A., Blaskovich, M.A.T., Halai, R., Cooper, M.A., 2014. Glycopeptide antibiotics: Back to the future. J Antibiotics 67, 631–644.

Ceccarelli, G., Alessandri, F., d'Ettorre, G., Borrazzo, C., Spagnolello, O., Oliva, A., Ruberto, F., Mastroianni, C.M., Pugliese, F., Venditti, M., University, I.C.C.-19 S.G. of S., 2020. Is teicoplanin a complementary treatment option for COVID-19? The question remains. Int J Antimicrob Ag 56, 106029.

Ceccarelli, G., Alessandri, F., Oliva, A., Borrazzo, C., Dell'Isola, S., Ialungo, A.M., Rastrelli, E., Pelli, M., Raponi, G., Turriziani, O., Ruberto, F., Rocco, M., Pugliese, F., Russo, A., d'Ettorre, G., Venditti, M., 2021. The role of teicoplanin in the treatment of SARS-CoV-2 infection: A retrospective study in critically ill COVID-19 patients (Tei-COVID study). J Med Virol 93, 4319–4325.

Covington, A.K., Robinson, R.A., 1975. References standards for the electrometric determination, with ion-selective electrodes, of potassium and calcium in blood serum. Analytica Chimica Acta 78, 219–223.

Creeth, J.M., Harding, S.E., 1982. Some observations on a new type of point average molecular weight. Journal of Biochemical and Biophysical Methods 1, 25–34.

Dam, J., Schuck, P., 2004. Calculating sedimentation coefficient distributions by direct modeling of sedimentation velocity concentration profiles. Methods Enzymol 384, 185–212.

Dinu, V., Lu, Y., Weston, N., Lithgo, R., Coupe, H., Channell, G., Adams, G.G., Gómez, A.T., Sabater, C., Mackie, A., Parmenter, C., Fisk, I., Phillips-Jones, M.K., Harding, S.E., 2020. The antibiotic vancomycin induces complexation and aggregation of gastrointestinal and submaxillary mucins. Sci Rep-uk 10, 960.

Green, A.A., 1933. The preparation of acetate and phosphate buffer solutions of known pH and ionic strength. Journal of the American Chemical Society 6, 2331–2336.

Harding, S.E., 1997. The intrinsic viscosity of biological macromolecules. Progress in measurement, interpretation and application to structure in dilute solution. Prog Biophysics Mol Biology 68, 207–262.

Harding, S.E., 2018. The Svedberg Lecture 2017. From nano to micro: the huge dynamic range of the analytical ultracentrifuge for characterising the sizes, shapes and interactions of molecules and assemblies in Biochemistry and Polymer Science. Eur Biophys J 47, 697–707.

Harding, S.E., Horton, J.C., Cölfen, H., 1997. The ELLIPS suite of macromolecular conformation algorithms. Eur Biophys J 25, 347–359.

Harding, S.E., Johnson, P., 1985a. The concentration-dependence of macromolecular parameters. Biochem J 231, 543–547.

Harding, S.E., Johnson, P., 1985b. Physicochemical studies on turnip-yellow-mosaic virus. Homogeneity, relative molecular masses, hydrodynamic radii and concentration-dependence of parameters in non-dissociating solvents. Biochem J 231, 549–555.

Harding, S.E., Sattelle, D.B., Bloomfield, V.A., 1992. Laser Light Scattering in Biochemistry. Royal Society Chemistry, Cambridge, UK.

Hughes, C.S., Longo, E., Phillips-Jones, M.K., Hussain, R., 2017. Characterisation of the selective binding of antibiotics vancomycin and teicoplanin by the VanS receptor regulating type A vancomycin resistance in the enterococci. Biochimica Et Biophysica Acta Bba - Gen Subj 1861, 1951–1959.

Hunt, A.H., Molloy, R.M., Occolowitz, J.L., Marconi, G.G., Debono, M., 1984. Structure of the major glycopeptide of the teicoplanin complex. J Am Chem Soc 106, 4891–4895.

Kaye, S., 2017. Microbial keratitis and the selection of topical antimicrobials. Bmj Open Ophthalmol 1, e000086.

Kaye, S.B., Neal, T., Nicholson, S., Szkurlat, J., Bamber, S., Baddon, A.C., Anderson, S., Seddon, K., Dwyer, N., Lovering, A.M., Smith, G., 2009. Concentration and bioavailability of ciprofloxacin and teicoplanin in the cornea. Investigative Opthalmology Vis Sci 50, 3176.

Khamesipour, F., Hashemian, S.M., Velayati, A.A., Tabarsi, P., 2015. A Review of Teicoplanin Used in the Prevention and Treatment of Serious Infections Caused by Gram-Positive Bacteria and Compared Its Effects with Some other Antibiotics. Biomedical and Pharmacology Journal 8, 513-521.

Kratky, O., Leopold, H., Stabinger, H., 1973. The determination of the partial specific volume of proteins by the mechanical oscillator technique. Methods in Enzymology 27, 98–110.

Leclercq, R., Derlot, E., Eber, M.V., Duval, J., Courvalin, P., 1989. Transferable vancomycin and teicoplanin resistance in Enterococcus faecium. Antimicrobial Agents and Chemotherapy 33, 10–15.

Nobbmann, U., Connah, M., Fish, B., Varley, P., Gee, C., Mulot, S., Chen, J., Zhou, L., Lu, Y., Sheng, F., Yi, J., Harding, S.E., 2007. Dynamic light scattering as a relative tool for assessing the molecular integrity and stability of monoclonal antibodies. Biotechnology Genetic Eng Rev 24, 117–128.

Olademehin, O.P., Shuford, K.L., Kim, S.J., 2022. Molecular dynamics simulations of the secondary-binding site in disaccharide-modified glycopeptide antibiotics. Sci Rep-uk 12, 7087.

Ortega, A., Torre, J.G. de la, 2007. Equivalent radii and ratios of radii from solution properties as indicators of macromolecular conformation, shape, and flexibility. Biomacromolecules 8, 2464–2475.

Parenti, F., 1986. Structure and mechanism of action of teicoplanin. Journal of Hospital Infection 7, 79–83.

Parenti, F., Beretta, G., Berti, M., Arioli, V., 2006. Teichomycins, new antibioitcs from *Actinoplanes teichomyceticus* NOV. SP. J Antibiotics 31, 276–283.

Pea, F., 2020. Teicoplanin and therapeutic drug monitoring: An update for optimal use in different patient populations. J Infect Chemother 26, 900–907.

Pea, F., Brollo, L., Viale, P., Pavan, F., Furlanut, M., 2003. Teicoplanin therapeutic drug monitoring in critically ill patients: a retrospective study emphasizing the importance of a loading dose. J Antimicrob Chemoth 51, 971–975.

Phillips-Jones, M.K., Channell, G., Kelsall, C.J., Hughes, C.S., Ashcroft, A.E., Patching, S.G., Dinu, V., Gillis, R.B., Adams, G.G., Harding, S.E., 2017a. Hydrodynamics of the VanA-type VanS histidine kinase: an extended solution conformation and first evidence for interactions with vancomycin. Sci Rep-uk 7, 46180.

Phillips-Jones, M.K., Harding, S.E., 2018. Antimicrobial resistance (AMR) nanomachines—mechanisms for fluoroquinolone and glycopeptide recognition, efflux and/or deactivation. Biophysical Rev 10, 347–362.

Phillips-Jones, M.K., Lithgo, R., Dinu, V., Gillis, R.B., Harding, J.E., Adams, G.G., Harding, S.E., 2017b. Full hydrodynamic reversibility of the weak dimerization of vancomycin and elucidation of its interaction with VanS monomers at clinical concentration. Sci Rep-uk 7, 12697.

Provencher, S.W., 1992. Low-bias macroscopic analysis of polydispersity. In: Harding, S.E., Sattelle, D.B., Bloomfield, V.A. (Eds.), Laser Light Scattering in Biochemistry. Royal Society of Chemistry, Cambridge, UK, pp. 92–111.

Reynolds, P.E., 1989. Structure, biochemistry and mechanism of action of glycopeptide antibiotics. European Journal of Clinical Microbiology and Infectious Diseases 8, 943–950.

Schachman, H.K., 1950. Ultracentrifugation Biochemistry. Academic Press: New York, NY, USA; London, UK.

Scheinfeld, N., 2006. Dalbavancin: A review for dermatologists. Dermatology Online Journal 12, 6.

Schuck, P., Gillis, R.B., Besong, T.M.D., Almutairi, F., Adams, G.G., Rowe, A.J., Harding, S.E., 2014. SEDFIT–MSTAR: molecular weight and molecular weight distribution analysis of polymers by sedimentation equilibrium in the ultracentrifuge. Analyst 139, 79–92.

Solomon, O.F., Ciută, I.Z., 1962. Détermination de la viscosité intrinsèque de solutions de polymères par une simple détermination de la viscosité. Journal of Applied Polymer Science 6, 683–686.

Sueke, H., Kaye, S., Wilkinson, M.C., Kennedy, S., Kearns, V., Zheng, Y., Roberts, P., Tuft, S., Neal, T., 2015. Pharmacokinetics of meropenem for use in bacterial keratitis. Investigative Opthalmology Vis Sci 56, 5731.

Taber, L.E., 1980. Study of vacuum oven drying in official method for moisture in eggs and egg products 63, 941–942.

Tesarová, E., Tuzar, Z., Nesmerák, K., Bosáková, Z., Gas, B., 2001. Study on the aggregation of teicoplanin. Talanta 4, 643–53.

Vimberg, V., 2021. Teicoplanin—A new use for an old drug in the COVID-19 era? Pharm 14, 1227.

Vimberg, V., Gazak, R., Szűcs, Z., Borbás, A., Herczegh, P., Cavanagh, J.P., Zieglerova, L., Závora, J., Adámková, V., Novotna, G.B., 2019. Fluorescence assay to predict activity of the glycopeptide antibiotics. J Antibiotics 72, 114–117.

Wan, H., Blomberg, L.G., 1997. Chiral separation of DL-peptides and enantioselective interactions between teicoplanin and D-peptides in capillary electrophoresis. Electrophoresis 18, 943–949.

Wenisch, C., Parschalk, B., Hasenhündl, M., Hirschl, A.M., Graninger, W., 1996. Comparison of vancomycin, teicoplanin, metronidazole, and fusidic acid for the treatment of Clostridium difficile—associated diarrhea. Clin Infect Dis 22, 813–818.

Wilson, A.P.R., 2000. Clinical pharmacokinetics of teicoplanin. Clin Pharmacokinet 39, 167–183.

Yu, F., Pan, T., Huang, F., Ying, R., Liu, J., Fan, H., Zhang, J., Liu, W., Lin, Y., Yuan, Y., Yang, T., Li, R., Zhang, X., Lv, X., Chen, Q., Liang, A., Zou, F., Liu, B., Hu, F., Tang, X., Li, L., Deng, K., He, X., Zhang, H., Zhang, Y., Ma, X., 2022. Glycopeptide antibiotic teicoplanin inhibits cell entry of SARS-CoV-2 by suppressing the proteolytic activity of cathepsin L. Front Microbiol 13, 884034.

Zanol, M., Cometti, A., Borghi, A., Lancini, G.C., 1988. Isolation and structure determination of minor components of teicoplanin. Chromatographia 26, 234–236.

Zeng, D., Debabov, D., Hartsell, T.L., Cano, R.J., Adams, S., Schuyler, J.A., McMillan, R., Pace, J.L., 2016. Approved glycopeptide antibacterial drugs: mechanism of action and resistance. Csh Perspect Med 6, a026989.

Zhou, N., Pan, T., Zhang, Junsong, Li, Q., Zhang, X., Bai, C., Huang, F., Peng, T., Zhang, Jianhua, Liu, C., Tao, L., Zhang, H., 2016. Glycopeptide antibiotics potently inhibit cathepsin L in the late endosome/lysosome and block the entry of Ebola virus, middle east respiratory syndrome coronavirus (MERS-CoV), and severe acute respiratory syndrome coronavirus (SARS-CoV)*. J Biol Chem 291, 9218–9232.

Chapter 5: A comparative hydrodynamic and imaging study on teicoplanin A2 and bovine submaxillary mucin as a model ocular mucin.

5.1. Introduction

Teicoplanin is the 'last resort of defence' drug to treat severe infections of Gram-positive bacteria including methicillin-resistant *Staphylococcus aureus* (MRSA) and enterococci (Binda et al., 2014). Its chemical structure was first determined in 1984 (Barna et al., 1984; Malabarbra et al., 1984). Figure 1-4 shows that the core aglycone structure of teicoplanin is a linear heptapeptide, combined with three monosaccharide residues: α-D-mannose, *N*-acetyl-β-D-glucosamine, and one of five subtypes of *N*-acyl-β-D-glucosamines depending on teicoplanin A2-1 through A2-5 (Wilson, 2000). The mixture of five subtypes of teicoplanin is produced by *Actinoplanes teicomyceticus* (Borghi et al., 1991) and is generally administered as a single product in clinical practice (van Groesen et al., 2022). The prominent difference with vancomycin is the presence of a long fatty acid chain attached to the (*N*-acyl-) β-D-glucosamine residue, compared with vancomycin bearing a non-acylated disaccharide residue as shown in Figure 1-4 (Nicolaou et al., 1999). Both glycan antibiotics show antibacterial activity in the same manner. Namely, they bind to the membranous protein (Lipid II) and prevent this peptidoglycan precursor from insertion into the bacterial cell wall (Blaskovich et al., 2018). However, to

increase their affinity for the peptidyl D-Ala-D-Ala motif of Lipid II, vancomycin cooperatively dimerises in a back-to-back manner, while teicoplanin does not show dimerization and uses its hydrophobic tail to anchor itself at the bacterial membrane (Beauregard et al., 1995). Figure 5-1 shows the suggested binding mechanisms of vancomycin, compared with teicoplanin.

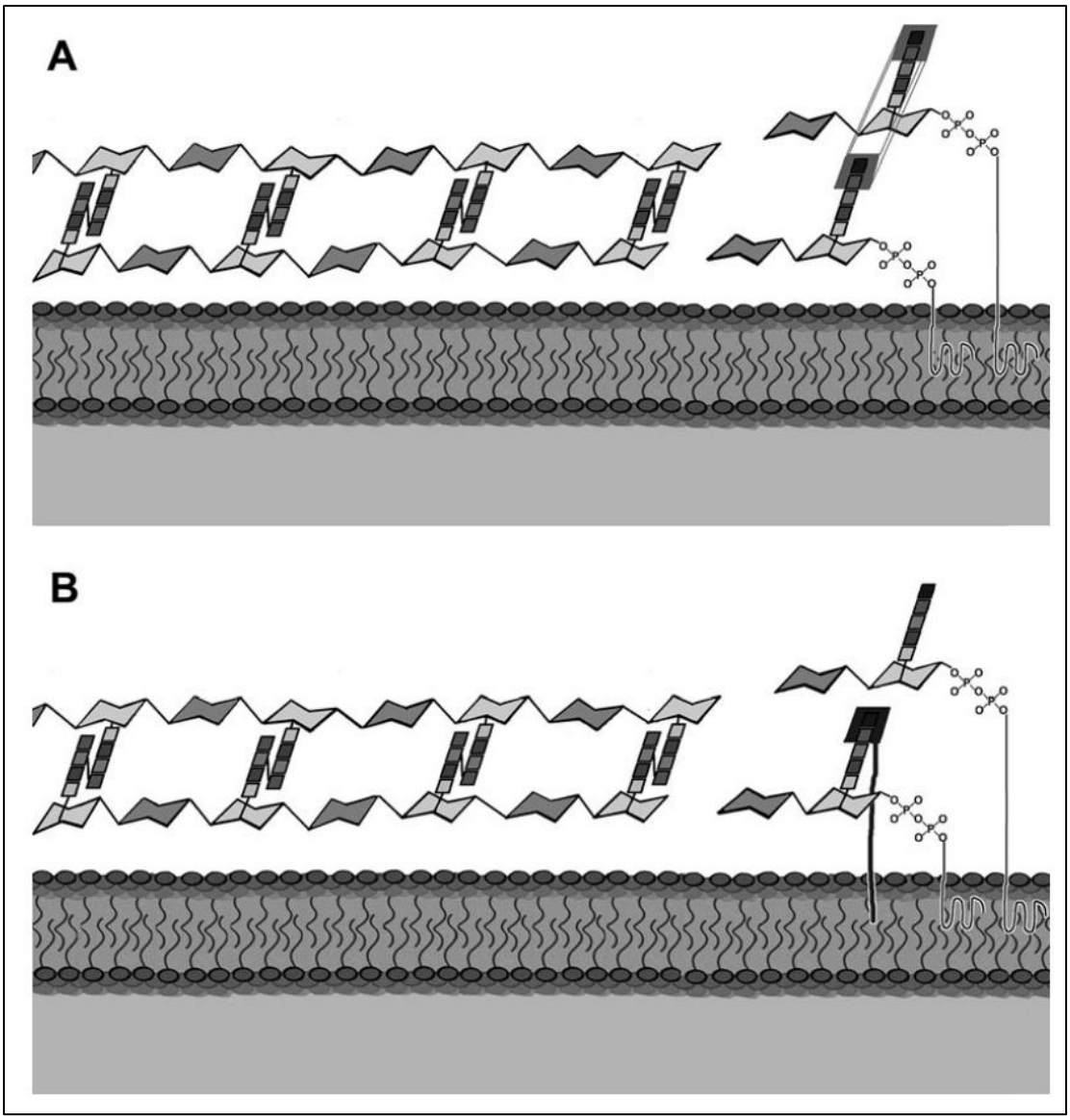

Figure 5-1: The suggested binding mechanisms of vancomycin (A) and teicoplanin (B) cited from Treviño et al. (2014). In this diagram, vancomycin molecules (transparent black squares) conduct back-to-back dimerization (A), while a teicoplanin monomer (black square) uses its long acyl chain attached to a phospholipid bilayer cell membrane (B) so that teicoplanin can be located next to a peptidoglycan precursor.

Glycan antibiotics are used in ophthalmology. Bacterial infections of the eyes range from relatively easily treated ones, such as conjunctivitis and blepharitis, to more serious ones including keratitis, and notoriously endophthalmitis (Forrester et al., 2016). The significance of MRSA strains for ocular infections is on the increase. For example, Harford et al. (2022) reported that in the U.K. the percentage of MRSA-positive cases from eye swabs was 2% on average in 2013-2019. Those cases are rising in the U.S. (Asbell et al., 2008) and South India (Lalitha et al., 2017). Therefore, the eradication of MRSA strains on ocular surfaces is routinely performed for proven positive patients in pre-operative screening. Those patients receive chloramphenicol drops before eye surgery and intracameral vancomycin intraoperatively (Harford et al., 2022). Vancomycin eye drops (50 mg/mL) are also used for the treatment of MRSA-positive keratitis (Tabbara, 2014). On the other hand, teicoplanin drops are reported to have no or little corneal penetration in rabbits (Carney et al., 1988) and in patients at 10 mg/mL (Kaye et al., 2009). For orbital cellulitis, intravenous teicoplanin can be applied to patients with penicillin allergy, along with oral ciprofloxacin and metronidazole (NHS, 2022).

However, the emergence of further resistant species against these glycan antibiotics becomes a burning issue for antibiotic selection for ocular infections. Vancomycin- and teicoplanin-resistant enterococcal species were reported in the U.S. (Sahm et

al., 1989) and Europe (Leclercq et al., 1989; Uttley et al., 1988) before the 1990s. Resistance gene clusters are transferred between bacterial cells through plasmids (van Groesen et al., 2022). Glycan antibiotics attach to the D-Ala-D-Ala motif of Lipid II through five hydrogen bonds, though these resistance operons modify that targeted motif into D-Ala-D-Lac for *vanA*, *vanB*, *vanD*, *vanF*, and *vanM*, and D-Ala-D-Ser for *vanC*, *vanE*, *vanG*, *vanL*, and *vanN* (Ahmed and Baptiste, 2018). This modification reduces the number of hydrogen bonds and the Lipid II affinity. Overuse and misuse of antibiotics are considered major causes of antimicrobial resistance (Byrne et al., 2019). This is due to excessive exposure of bacterial populations to antibiotics. These human activities lead to selection pressure, increasing resistance genes in microbes (Peterson and Kaur, 2018).

Ocular mucins may also contribute to antimicrobial resistance (AMR). There is no doubt that the mucin layer of tear films protects against bacterial adherence (Forrester et al., 2016). For example, it is reported that ocular mucus, as well as bovine submaxillary mucin (BSM), inhibited the adherence of *Pseudomonas aeruginosa* on the rabbit corneal epithelium (Fleiszig et al., 1994). However, it is also reported that antibiotics bind to mucins of intestinal (Niibuchi et al., 1986) and respiratory (Ramphal et al., 1988) tracts, showing a substantial reduction of their microbial activity (Huang et al., 2015). Samad et al. (2019) suggested that mucin

glycoproteins (MUC5AC, MUC2, and MUC5B) interacted with two antibiotics against *P. aeruginosa* (polymyxin and fluoroquinolone), increasing its growth after exposure to antibiotics. Dinu et al. (2020) reported that gastrointestinal mucins and BSM induced aggregation with vancomycin. Therefore, mucin components of tear films might also exacerbate AMR through their interactions with antibiotics.

In this study, commercially available BSM was used as model ocular mucin to explore interactions with teicoplanin. BSM has been widely used as a tear film model for the evaluation of contact lenses (Rabiah et al., 2020, 2019; Sterner et al., 2017) and for the interactions with proteins as a tear fluid mucin model (Setälä et al., 2010). Setälä et al. (2010) especially mentioned the validity of BSM as an ocular mucin model for *in vitro* interaction experiments, pointing out that both ocular mucins and BSM interacted with phospholipid transfer protein. In contrast, it should be noted that BSM may not necessarily behave like ocular mucins, such as MUC5AC, the most abundant and gel-forming mucin since commercially available BSM is not a gel-forming mucin (Zhong, 2016). Furthermore, Rivera and Tessarollo (2008) warned against dependence on a single animal model to extrapolate its findings to human pathophysiology, such as human carcinogenesis (Mak et al., 2014) and inflammatory diseases (Seok et al., 2013; Shay et al., 2013). However, it is worth conducting preliminary *in vitro* interaction experiments with

BSM as a substitute for whole mucin components of tear films just before sufficiently collecting human ocular mucins.

This interaction study is based on a relatively novel combination of hydrodynamic and microscopic methods. Sedimentation velocity in the analytical ultracentrifuge (SV-AUC) is the golden standard method used to evaluate the molecular integrity of various systems, such as glycoproteins. SV-AUC gives sedimentation coefficient distributions and sedimentation coefficients relating to molecular sizes (Zaccai et al., 2017). Dynamic light scattering (DLS) also provides macromolecular sizes complementary to SV-AUC (Harding et al., 2015). These hydrodynamic results can be confirmed by environmental scanning electron microscopy (ESEM) and Low-vacuum SEM visualising macromolecular aggregates from samples. The combination of these methods was first used by Dinu et al. (2020) to assess the aggregation of vancomycin with mucins, such as BSM. Many studies are designed to focus on how glycan antibiotics bind to Lipid II (Phillips-Jones et al., 2017) and the genomic profiles of resistant microbes (Samad et al., 2019), though the study on environmental factors including mucin-antibiotic binding, is important as well. Additionally, the hydrodynamic and microscopic methods will evaluate teicoplanin regarding the degree of interactions with BSM as an outer mucus model.

5.2. Materials and methods

5.2.1. Teicoplanin

Teicoplanin A2 powder (the mixture of teicoplanin A2-1 with monomer molar mass M_1 = 1877.6 g/mol, teicoplanin A2-2 and A2-3 with M_1 = 1879.7 g/mol, and teicoplanin A2-4 and A2-5 with M_1 = 1893.7 g/mol) was obtained from Sigma-Aldrich, the United Kingdom. A refractive increment *dn/dc* of 0.188 mL/g was used (Tesarová et al., 2001). The stock solution concentration was then measured with a differential refractometer (Atago DD7, Tokyo, Japan). The final concentrations (0.125 mg/mL, 1.25 mg/mL, and 12.5 mg/mL) of teicoplanin A2 were prepared in a phosphate-chloride buffered saline solution (PBS or "Paley buffer") at pH~6.8, ionic strength of I = 0.1 mol/L (Green, 1933).

5.2.2. Bovine submaxillary mucin, BSM

BSM (Sigma-Aldrich, U.K., catalogue no. M3895, type I-S) was purchased and then dissolved in the PBS buffer described previously. A refractive increment *dn/dc* of 0.181 mL/g for BSM (Dinu et al., 2019) was used. The stock solution concentration was then determined with the differential refractometer (Atago DD7, Tokyo, Japan).

5.2.3. Sedimentation velocity in the analytical ultracentrifuge (SV-AUC)

SV-AUC experiments were conducted at 20.0°C with the Optimal XL-I analytical ultracentrifuge (Beckman, Palo Alto, U.S.A.) coupled to Rayleigh interference optics. Reference solvent (PBS) of 420 µL and sample solutions (teicoplanin A2, BSM, and mixtures of teicoplanin A2 and BSM) of 400 µL were injected into the channels of 12 mm double-sectored cells with sapphire windows and rotated at 47500 rpm for a run time of ~24 h until the specimen completely sedimented. The data was then obtained by the interference system to monitor changes in the concentration of samples in fringe units over radial displacement and the obtained data were analysed in the SEDFIT algorithm (Dam and Schuck, 2004).

This algorithm produces by the least squares ls-g*(*s*) method the sedimentation coefficient distribution, *g(s)* versus $s_{T,b}$, where *s* is the sedimentation coefficient at temperature *T* and in buffer *b*. The value of $s_{T,b}$, given by the unit of Svedberg (S) = 10^{-13} seconds, was normalised to standard conditions with viscosity and density of water solvent at 20°C, $s_{20,w}$, using the equation (Schachman, 1950):

$$s_{20,w} = \frac{1 - \bar{v} \cdot \rho_{20,w}}{1 - \bar{v} \cdot \rho_{T,b}} \cdot \frac{\eta_{T,b}}{\eta_{20,w}} \cdot s_{T,b} \qquad (5\text{-}1)$$

where $\rho_{T,b}$ and $\eta_{T,b}$ are the density and the viscosity of buffer *b* at temperature *T*, respectively. The following sets of samples were used: 1 mg/mL BSM control due to the total concentration of ocular mucins (Ablamowicz and Nichols, 2018),

teicoplanin A2 control (0.125 mg/mL, 1.25 mg/mL, and 12.5 mg/mL), and the mixtures (1 mg/mL BSM + 0.125 mg/mL teicoplanin A2, 1 mg/mL BSM + 1.25 mg/mL teicoplanin A2, and 1 mg/mL BSM + 12.5 mg/mL teicoplanin A2).

5.2.4. Dynamic light scattering (DLS)

DLS experiments were performed on the fixed scattering angle Zetasizer Nano-S system (Malvern Instruments Ltd., Malvern, U.K.) coupled to a 4mV He-Ne laser at 632.8 nm (Harding et al., 1992; Nobbmann et al., 2007). Sample measurements were made in a quartz cuvette at 20.0°C using a scattering angle of 173°. The data were obtained and analysed with the "Zetasizer Software (Version 7.1)" (Malvern Instruments Ltd, Malvern, U.K.). The CONTIN programme (Provencher, 1992) gives volume distributions of translational diffusion coefficients, D_z. The z-average hydrodynamic radii, r_z, (nm) were then determined from D_z using the Stokes-Einstein equation (Harding et al., 1992):

$$r_z = \frac{k_B T}{6\pi\eta D_z} \tag{5-2}$$

where k_B is the Boltzmann constant given by the units of J/K.

In these experiments, the non-ideality effects were assumed to be insignificant because the sample solutions are sufficiently dilute and sample sizes are small. Therefore, an extrapolation to zero concentration is unnecessary. Additionally, for

translational diffusion, non-ideality is related to the two major factors in the hydrodynamic and thermodynamic terms, though these factors can compensate for and thus cancel each other (Harding and Johnson, 1985a, 1985b). Moreover, the teicoplanin samples – whether monomeric or multimeric forms in solution – were assumed not to be asymmetric. Therefore, the measured values of D_z were independent of the angle and extrapolation to zero angles was unnecessary.

5.2.5. Environmental Scanning Electron Microscopy (ESEM) analysis

Microscopic experiments of teicoplanin and BSM samples were performed using a Thermofisher Scientific (Waltham, U.S.A) FEI Quanta 650 ESEM. The samples were cooled to 2.0°C using a Peltier cooling stage. The relative humidity in the chamber was then maintained at 80-90% by the pressure of water vapour. The accelerating voltage of 15 kV was applied for all samples.

5.3. Results and discussion

5.3.1. Analytical Ultracentrifugation (AUC) of teicoplanin-BSM solutions

Figure 5-2 shows the sedimentation coefficient distributions for the interactions of teicoplanin with BSM 1 mg/mL as an ocular mucin model. The values of $s_{20,w}$ of BSM control of 1mg/mL, and teicoplanin control of 0.125 mg/mL

(Figure 5-2a), 1.25 mg/mL (Figure 5-2b), and 12.5 mg/mL (Figure 5-2c) are 4.58S (BSM), 0.95S (0.125 mg/mL teicoplanin), 4.52S (1.25 mg/mL teicoplanin), and 3.83S (12.5 mg/mL teicoplanin). For the mixture of BSM and 0.125 mg/mL teicoplanin (Figure 5-2a), there was no clear interaction between each component ($s_{20,w}$ of the mixture was 5.42S). On one hand, for Figure 5-2b, there was a little shift for BSM and 1.25 mg/mL teicoplanin ($s_{20,w}$ of the mixture was 5.89S), and there were some aggregates in ~25S and ~35S. For Figure 5-2c, there was a clear shift for BSM and 12.5 mg/mL teicoplanin ($s_{20,w}$of the mixture was 6.29S). Furthermore, there were some aggregates in ~30S and ~40S. For both Figure 5-2b and Figure 5-2c, there was a partial loss of teicoplanin peak at ~0.9S (teicoplanin unimer) in the mixture of BSM and 1.25 mg/mL teicoplanin (Figure 5-2b).

Generally, the larger the value of $s_{20,w}$ is, the bigger the molecule is (Zaccai et al., 2017). For the mixtures of BSM with 1.25 mg/mL (Figure 5-2a) and 12.5 mg/mL (Figure 5-2b) teicoplanin samples, the values of $s_{20,w}$ changed from 4.52S for 1.25 mg/mL teicoplanin control into 5.89S for the mixture and from 3.83S for 12.5 mg/mL teicoplanin control into 6.29S for the mixture (Also see Figure 5-4). However, in SV-AUC, the shape of molecules also affects values of $s_{20,w}$. Thus, DLS experiments needed to be performed to give further evidence.

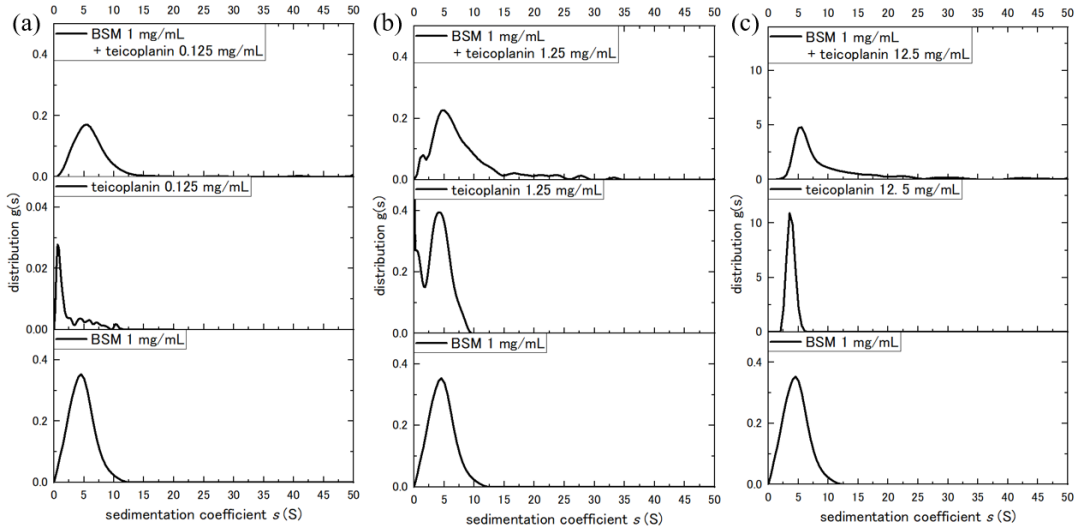

Figure 5-2: The sedimentation coefficient distributions of the interactions of BSM with 0.125 mg/mL teicoplanin (Figure 5-2a), 1.25 mg/mL teicoplanin (Figure 5-2b), and 12.5 mg/mL teicoplanin (Figure 5-2c).

5.3.2. Dynamic light scattering (DLS)

Further evidence of BSM-teicoplanin aggregation is shown in Figure 5-3 providing the distributions of the apparent translational diffusion coefficient changed in the apparent radii through the Stokes-Einstein equation, Equation (5-2). There was a partial loss of mucin components (at 30 nm and 3000 nm) in the mixture of BSM and 1.25 mg/mL teicoplanin, shown by the two yellow downward arrows in Figure 5-4. There was also a complete loss of these two components in the mixture of BSM and 12.5 mg/mL teicoplanin, and the new aggregates emerge at 300 nm shown by the single yellow upward arrow. These results from DLS experiments appear to confirm SV-AUC results in terms of the interactions of the mixtures.

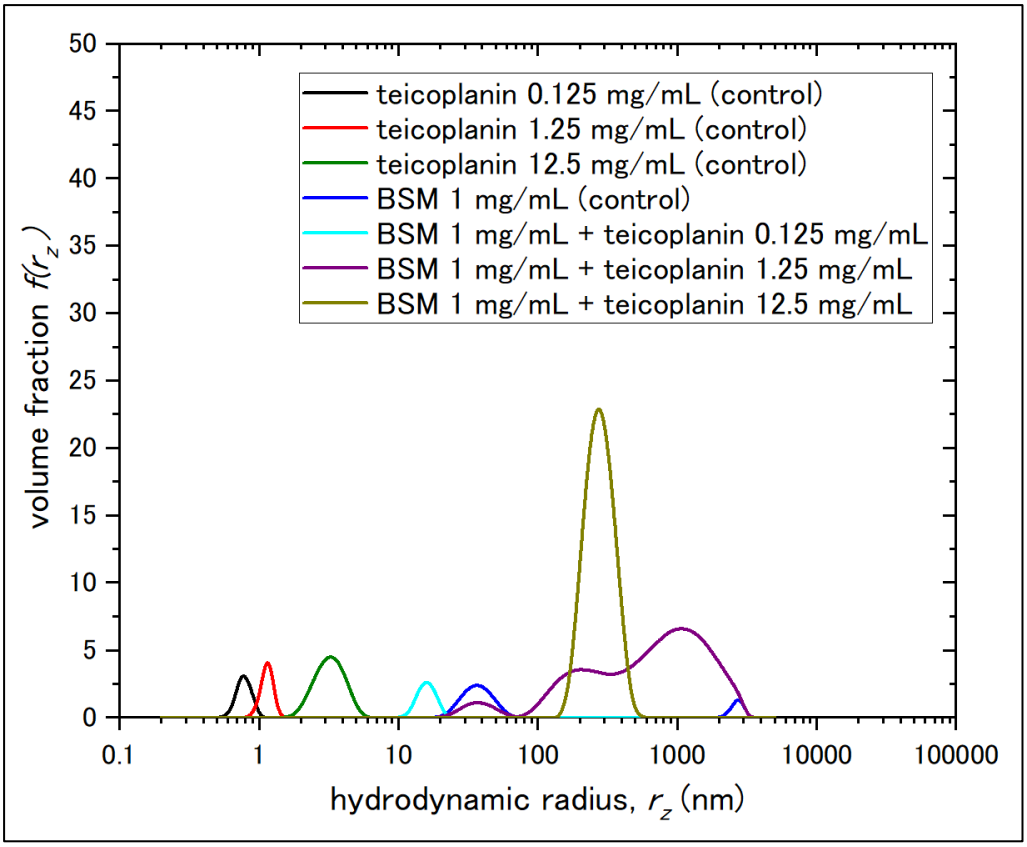

Figure 5-3: The distributions of z-average apparent hydrodynamic radii, r_z from DLS measurements on BSM with teicoplanin 0.125 mg/mL, 1.25 mg/mL, and 12.5 mg/mL. The different colours denote each sample: teicoplanin controls (0.125 mg/mL for the black line, 1.25 mg/mL for the red line, and 12.5 mg/mL for the green line), BSM control (blue line), the mixture of BSM and 0.125 mg/mL (sky blue line), the mixture of BSM and 1.25 mg/mL (purple line), and the mixture of BSM and 12.5 mg/mL (dark yellow line).

5.3.3. Imaging of teicoplanin-BSM aggregates

Figure 5-4 shows the two images of teicoplanin-BSM aggregates in the mixtures of BSM with 1.25 mg/mL (Figure 5-4b) and 12.5 mg/mL (Figure 5-4c and 5-4d), together with BSM control (Figure 5-4a). The technique of environmental scanning electron microscopy (ESEM) was used with the samples under the same conditions as previous AUC and DLS measurements (PBS at pH ~6.8 and ionic strength of I = 0.1 M) before drying. These samples were then observed under controlled dehydration and operating pressure of ~5 Torr in the ESEM chamber. The ESEM analysis showed very large aggregates in both mixtures, reinforcing the hydrodynamic results of the interactions of teicoplanin with BSM. To observe aggregation at the nanoscale, atomic force microscopy was utilised to visualise all samples.

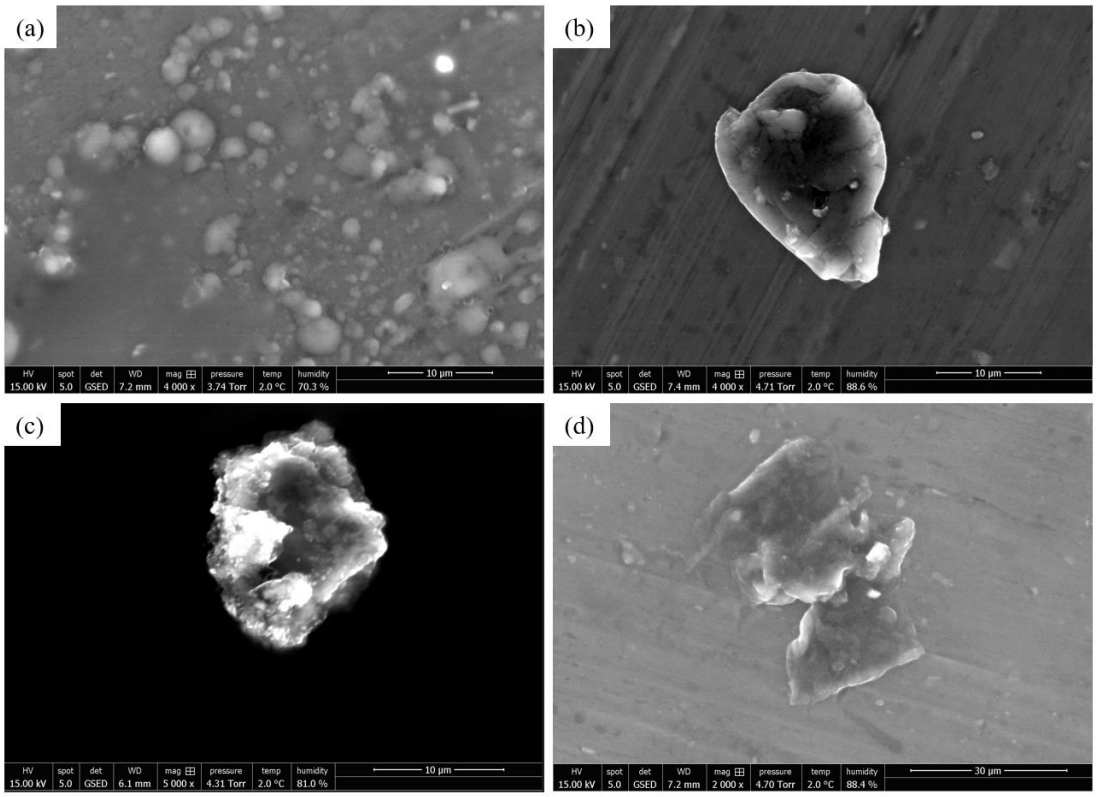

Figure 5-4: Showing example ESEM images for 1 mg/mL BSM control (a) and the mixture of BSM with 1.25 mg/mL teicoplanin (b) and 12.5 mg/mL (c, d).

5.4. Conclusions

In conclusion, teicoplanin A2 has partial interactions with BSM at > 1.25 mg/mL, based on hydrodynamic and microscopic assessments. Additionally, there are some teicoplanin-BSM aggregates at > 1.25 mg/mL, preventing teicoplanin unimer from having its antibiotic activity in the mucin-rich environment. The partial interactions and aggregation of teicoplanin with BSM have three consequences, as follows – (1) since teicoplanin A2 uses its hydrophobic tail to allocate itself near the Lipid II precursor as a monomer (Beauregard et al., 1995), the multimeric formation with mucins inevitably reduce its antimicrobial activity. (2) In addition, since aggregates are more likely to be removed and transferred into nasolacrimal ducts by blinking (Gipson and Argüeso, 2003), total concentrations of teicoplanin decrease on ocular surfaces. (3) Most importantly, there is a good possibility that aggregations of teicoplanin with mucins result in longer exposure to antibiotics, leading to more selection pressure towards antimicrobial resistance between bacterial populations. Therefore, teicoplanin eye drops may be preferred to be at least < 1.25 mg/mL or more preferably, around 0.125 mg/mL, where there were no interactions and aggregates with BSM.

However, the validity of BSM as the ocular mucin model – although a good first step – remains questionable for the study of antibiotics in ophthalmology. Many

studies have used commercially available BSM as the ocular mucin model (Rabiah et al., 2020, 2019; Setälä et al., 2010; Sterner et al., 2017), though there are some differences with ocular mucins, especially gel-forming mucins including MUC5AC. For instance, commercially available BSM is not a gel-forming mucin as MUC5AC (Zhong, 2016). On the other hand, it is also reported that the mucus layer on the ocular surface is not the same as the truly gel-forming layer presented in respiratory and intestinal tracts, due to its relatively thin (1μm) mucus layer (Hodges and Dartt, 2013). Whatever the ocular mucus layer would be, it should be noted that differences with human ocular mucins also need to be explored in terms of the interaction study with teicoplanin. This current study, nonetheless, provides a firm groundwork for further comparative studies using BSM and, when evaluated in sufficiently quantity, ocular mucins.

5.5. References

Ablamowicz, A. F. and Nichols, J. J., 2018. Concentrations of MUC16 and MUC5AC using three tear collection methods. Molecular Vision 23, 529-537.

Ahmed, M.O., Baptiste, K.E., 2018. Vancomycin-resistant Enterococci: A review of antimicrobial resistance mechanisms and perspectives of human and nimal Health. Microbial Drug Resistance 24, 590–606.

Asbell, P.A., Sahm, D.F., Shaw, M., Draghi, D.C., Brown, N.P., 2008. Increasing prevalence of methicillin resistance in serious ocular infections caused by Staphylococcus aureus in the United States: 2000 to 2005. J Cataract Refract Surg 34, 814–818.

Barna, J.C.J., Williams, D.H., Stone, D.J.M., Leung, T.W.C., Doddrell, D.M., 1984. Structure elucidation of the teicoplanin antibiotics. J Am Chem Soc 106, 4895–4902.

Beauregard, D.A., Williams, D.H., Gwynn, M.N., Knowles, D.J., 1995. Dimerization and membrane anchors in extracellular targeting of vancomycin group antibiotics. Antimicrob Agents Ch 39, 781–785.

Binda, E., Marinelli, F., Marcone, G.L., 2014. Old and new glycopeptide antibiotics: Action and resistance. Antibiotics 3, 572–594.

Blaskovich, M.A.T., Hansford, K.A., Butler, M.S., Jia, Z., Mark, A.E., Cooper, M.A., 2018. Developments in glycopeptide antibiotics. Acs Infect Dis 4, 715–735.

Borghi, A., Edwards, D., Zerilli, L.F., Lancini, G.C., 1991. Factors affecting the normal and branched-chain acyl moieties of teicoplanin components produced by Actinoplanes teichomyceticus. Microbiology 137, 587–592.

Byrne, M.K., Miellet, S., McGlinn, A., Fish, J., Meedya, S., Reynolds, N., Oijen, A.M. van, 2019. The drivers of antibiotic use and misuse: the

development and investigation of a theory driven community measure. BMC Public Health 1425.

Carney, M., Kao, G., Peyman, G.A., Fiscella, R., Staneck, J., 1988. The intraocular penetration and retinal toxicity of teicoplanin. Ophthalmic Surg 19, 119–23.

Dam, J., Schuck, P., 2004. Calculating sedimentation coefficient distributions by direct modeling of sedimentation velocity concentration profiles. Methods Enzymol 384, 185–212.

Dinu, V., Gillis, R.B., MacCalman, T., Lim, M., Adams, G.G., Harding, S.E., Fisk, I.D., 2019. Submaxillary mucin: its effect on aroma release from acidic drinks and new insight into the effect of aroma compounds on its macromolecular integrity. Food Biophys 14, 278–286.

Dinu, V., Lu, Y., Weston, N., Lithgo, R., Coupe, H., Channell, G., Adams, G.G., Gómez, A.T., Sabater, C., Mackie, A., Parmenter, C., Fisk, I., Phillips-Jones, M.K., Harding, S.E., 2020. The antibiotic vancomycin induces complexation and aggregation of gastrointestinal and submaxillary mucins. Sci Rep-uk 10, 960.

Fleiszig, S.M., Zaidi, T.S., Ramphal, R., Pier, G.B., 1994. Modulation of Pseudomonas aeruginosa adherence to the corneal surface by mucus. Infection and Immunity 62, 1799–804.

Forrester, J.V., Dick, A.D., McMenamin, P.G., Roberts, F., Pearlman, E., 2016. The Eye Basic Sciences in Practice, Fourth. ed. Elsevier, London.

Gipson, I.K., Argüeso, P., 2003. Role of mucins in the function of the corneal and conjunctival epithelia. International Review of Cytology 231, 1–49.

Green, A.A., 1933. The preparation of acetate and phosphate buffer solutions of known pH and ionic strength. Journal of the American Chemical Society 6, 2331–2336.

Groesen, E. van, Innocenti, P., Martin, N.I., 2022. Recent Advances in the Development of Semisynthetic Glycopeptide Antibiotics: 2014–2022. Acs Infect Dis 8, 1381–1407.

Harding, S.E., Abdelhameed, A.S., Gillis, R.B., Morris, G.A., Adams, G.G., 2015. Chapter 13 Characterization of capsular polysaccharides and their glycoconjugates by hydrodynamic methods. In: Lepenies, B. (Ed.), carbohydrate-based vaccines: methods and protocols, methods in molecular Biology 1331. Springer Science+Business Media, New York, pp. 211–227.

Harding, S.E., Johnson, P., 1985a. Physicochemical studies on turnip-yellow-mosaic virus. Homogeneity, relative molecular masses, hydrodynamic radii and concentration-dependence of parameters in non-dissociating solvents. Biochem J 231, 549–555.

Harding, S.E., Johnson, P., 1985b. The concentration-dependence of macromolecular parameters. Biochem J 231, 543–547.

Harding, S.E., Sattelle, D.B., Bloomfield, V.A., 1992. Laser Light Scattering in Biochemistry. Royal Society Chemistry, Cambridge, UK.

Harford, D.A., Greenan, E., Knowles, S.J., Fitzgerald, S., Murphy, C.C., 2022. The burden of methicillin-resistant Staphylococcus aureus in the delivery of eye care. Eye 36, 1368–1372.

Hodges, R.R., Dartt, D.A., 2013. Tear film mucins: Front line defenders of the ocular surface; comparison with airway and gastrointestinal tract mucins. Exp Eye Res 117, 62–78.

Huang, J.X., Blaskovich, M.A.T., Pelingon, R., Ramu, S., Kavanagh, A., Elliott, A.G., Butler, M.S., Montgomery, A.B., Cooper, M.A., 2015. Mucin binding reduces colistin antimicrobial activity. Antimicrobial Agents and Chemotherapy 59, 5925–31.

Kaye, S.B., Neal, T., Nicholson, S., Szkurlat, J., Bamber, S., Baddon, A.C., Anderson, S., Seddon, K., Dwyer, N., Lovering, A.M., Smith, G., 2009. Concentration and bioavailability of ciprofloxacin and teicoplanin in the cornea. Investigative Opthalmology Vis Sci 50, 3176.

Lalitha, P., Manoharan, G., Karpagam, R., Prajna, N.V., Srinivasan, M., Mascarenhas, J., Das, M., Porco, T.C., Lietman, T.M., Cevallos, V.,

Keenan, J.D., 2017. Trends in antibiotic resistance in bacterial keratitis isolates from South India. Brit J Ophthalmol 101, 108.

Leclercq, R., Derlot, E., Eber, M.V., Duval, J., Courvalin, P., 1989. Transferable vancomycin and teicoplanin resistance in Enterococcus faecium. Antimicrobial Agents and Chemotherapy 33, 10–15.

Mak, I. W. Y., Evaniew, N., Ghert, M. 2014. Lost in translation: animal models and clinical trials in cancer treatment. Am J Transl Res 6(2), 114-118.

Malabarbra, A., Strazzolini, P., Depaoli, A., Landi, M., Berti, M., Cavalleri, B., 1984. Teicoplanin, antibiotics from *Actinoplanes teichomyceticus* NOV. SP. J Antibiotics 37, 988–999.

NHS, L.U.H., 2022. Ophthalmology infection treatment guidelines 4th edition.

Nicolaou, K.C., Boddy, C.N.C., Brase, S., Winssinger, N., 1999. Chemistry, biology, and medicine of the glycopeptide antibiotics. Angewandte Chemie International Edition 38, 2096–2152.

Niibuchi, J.-J., Aramaki, Y., Tsuchiya, S., 1986. Binding of antibiotics to rat intestinal mucin. International Journal of Pharmaceutics 30, 181–187.

Nobbmann, U., Connah, M., Fish, B., Varley, P., Gee, C., Mulot, S., Chen, J., Zhou, L., Lu, Y., Sheng, F., Yi, J., Harding, S.E., 2007. Dynamic light scattering as a relative tool for assessing the molecular integrity and stability of monoclonal antibodies. Biotechnology Genetic Eng Rev 24, 117–128.

Peterson, E., Kaur, P., 2018. Antibiotic resistance mechanisms in bacteria: Relationships between resistance determinants of antibiotic producers, environmental bacteria, and clinical pathogens. Front Microbiol 9, 2928.

Phillips-Jones, M.K., Lithgo, R., Dinu, V., Gillis, R.B., Harding, J.E., Adams, G.G., Harding, S.E., 2017. Full hydrodynamic reversibility of the weak dimerization of vancomycin and elucidation of its interaction with VanS monomers at clinical concentration. Sci Rep-uk 7, 12697.

Provencher, S.W., 1992. Low-bias macroscopic analysis of polydispersity. In: Harding, S.E., Sattelle, D.B., Bloomfield, V.A. (Eds.), Laser Light Scattering in Biochemistry. Royal Society of Chemistry, Cambridge, UK, pp. 92–111.

Rabiah, N.I., Sato, Y., Kannan, A., Kress, W., Straube, F., Fuller, G.G., 2020. Understanding the adsorption and potential tear film stability properties of recombinant human lubricin and bovine submaxillary mucins in an in vitro tear film model. Colloids Surfaces B Biointerfaces 195, 111257.

Rabiah, N.I., Scales, C.W., Fuller, G.G., 2019. The influence of protein deposition on contact lens tear film stability. Colloids Surfaces B Biointerfaces 180, 229–236.

Ramphal, R., Lhermitte, M., Filliat, M., Roussel, P., 1988. The binding of anti-pseudomonal antibiotics to macromolecules from cystic fibrosis sputum. Journal of Antimicrobial Chemotherapy 22, 483–90.

Rivera, J., Tessarollo, L. 2008. Genetic Background and the Dilemma of Translating Mouse Studies to Humans. Immunity 28(1), 1-4.

Sahm, D.F., Kissinger, J., Gilmore, M.S., Murray, P.R., Mulder, R., Solliday, J., Clarke, B., 1989. In vitro susceptibility studies of vancomycin-resistant Enterococcus faecalis. Antimicrobial Agents and Chemotherapy 33, 1588–1591.

Samad, T., Co, J.Y., Witten, J., Ribbeck, K., 2019. Mucus and Mucin Environments Reduce the Efficacy of Polymyxin and Fluoroquinolone Antibiotics against Pseudomonas aeruginosa. Acs Biomater Sci Eng 5, 1189–1194.

Schachman, H.K., 1950. Ultracentrifugation in Biochemistry. Academic Press, New York, NY, USA; London, UK.

Seok, J., Warren, H. S., Cuenca, A. G. et al. Genomic responses in mouse models poorly mimic human inflammatory diseases. PNAS 110(9), 3507-3512.

Setälä, N.L., Holopainen, J.M., Metso, J., Yohannes, G., Hiidenhovi, J., Andersson, L.C., Eriksson, O., Robciuc, A., Jauhiainen, M., 2010. Interaction of phospholipid transfer protein with human tear fluid mucins[S]. J Lipid Res 51, 3126–3134.

Shay, T., Jojic, V., Zuk, O. et al., 2013. Conservation and divergence in the transcriptional programs of the human and mouse immune systems. PNAS 110(8), 2946-2951.

Sterner, O., Karageorgaki, C., Zürcher, M., Zürcher, S., Scales, C.W., Fadli, Z., Spencer, N.D., Tosatti, S.G.P., 2017. Reducing friction in the eye: A comparative study of lubrication by surface-anchored synthetic and natural ocular mucin analogues. Acs Appl Mater Inter 9, 20150–20160.

Tabbara, K.F., 2014. Antimicrobial agents in ophthalmology. Ocular Infect 19–35.

Tesarová, E., Tuzar, Z., Nesmerák, K., Bosáková, Z., Gas, B., 2001. Study on the aggregation of teicoplanin. Talanta 4, 643–53.

Treviño, J., Bayón, C., Ardá, A., Marinelli, F., Gandolfi, R., Molinari, F., Jimenez-Barbero, J., Hernáiz, M.J., 2014. New insights into glycopeptide antibiotic binding to cell wall precursors using SPR and NMR spectroscopy. Chem European J 20, 7363–7372.

Uttley, A.H., Collins, C.H., Naidoo, J., George, R.C., 1988. Vancomycin-resistant enterococci. Lancet 57–58.

Wilson, A.P.R., 2000. Clinical pharmacokinetics of teicoplanin. Clin Pharmacokinet 39, 167–183.

Zaccai, N.R., Serdyuk, I.N., Zaccai, J., 2017. Methods in Molecular Biophysics, Second. ed. Cambridge University Press, Cambridge.

Zhong, X., 2016. Mucin preparation and assembly into new biomaterials. KTH, School of Technology and Health (STH), Medical Engineering, 1-41.

Chapter 6: General Conclusion

6.1. Hydrodynamic analysis of hyaluronic acid and tamarind seed polysaccharides

6.1.1. Hydrodynamic properties of both polysaccharides

This current thesis has presented the hydrodynamic data on hyaluronic acid (HA) and tamarind seed polysaccharides (TSP) before focusing on their ability to interact with each other. These hydrodynamic properties were examined based on sedimentation velocity in the analytical ultracentrifuge (SV-AUC), size exclusion chromatography coupled to multi-angle laser light scattering (SEC-MALS), and capillary viscometry.

Both HA and TSP showed unimodal behaviour in the sedimentation coefficient distributions from SV-AUC and the elution profiles from SEC-MALS. The Gralén equation, or Equation (3-2), provides values of $s^0_{20,w}$ and k_s when values of $s_{20,w}$ are extrapolated to zero concentration. HA and TSP showed $s^0_{20,w} = (4.7 \pm 0.2)\ S$ and $(5.4 \pm 0.2)\ S$, as well as $k_s = (1170 \pm 20)\ mL/g$ and $(240 \pm 30)\ mL/g$, respectively. SEC-MALS analysis of HA and TSP yields the weight-average molar masses M_w = (680 ± 30) kDa and (830 ± 30) kDa, respectively. SEC-MALS generated the Mark-Houwink-Kuhn-Sakurada (MHKS) coefficient (a) from the double-logarithmic plot of $[\eta]$ versus M_w,

showing $a \sim 1.1$ for $M_w < 800$ kDa and ~0.55 for $M_w > 800$ kDa of HA, and $a = 0.63$ for TSP. This means that HA was a stiff rod for $M_w < 800$ kDa while a flexible random coil for $M_w > 800$ kDa. The conformation of TSP was shown to be a flexible random coil. Furthermore, the different approach based on the Ostwald capillary viscometer gave $[\eta] = (1475 \pm 30)\ \mathrm{mL/g}$ for HA and $(675 \pm 20)\ \mathrm{mL/g}$ for TSP, respectively.

HA has been hailed as one of the most recommended eye drops due to its characteristics, such as longer retention time on ocular surfaces (Forrester et al., 2016). This thesis showed that HA was highly viscous according to the intrinsic viscosity measurement. TSP is also highly viscous, but its intrinsic viscosity is half as small as HA. On one hand, TSP is found to be mucoadhesive (Uccello-Barretta et al., 2013) and to have the ability to bind with HA (Uccello-Barretta et al., 2010) based on the NMR studies. Thus, there is a reasonable assumption that the mixture of HA and TSP makes their retention time longer than each component since TSP works as a bridge between HA and ocular mucins.

6.1.2. Interactions between both polysaccharides

The three complementary approaches (SEC-MALS, SV-AUC, and capillary

viscometry) have been applied to the interaction study of the two components of HydraMed®. SEC-MALS profiles showed that for the mixture of HA and TSP (HA/TSP), elution time was slightly shifted to a lower time compared to that of HA and TSP, respectively. This shift in elution profiles would mean that there were some aggregation or weak interactions in the HA/TSP solution. The molar mass determination by SEC-MALS also showed M_w = (720 ± 30) kDa for HA/TSP, which was slightly smaller than the predicted values (755 kDa) obtained from each component, (680 ± 30) kDa for HA and (830 ± 30) kDa for TSP. However, this SEC-MALS result should be confirmed by another method. In contrast, SV-AUC provided the sedimentation coefficient distributions from HA, TSP, and HA/TSP, showing there was no shift to a larger value in $s^0_{20,w}$ values from each component to the mixture. These results were confirmed by the intrinsic viscosity measurement, presenting the data that the $[\eta]$ value of HA/TSP are almost the same as the calculated one obtained from that of HA and TSP, respectively. These observations mean that there were no aggregations or supramolecular complexes in the HA/TSP solution at commercially available concentrations.

This feature – no aggregation or complexation in the mixture – of HydraMed® is more favourable to the application of eye drops regarding quality control. In

addition, the SEC-MALS results implied potential weak or partial interactions between the two polysaccharides, and therefore, reinforced the previous study by NMR spectroscopy (Uccello-Barretta et al., 2010). On one hand, the other favourable feature – the mucoadhesivity of each component – remains unexplored by the hydrodynamic methods. Thus, the next step in the eye-drop study is to further examine the ability to interact with bovine submaxillary mucin (BSM) as the model mucin, regardless of the validity of the ocular mucin model.

6.2. Hydrodynamic analysis of glycan antibiotic teicoplanin A2

6.2.1. Self-association of teicoplanin

This current thesis has also pursued the other main theme: the antibiotic study, as well as the eye-drop study. The mucus layers (including secretary mucins and membrane-associated mucins) of tear films protect humans from not only dry eye syndrome but also ocular infections (Forrester et al., 2016). One of the glycopeptide antibiotics, teicoplanin, is not as favourable a choice for topical eye injection compared to another glycan antibiotic vancomycin, based on the results of corneal absorption (Antoniadou et al., 1998; Kaye et al., 2009). The thesis hypothesized that the aggregational behaviour of teicoplanin may hinder

its entry into corneal cells which are the sites of ocular infections. The teicoplanin study has used other hydrodynamic methods in addition to SV-AUC: sedimentation equilibrium in the analytical ultracentrifuge (SE-AUC) and dynamic light scattering (DLS).

SV-AUC provided the distributions of sedimentation coefficients over 0.125-8 mg/mL, showing that the two extrapolated values of $s^0_{20,w}$ (S) in the plot of $s_{20,w}$ versus c (mg/mL) corresponded to the teicoplanin unimer at ~0.7S and 18-19mer at ~4.65S, respectively. These SV results were further reinforced by SE-AUC experiments, indicating that the molar masses of teicoplanin samples were plateaued to ~33-35 kDa, namely 18-19mers. The DLS measurements provided the hydrodynamic radius ~ 3.2 nm at 12.5 mg/mL corresponding to the 18-19mer teicoplanin. It was also confirmed that these hydrodynamic radii became smaller according to smaller concentrations, meaning that aggregated forms were disassembled to smaller sizes. Finally, the conformation analysis revealed that the overall shape of the teicoplanin assembly was a good approximation to a sphere of an axial ratio (a/b) = 1, which was in good agreement with previous reports of micellization of teicoplanin (Armstrong and Nair, 1997; Wan and Blomberg, 1997).

This study concluded that teicoplanin was more suitable for topical routes at <

0.5 mg/mL because the unimer form was prevalent at that range based on the SV results. The 18-19mer assembly leads to two following consequences – (1) teicoplanin particles may not have access to the sites of infections beyond the ocular epithelia unless they dilute so quickly. (2) In addition, teicoplanin works its antimicrobial activity as a monomer (Beauregard et al., 1995), and as a result, the assembly prevents teicoplanin from working properly. The current thesis on teicoplanin implies that its lower concentrations may be more effective against ocular infections caused by methicillin-resistant *Staphylococcus aureus* (MRSA), rather than 10 mg/mL (Kaye et al., 2009) and 25 mg/~0.5 mL (Antoniadou et al., 1998). On the other hand, there remains a question about whether lower concentrations, i.e., 0.5 mg/mL, could reach the therapeutic concentrations, i.e., 10-30 μg/mL (Wilson, 2000) at the sites of infection.

6.2.2. Interactions of teicoplanin with BSM as an ocular mucin model

The topical route of teicoplanin faces the other challenge for the treatment of ocular infections: the mucus barrier on ocular surfaces. Tear films can prevent bacterial adhesion on ocular epithelia (Forrester et al., 2016), though mucins induce complexation with one of the glycan antibiotics, vancomycin (Dinu et

al., 2020). This thesis has explored the interactions of teicoplanin with mucins because such interactive behaviours in tear films might deplete the clinical action of teicoplanin, in addition to the aggregational behaviours in solution. In order to examine to what degree teicoplanin binds to mucins, the interaction study used SV-AUC and DLS. Additionally, this study visualised aggregates with mucins by means of an appropriate microscopic method (see Dinu et al., 2020), namely environmental scanning electron microscopy (ESEM). BSM was used as the ocular mucin model.

SV-AUC gives distributions of sedimentation coefficients, showing a single peak. Generally, the larger the $s_{20,w}$ values are, the larger the sizes of particles are (Zaccai et al., 2017), whilst the shapes affect the sedimentation coefficient as well. At 0.125 mg/mL of teicoplanin, SV showed no interaction with 1 mg/mL of BSM. In contrast, at both 1.25 mg/mL and 12.5 mg/mL, teicoplanin was shown to have weak interactions with BSM as the $s_{20,w}$ values in each component were shifted to the larger values in the mixtures. Additionally, there were much higher values between ~30S and ~40S in the distributions at these concentrations, indicating the presence of the aggregates in the mixtures.

These results were reinforced by DLS, and furthermore, ESEM. DLS provides

distributions of hydrodynamic radii transformed from diffusion coefficients through the Stokes-Einstein equation. The results of DLS showed that there was a partial loss of macromolecular mucin components upon the addition of 1.25 mg/mL teicoplanin and then a complete loss upon the addition of 12.5 mg/mL teicoplanin. There were also new aggregates at the radius of 300 nm in the mixture of BSM (1 mg/mL) and teicoplanin (12.5 mg/mL). The microscopic method confirmed these hydrodynamic results, visualizing the presence of the aggregates at 1.25 mg/mL and 12.5 mg/mL of teicoplanin with BSM.

Based on the hydrodynamic and microscopic results, this study revealed that teicoplanin, as well as vancomycin, could induce aggregation with BSM. This behaviour should be an important point in antimicrobial activity, considering that total concentrations and the presence of an active form (a monomer for teicoplanin) of glycan antibiotics decrease at the sites of infection. In addition, the aggregational forms with mucins might trigger a further increase of multi-drug resistant species in the bacterial population due to long exposure to antibiotics. Our interaction study of teicoplanin – combining hydrodynamics with imaging – has provided extra evidence to support its binding of mucins in solution.

6.3. Suggestions for future work

This thesis has explored two main themes: the eye-drop and glycopeptide antibiotic studies based on hydrodynamic and microscopic techniques. These studies have provided the data on hydrodynamic properties of eye-drop components, teicoplanin self-association, and the interactions of teicoplanin with BSM. More importantly, the HydraMed® study of the thesis has shown that there were weak interactions but no aggregations in the commercial eye-drop formulation. The teicoplanin study has pointed out that effective concentrations were < 0.5 mg/mL to avoid aggregational behaviours and <12.5 mg/mL to avoid interactive behaviours with mucins in an aqueous solution. This information would contribute to the development of new topical routes for ocular infections.

On the other hand, the thesis has some limitations, especially with regard to the validity of the model ocular mucin. One of the biggest issues of this thesis is the use of genuine ocular mucins due to lack of availability, following the practice of previously published papers have also utilised commercially available BSM as model for ocular mucin (Rabiah et al., 2020, 2019; Setälä et al., 2010; Sterner et al., 2017). Both mucins are somewhat different (i.e., commercial BSM is not a gel-forming mucin as MUC5AC, one of the secretory ocular mucins). Hence, a

following step must be sufficient collection and characterisation of human ocular mucins for reinforcement of the eye-drop and glycan antibiotic projects described in this study.

6.4. References

Antoniadou, A., Vougioukas, N., Kavouklis, E., Chrissouli, Z., Giamarellou, H., 1998. Penetration of Teicoplanin (TEC) into Human Aqueous Humor (AH) after Subconjuctival (SCJ) and IV Administration. Clinical Infectious Diseases 27, 967.

Armstrong, D.W., Nair, U.B., 1997. Capillary electrophoretic enantioseparations using macrocyclic antibiotics as chiral selectors. Electrophoresis 12–13, 2331–42.

Beauregard, D.A., Williams, D.H., Gwynn, M.N., Knowles, D.J., 1995. Dimerization and membrane anchors in extracellular targeting of vancomycin group antibiotics. Antimicrob Agents Ch 39, 781–785.

Dinu, V., Lu, Y., Weston, N., Lithgo, R., Coupe, H., Channell, G., Adams, G.G., Gómez, A.T., Sabater, C., Mackie, A., Parmenter, C., Fisk, I., Phillips-Jones, M.K., Harding, S.E., 2020. The antibiotic vancomycin induces complexation and aggregation of gastrointestinal and submaxillary mucins. Sci Rep-uk 10, 960.

Forrester, J.V., Dick, A.D., McMenamin, P.G., Roberts, F., Pearlman, E., 2016. The Eye Basic Sciences in Practice, Fourth. ed. Elsevier, London.

Kaye, S.B., Neal, T., Nicholson, S., Szkurlat, J., Bamber, S., Baddon, A.C., Anderson, S., Seddon, K., Dwyer, N., Lovering, A.M., Smith, G., 2009. Concentration and bioavailability of ciprofloxacin and teicoplanin in the cornea. Investigative Opthalmology Vis Sci 50, 3176.

Rabiah, N.I., Sato, Y., Kannan, A., Kress, W., Straube, F., Fuller, G.G., 2020. Understanding the adsorption and potential tear film stability properties of recombinant human lubricin and bovine submaxillary mucins in an in vitro tear film model. Colloids Surfaces B Biointerfaces 195, 111257.

Rabiah, N.I., Scales, C.W., Fuller, G.G., 2019. The influence of protein deposition on contact lens tear film stability. Colloids Surfaces B Biointerfaces 180, 229–236.

Setälä, N.L., Holopainen, J.M., Metso, J., Yohannes, G., Hiidenhovi, J., Andersson, L.C., Eriksson, O., Robciuc, A., Jauhiainen, M., 2010. Interaction of phospholipid transfer protein with human tear fluid mucins[S]. J Lipid Res 51, 3126–3134.

Sterner, O., Karageorgaki, C., Zürcher, M., Zürcher, S., Scales, C.W., Fadli, Z., Spencer, N.D., Tosatti, S.G.P., 2017. Reducing friction in the eye: A comparative study of lubrication by surface-anchored synthetic and natural ocular mucin analogues. Acs Appl Mater Inter 9, 20150–20160.

Uccello-Barretta, G., Balzano, F., Vanni, L., Sansò, M., 2013. Mucoadhesive properties of tamarind-seed polysaccharide/hyaluronic acid mixtures: A nuclear magnetic resonance spectroscopy investigation. Carbohyd Polym 91, 568–572.

Uccello-Barretta, G., Nazzi, S., Zambito, Y., Colo, G.D., Balzano, F., Sansò, M., 2010. Synergistic interaction between TS-polysaccharide and hyaluronic acid: Implications in the formulation of eye drops. Int J Pharmaceut 395, 122–131.

Wan, H., Blomberg, L.G., 1997. Chiral separation of DL-peptides and enantioselective interactions between teicoplanin and D-peptides in capillary electrophoresis. Electrophoresis 18, 943–949.

Wilson, A.P.R., 2000. Clinical pharmacokinetics of teicoplanin. Clin Pharmacokinet 39, 167–183.

Zaccai, N.R., Serdyuk, I.N., Zaccai, J., 2017. Methods in Molecular Biophysics, Second. ed. Cambridge University Press, Cambridge.

Publications (3)

- Published:

  Chun, T., MacCalman, T., Dinu, V., Ottino, S., Phillips-Jones, M. K., and Harding, S. E. (2020) Hydrodynamic compatibility of hyaluronic acid and tamarind seed polysaccharide as ocular mucin supplements. *Polymers*. 12, 2272; doi: 10.3390/polym12102272

- Manuscript submitted:

  Chun, T., Pattem, J., Gillis, R. B., Dinu, V. T., Yakubov, G. E., Corfield, A. P. and Harding, S. E. (2022) Self-association of the glycan antibiotic teicoplanin A2 in aqueous solution studied by molecular hydrodynamics.

- Manuscript in preparation:

  Chun, T., Pattem, J., Gillis, R. B., Dinu, V. T., Yakubov, G. E., Weston, N., Parmenter, C., Corfield, A. P. and Harding, S. E. (2022) A comparative hydrodynamic and imaging study on teicoplanin A2 and bovine submaxillary mucin as a model ocular mucin.

Appendix: Supplementary environmental scanning electron microscopy images.

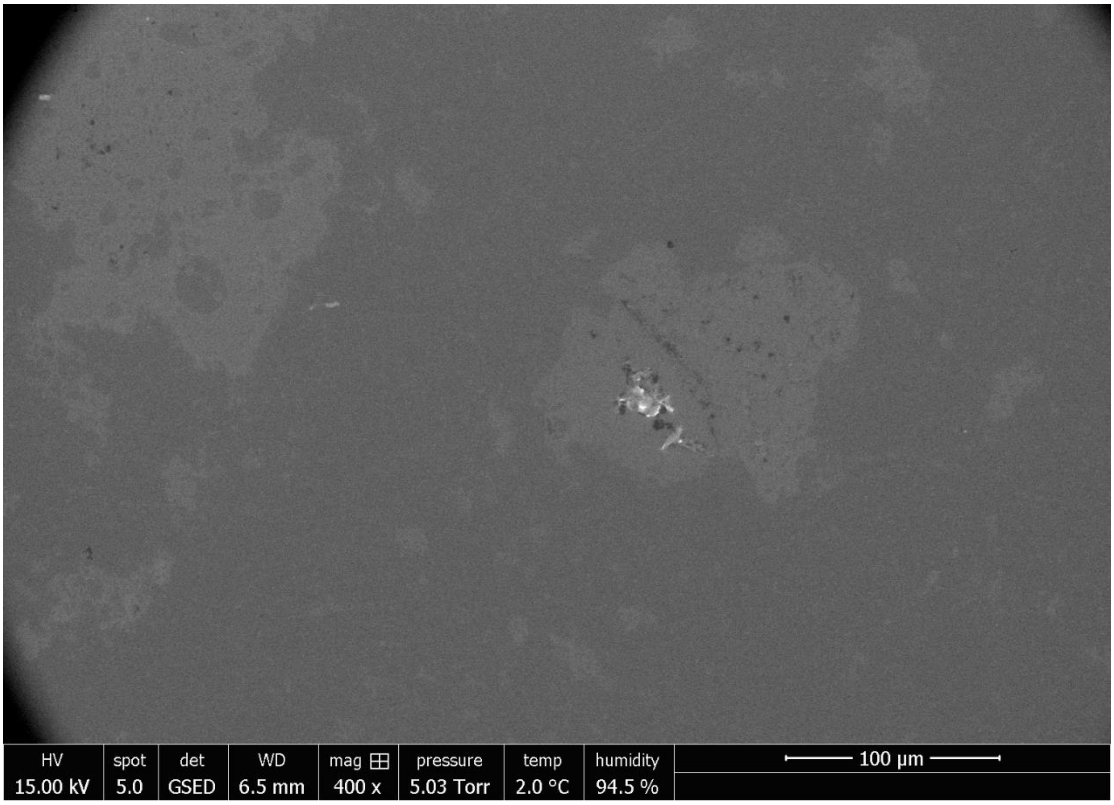

Figure A1: Environmental scanning electron micrographs of BSM control (1 mg/mL)

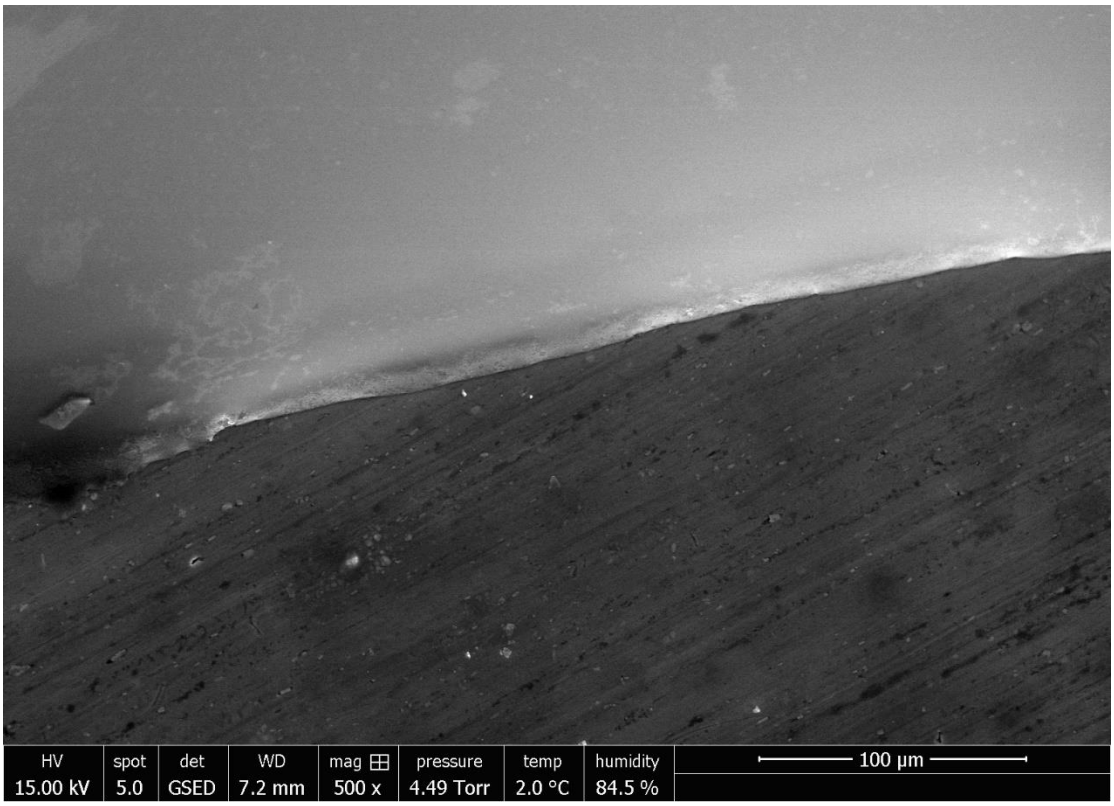

Figure A2: Environmental scanning electron micrographs of BSM control (1 mg/mL)

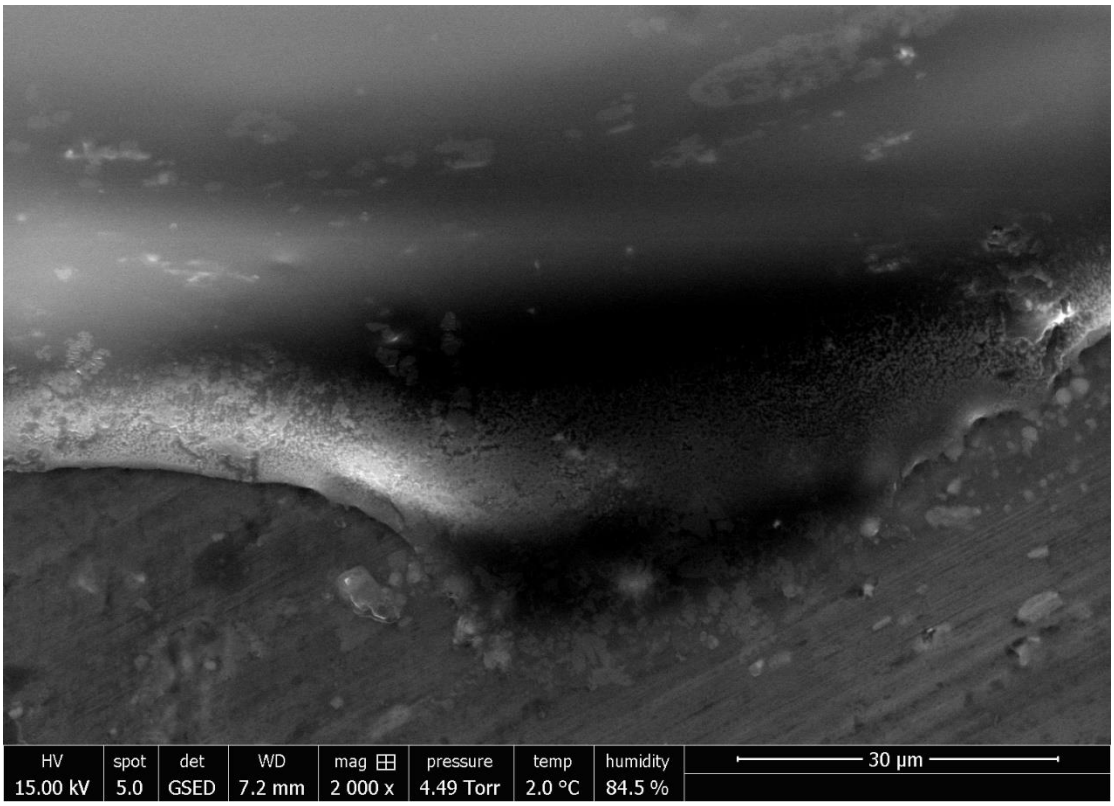

Figure A3: Environmental scanning electron micrographs of BSM control (1 mg/mL)

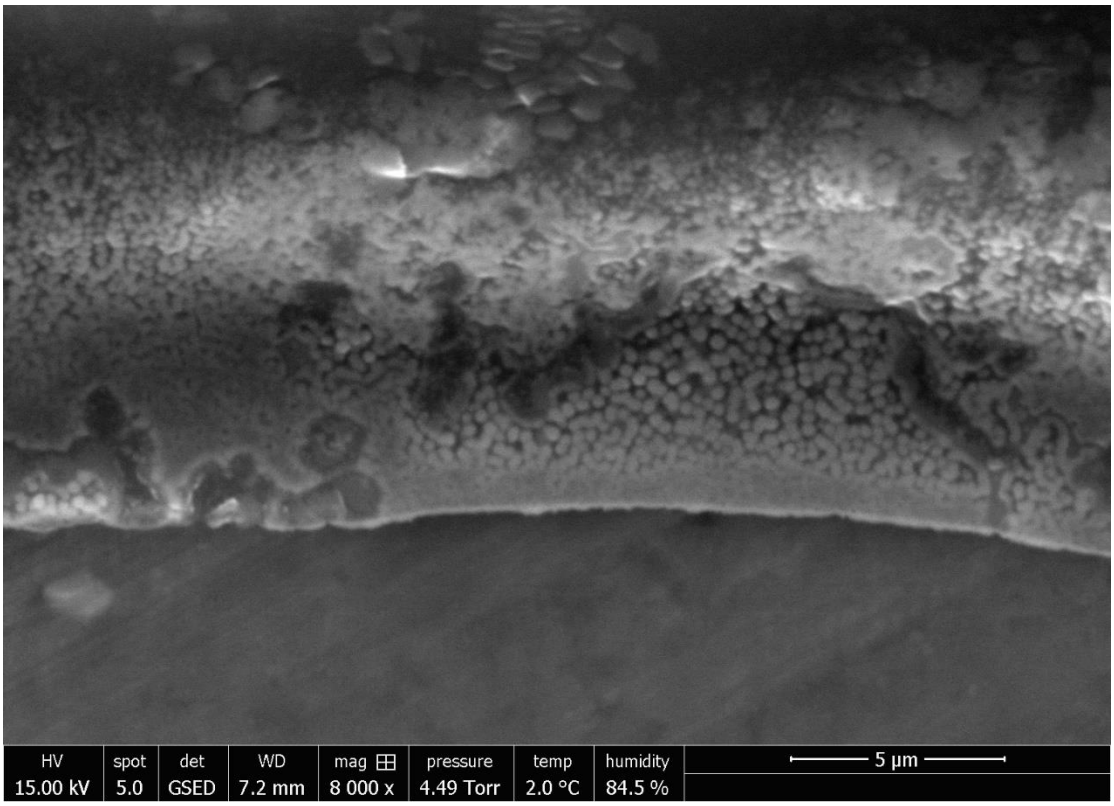

Figure A4: Environmental scanning electron micrographs of BSM control (1 mg/mL)

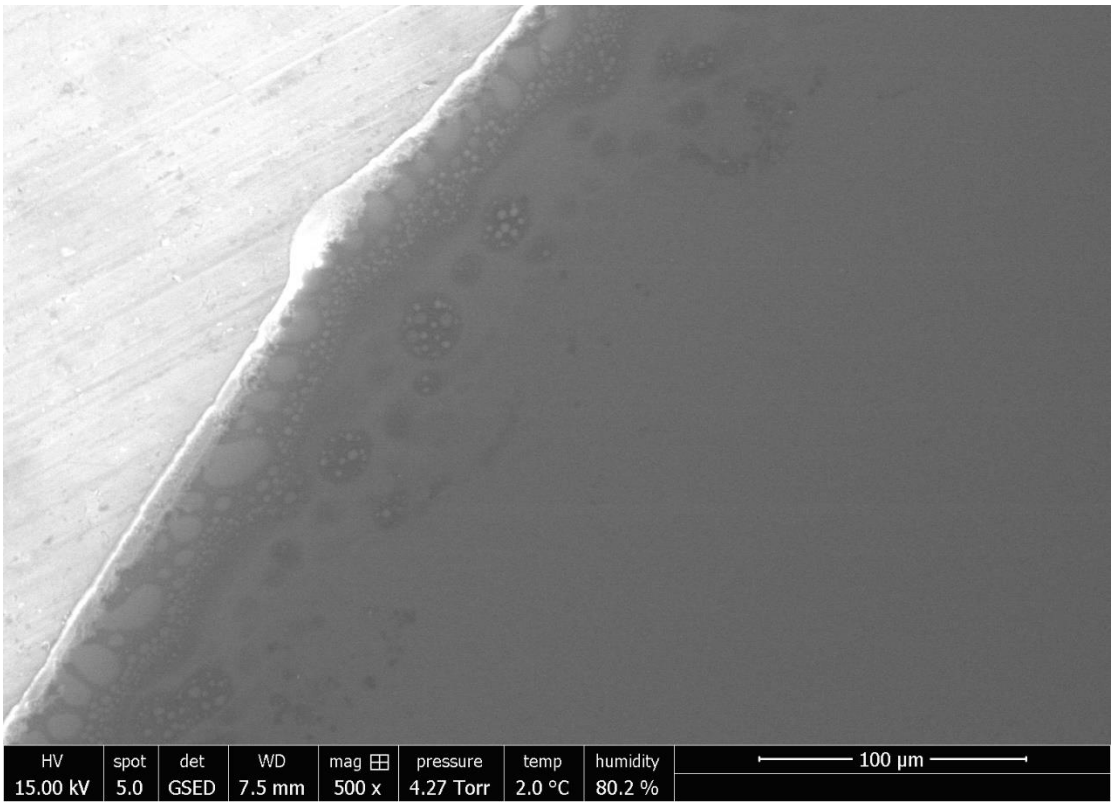

Figure A5: Environmental scanning electron micrographs of BSM control (1 mg/mL)

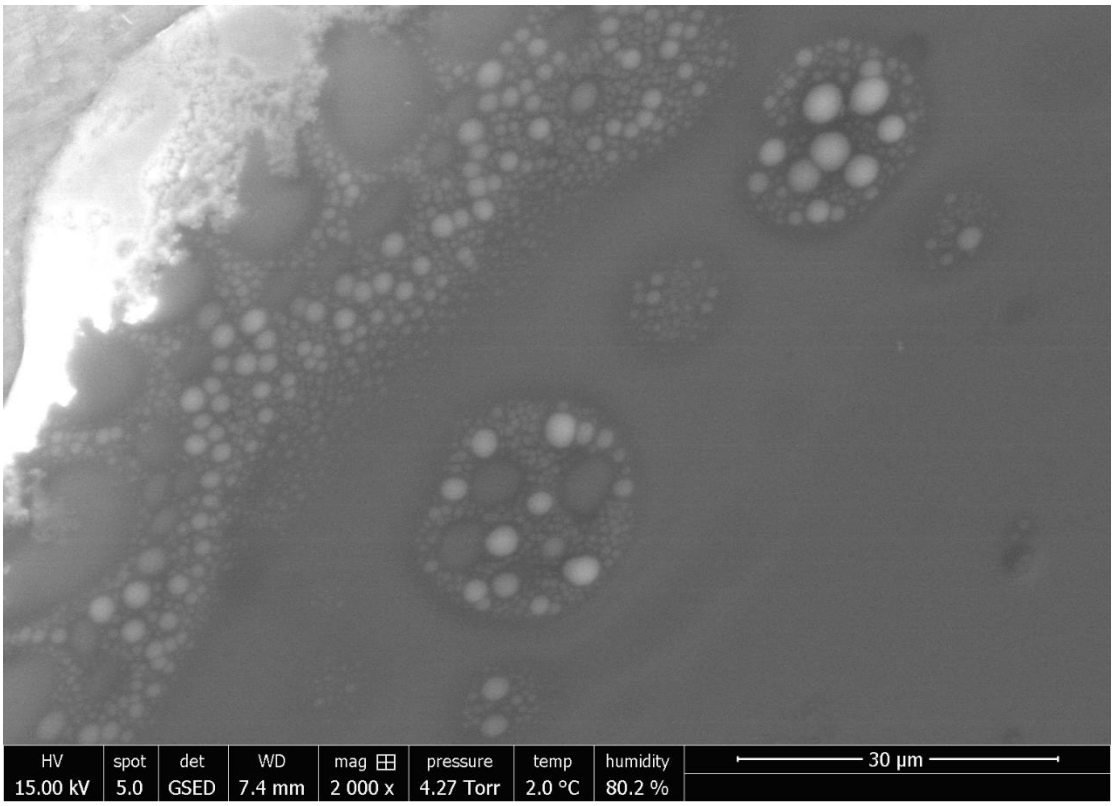

Figure A6: Environmental scanning electron micrographs of BSM control (1 mg/mL)

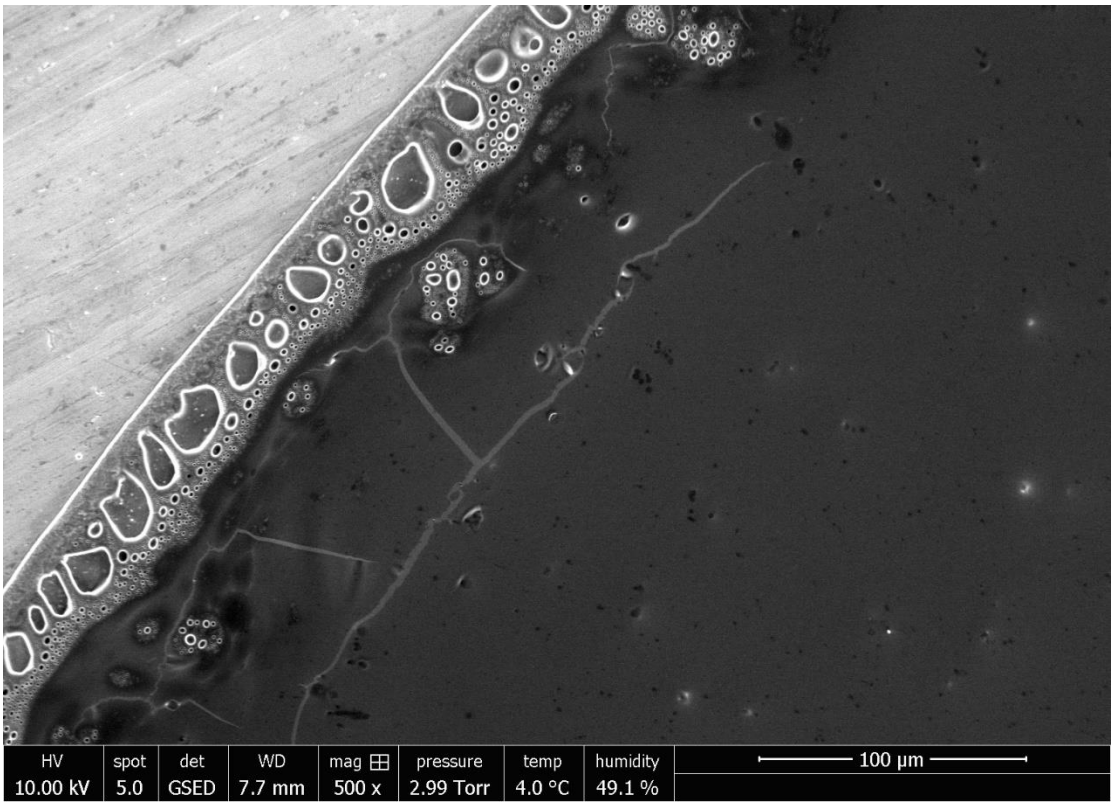

Figure A7: Environmental scanning electron micrographs of BSM control (1 mg/mL)

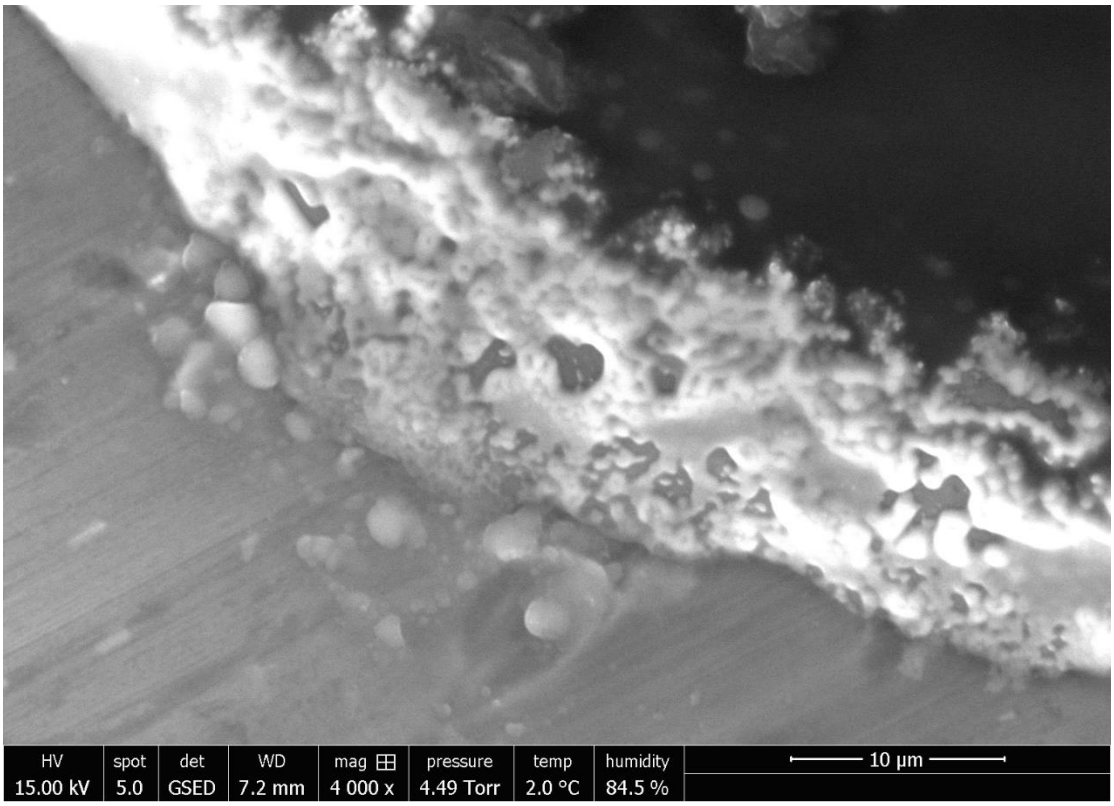

Figure A8: Environmental scanning electron micrographs of BSM control (1 mg/mL)

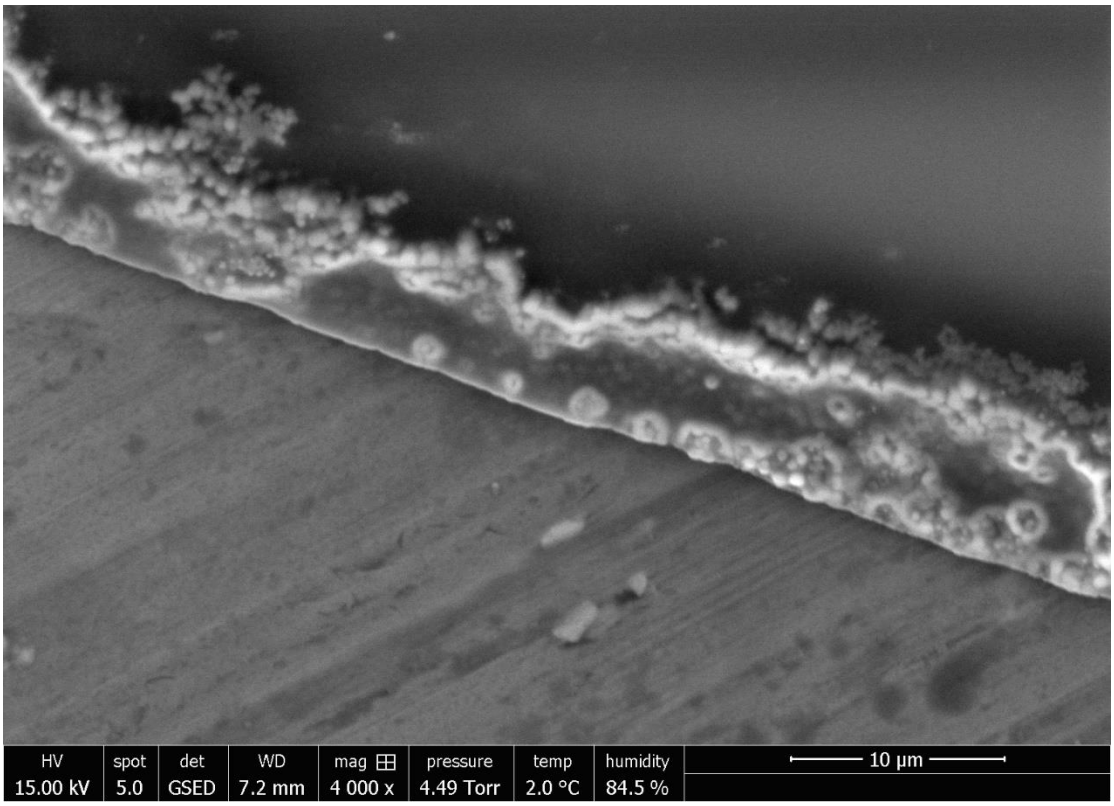

Figure A9: Environmental scanning electron micrographs of BSM control (1 mg/mL)

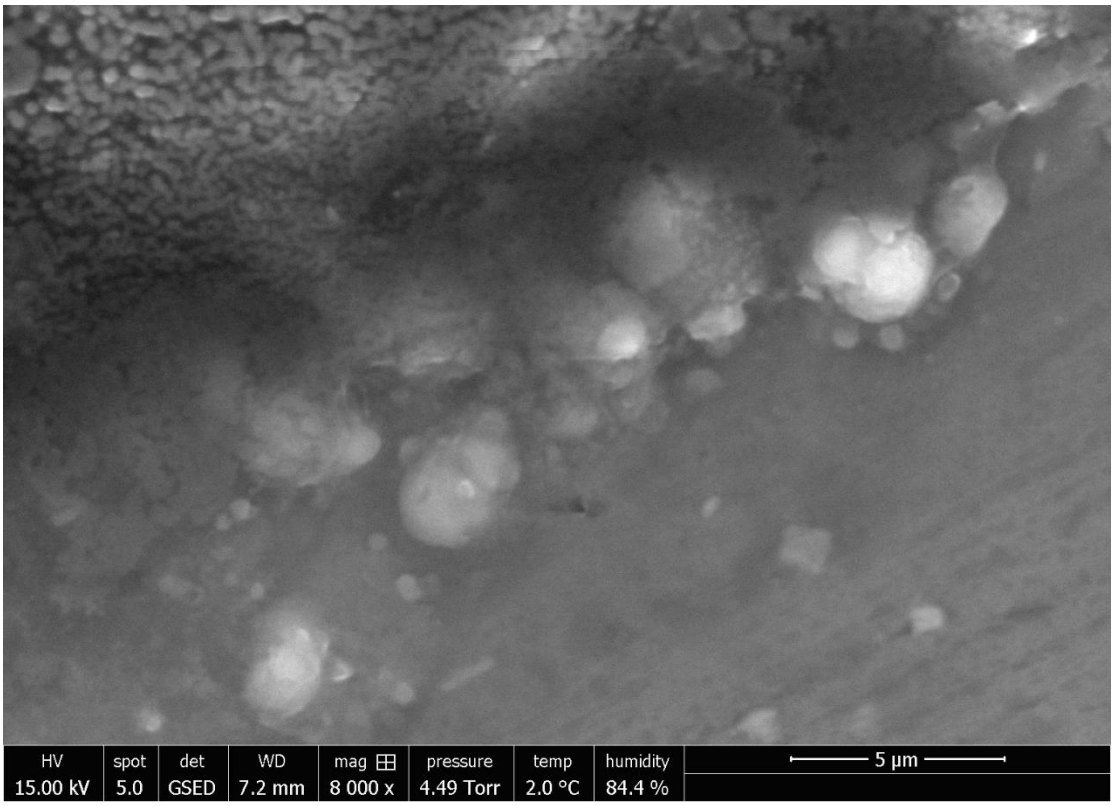

Figure A10: Environmental scanning electron micrographs of BSM control (1 mg/mL)

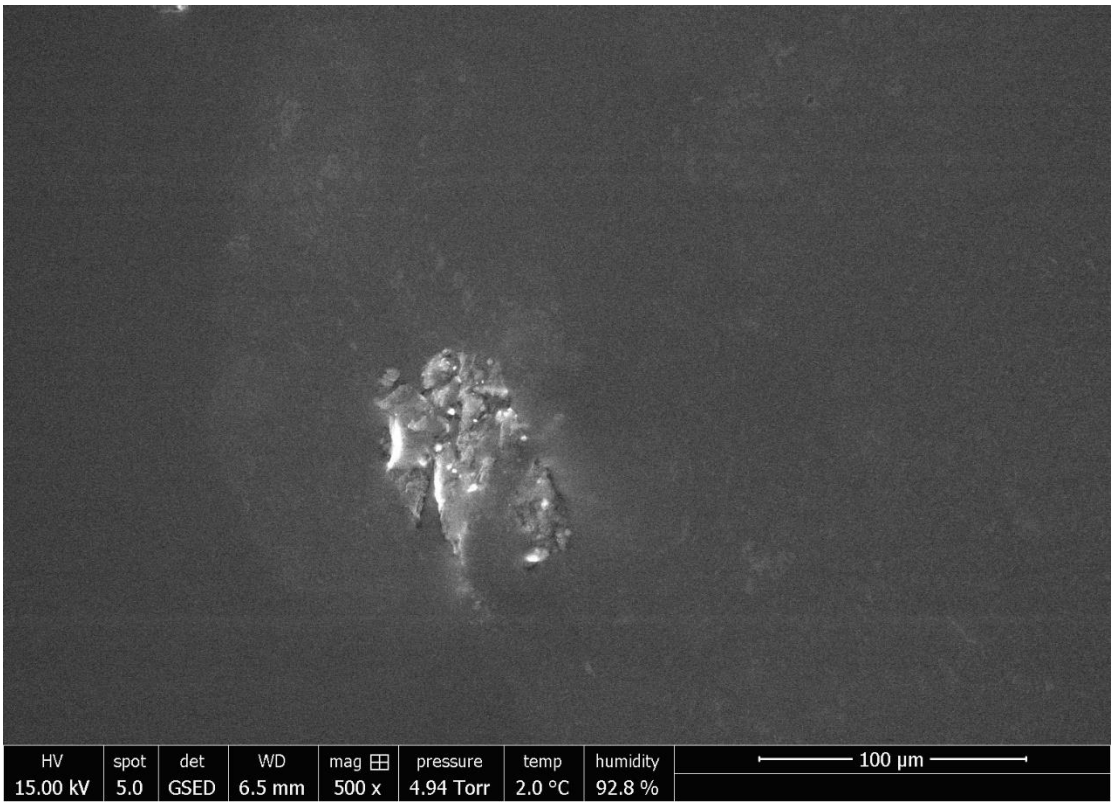

Figure A11: Environmental scanning electron micrographs of the mixture of BSM (1mg/mL) and teicoplanin (1.25 mg/mL)

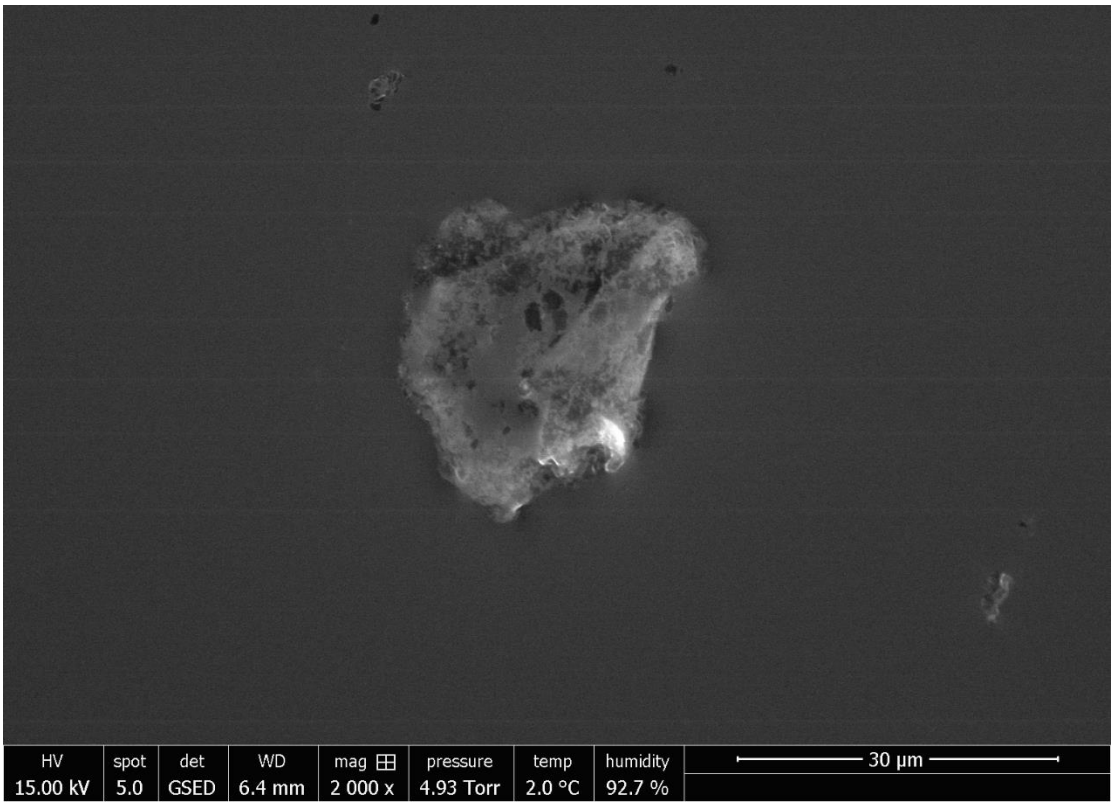

Figure A12: Environmental scanning electron micrographs of the mixture of BSM (1mg/mL) and teicoplanin (1.25 mg/mL)

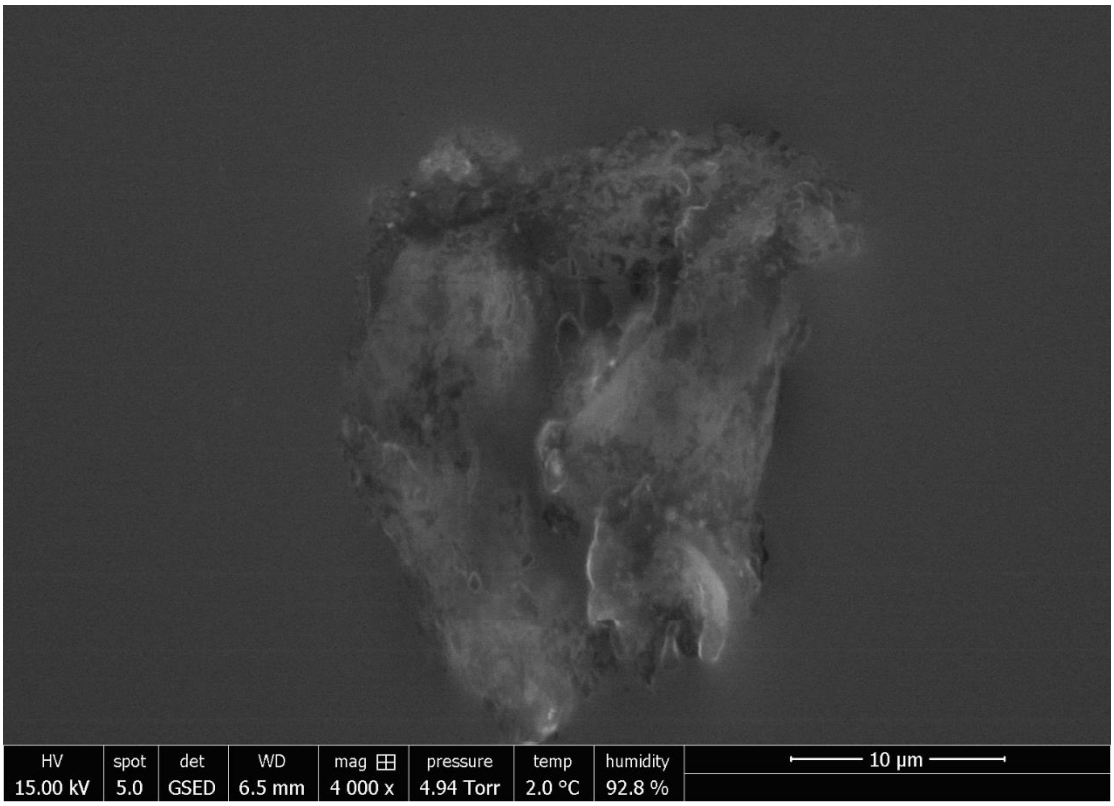

Figure A13: Environmental scanning electron micrographs of the mixture of BSM (1mg/mL) and teicoplanin (1.25 mg/mL)

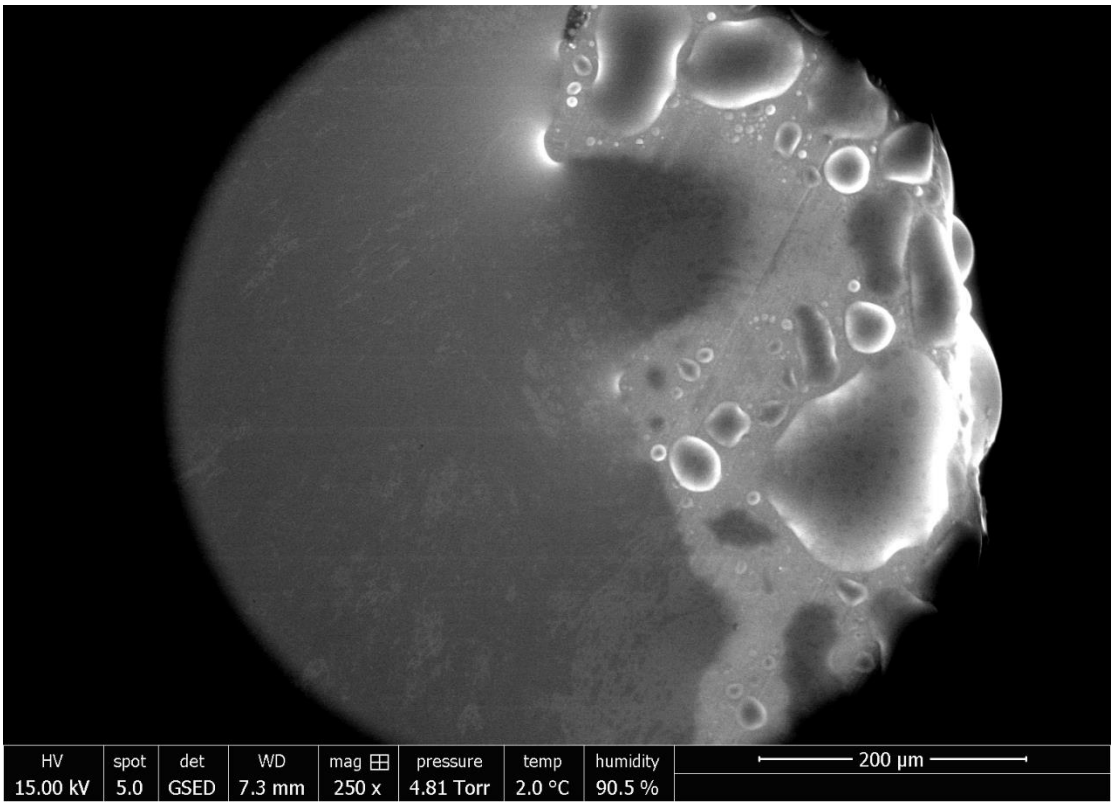

Figure A14: Environmental scanning electron micrographs of the mixture of BSM (1mg/mL) and teicoplanin (1.25 mg/mL)

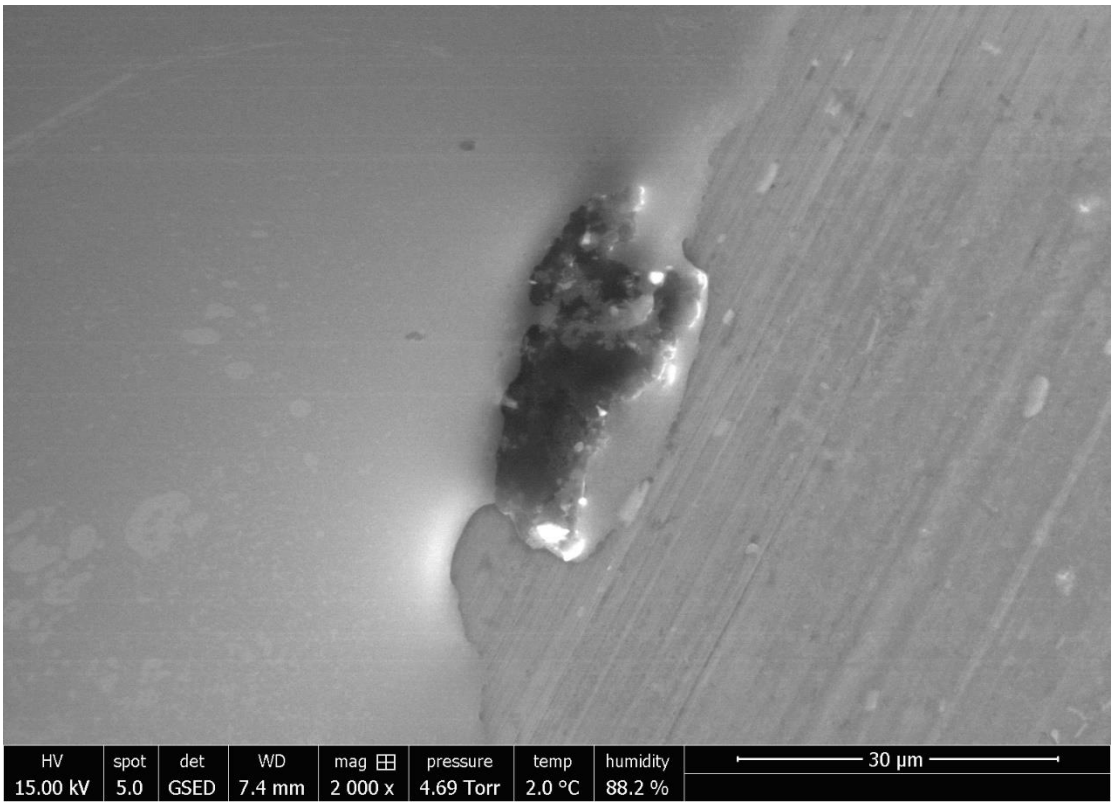

Figure A15: Environmental scanning electron micrographs of the mixture of BSM (1mg/mL) and teicoplanin (1.25 mg/mL)

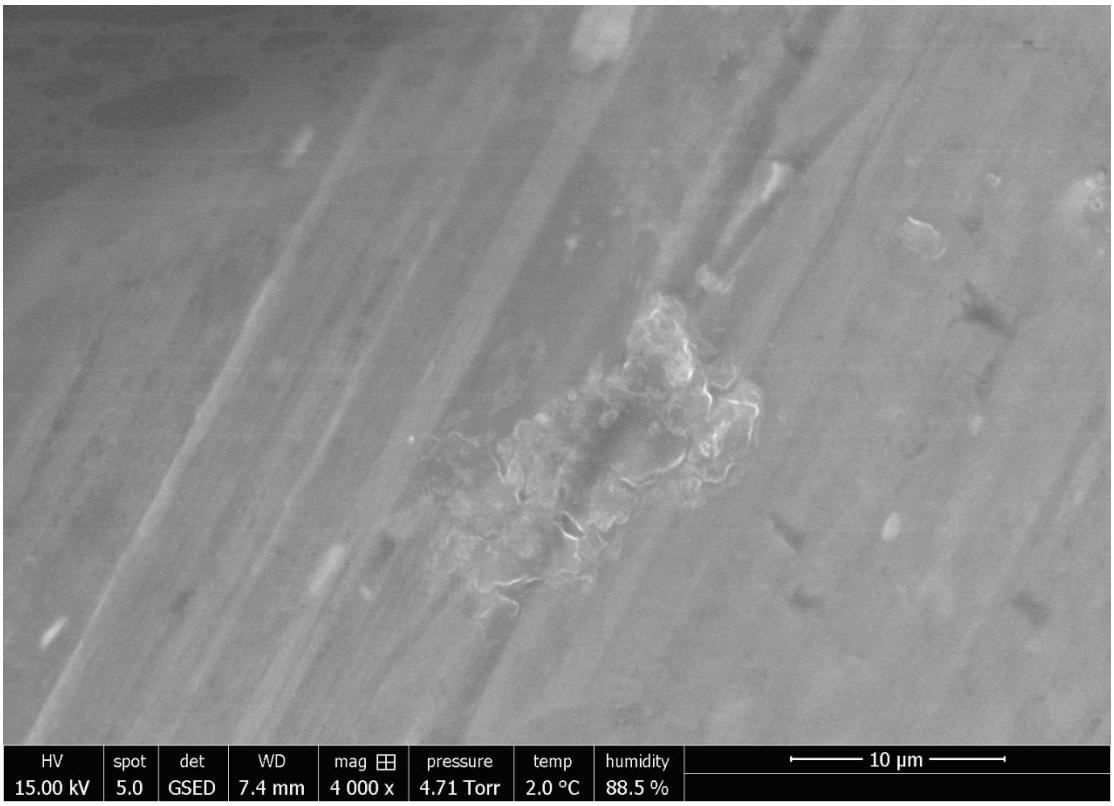

Figure A16: Environmental scanning electron micrographs of the mixture of BSM (1mg/mL) and teicoplanin (1.25 mg/mL)

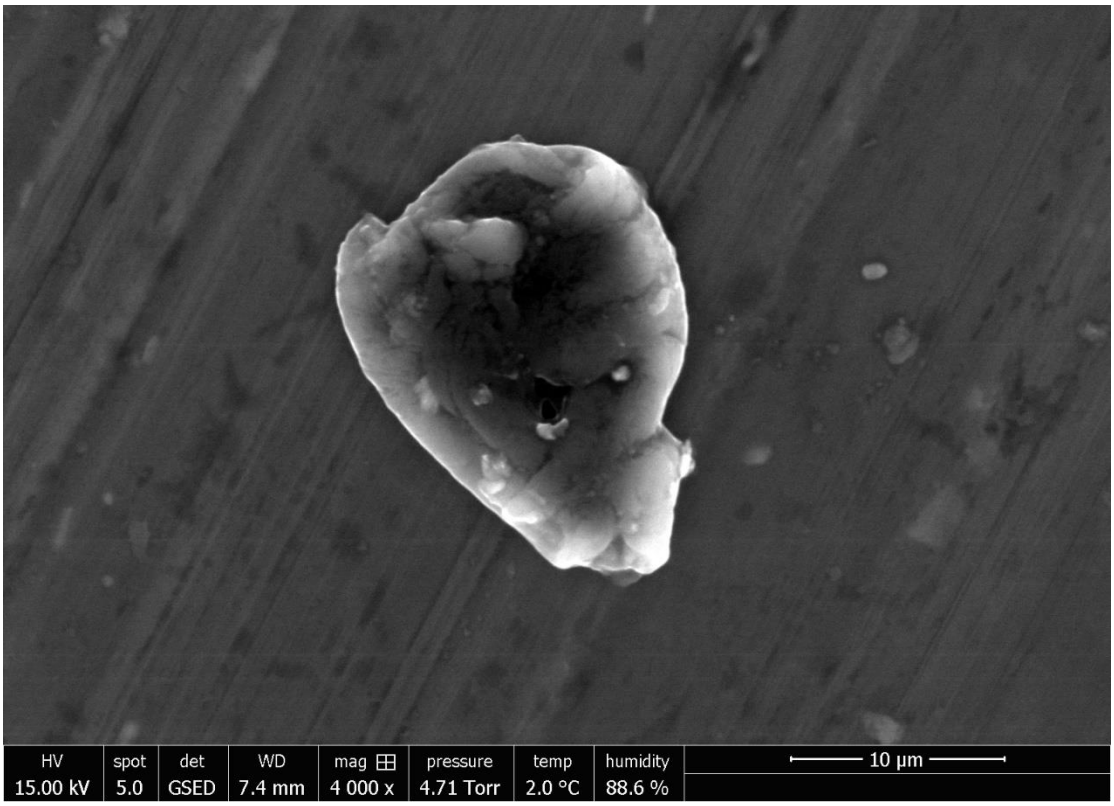

Figure A17: Environmental scanning electron micrographs of the mixture of BSM (1mg/mL) and teicoplanin (1.25 mg/mL)

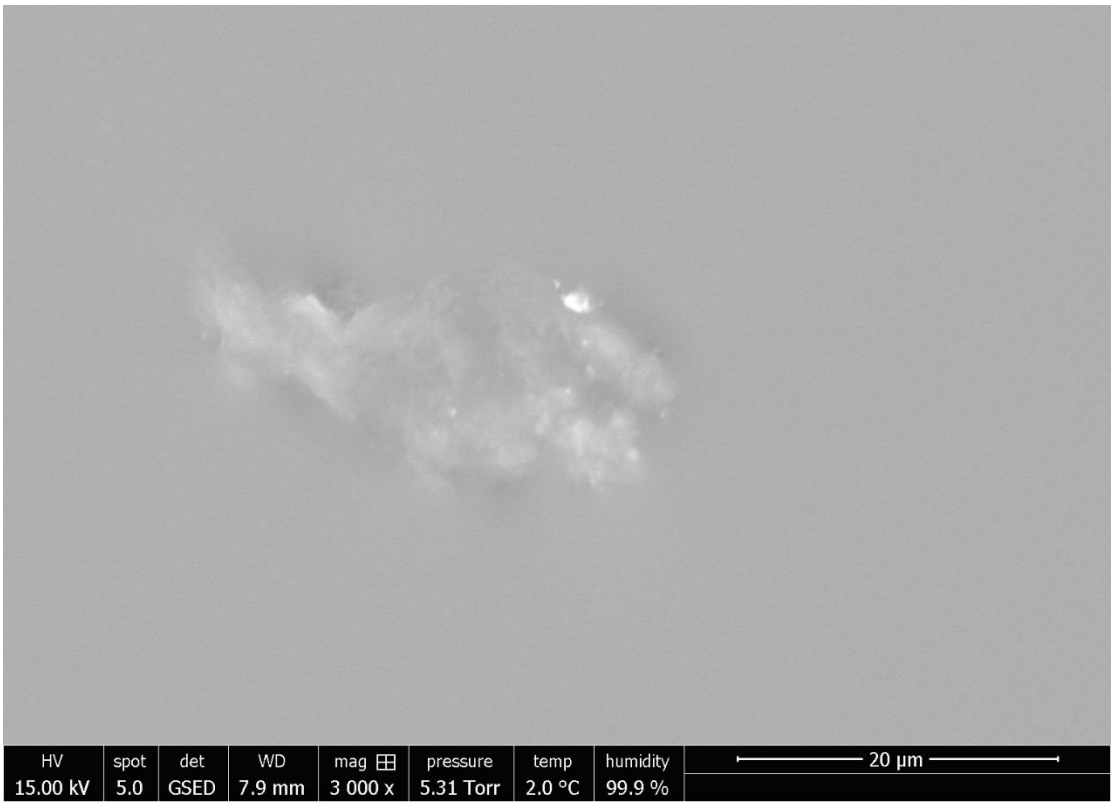

Figure A18: Environmental scanning electron micrographs of the mixture of BSM (1mg/mL) and teicoplanin (12.5 mg/mL)

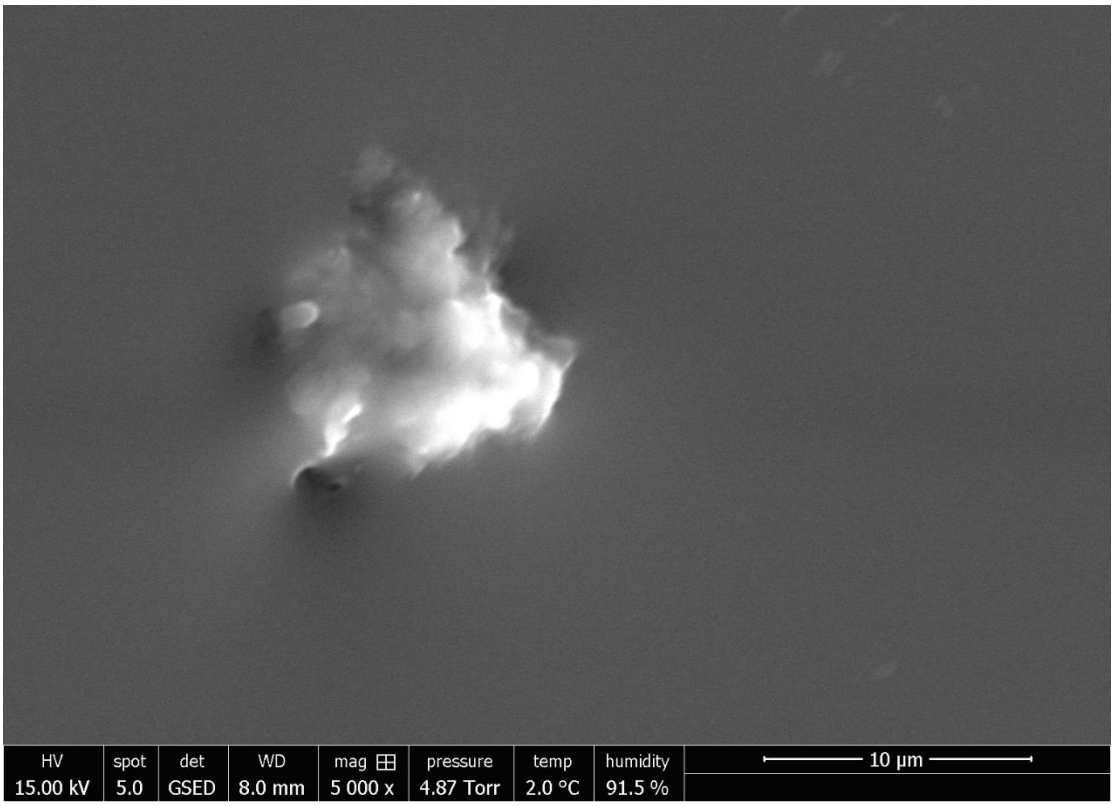

Figure A19: Environmental scanning electron micrographs of the mixture of BSM (1mg/mL) and teicoplanin (12.5 mg/mL)

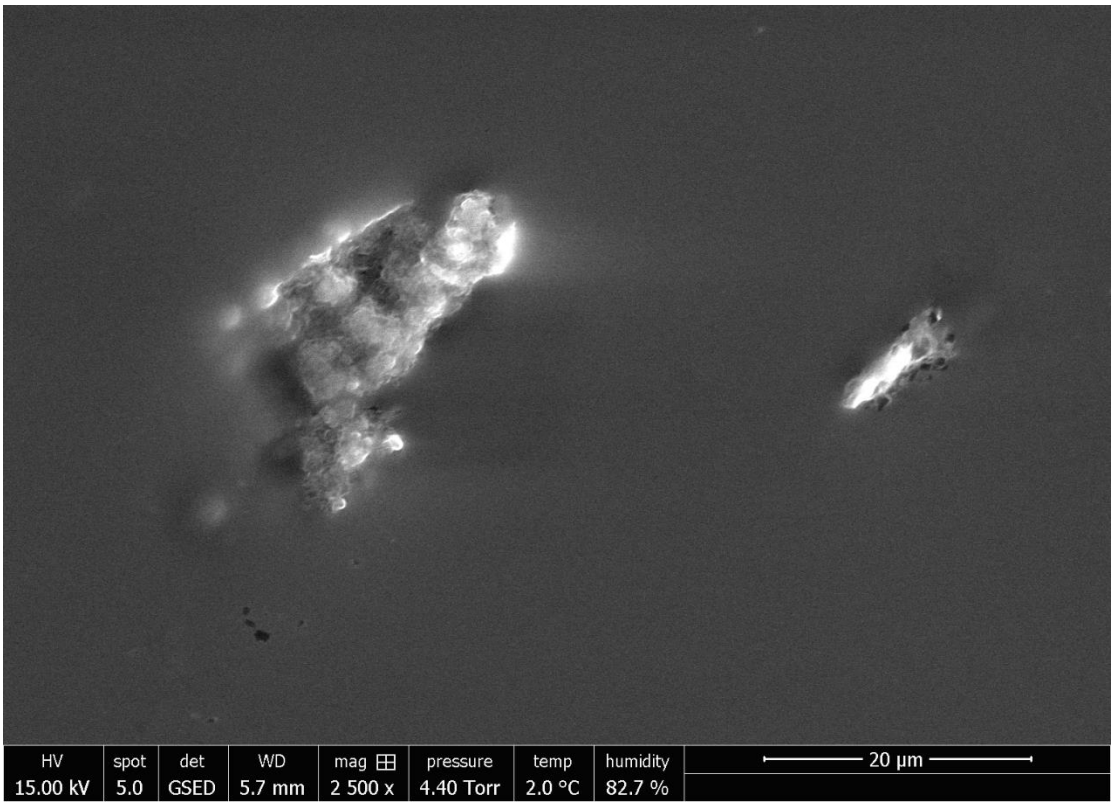

Figure A20: Environmental scanning electron micrographs of the mixture of BSM (1mg/mL) and teicoplanin (12.5 mg/mL)

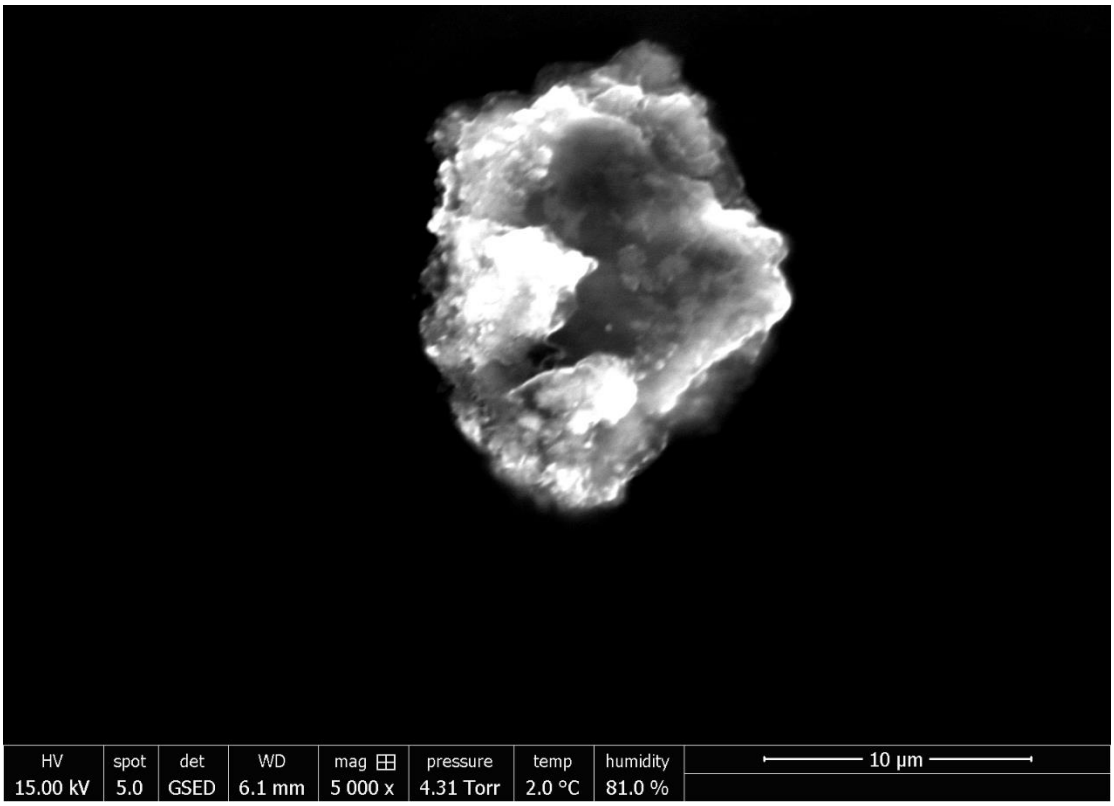

Figure A21: Environmental scanning electron micrographs of the mixture of BSM (1mg/mL) and teicoplanin (12.5 mg/mL)

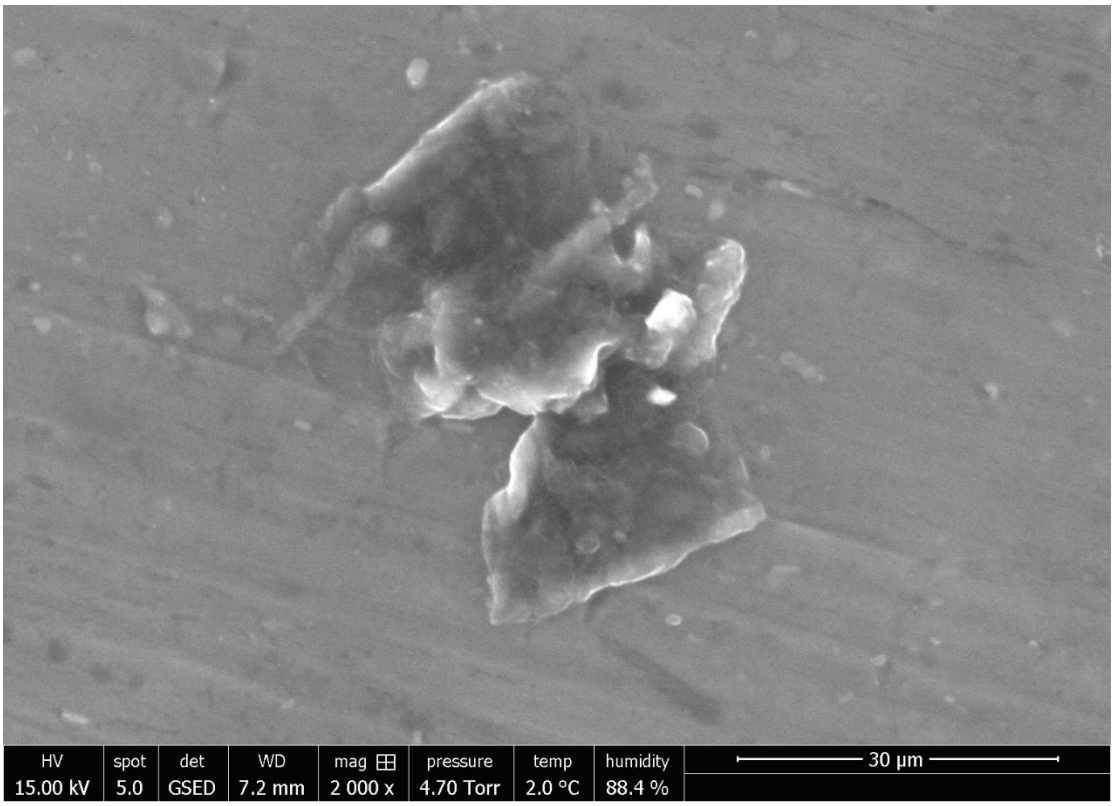

Figure A22: Environmental scanning electron micrographs of the mixture of BSM (1mg/mL) and teicoplanin (12.5 mg/mL)

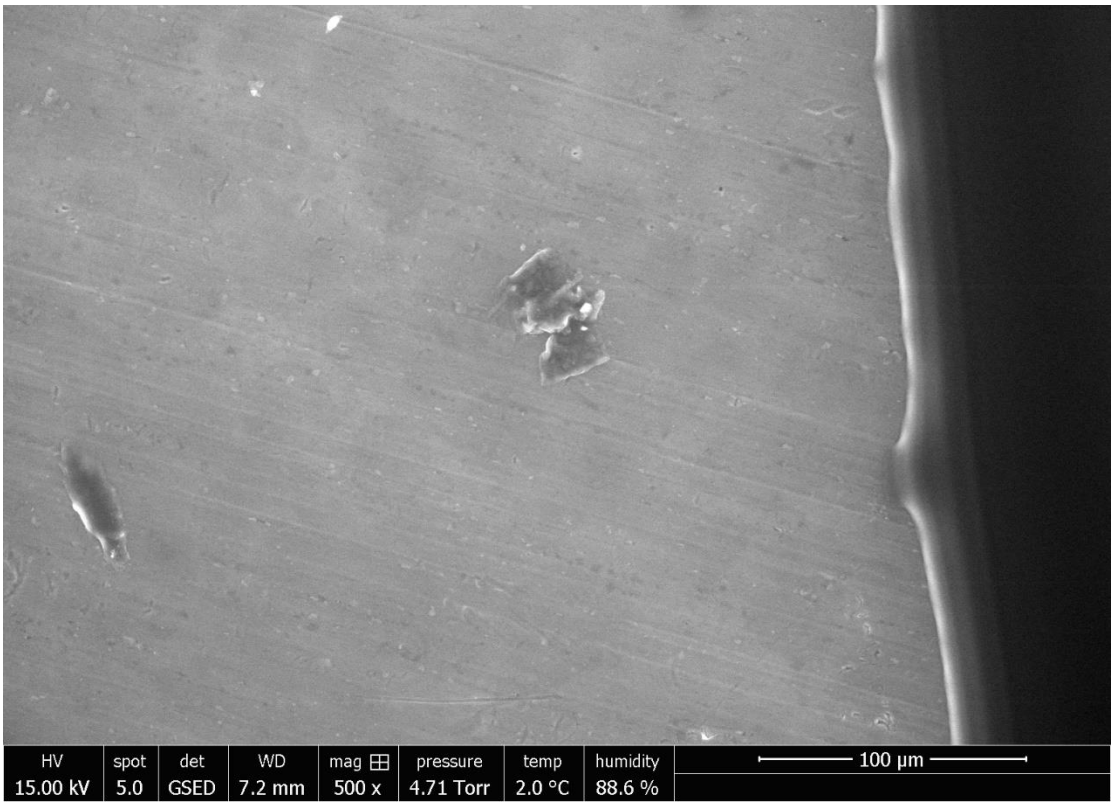

Figure A23: Environmental scanning electron micrographs of the mixture of BSM (1mg/mL) and teicoplanin (12.5 mg/mL)

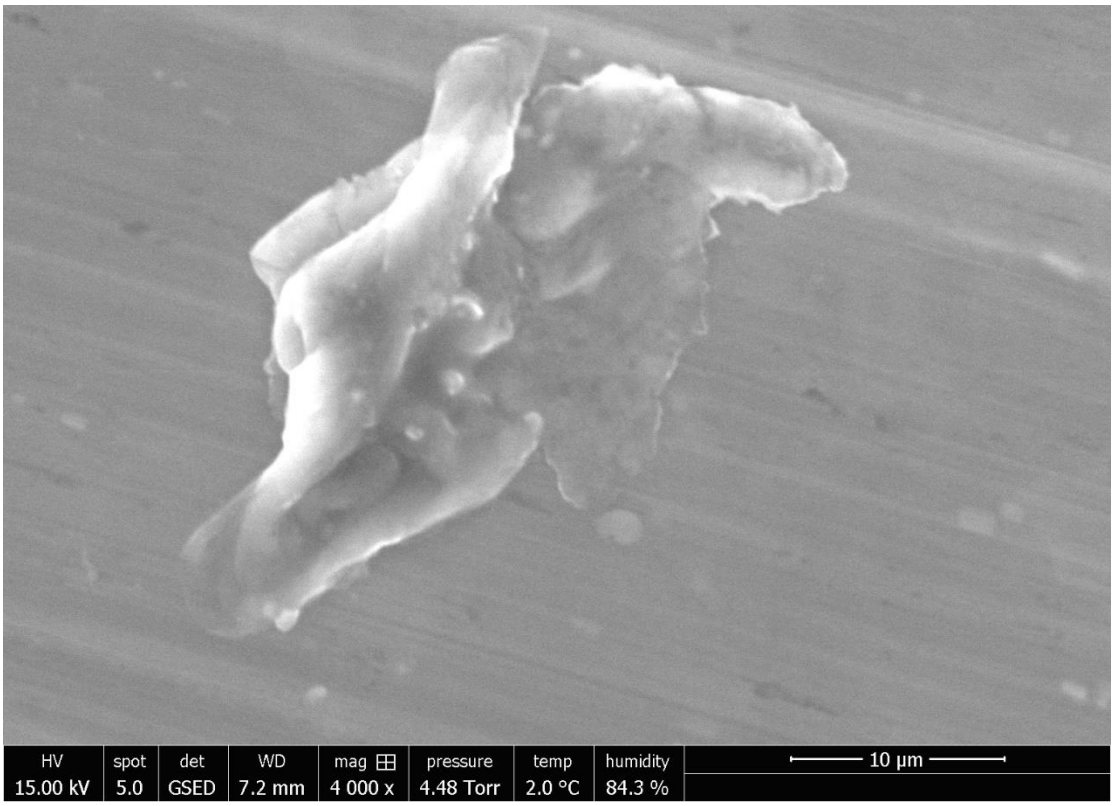

Figure A24: Environmental scanning electron micrographs of the mixture of BSM (1mg/mL) and teicoplanin (12.5 mg/mL)

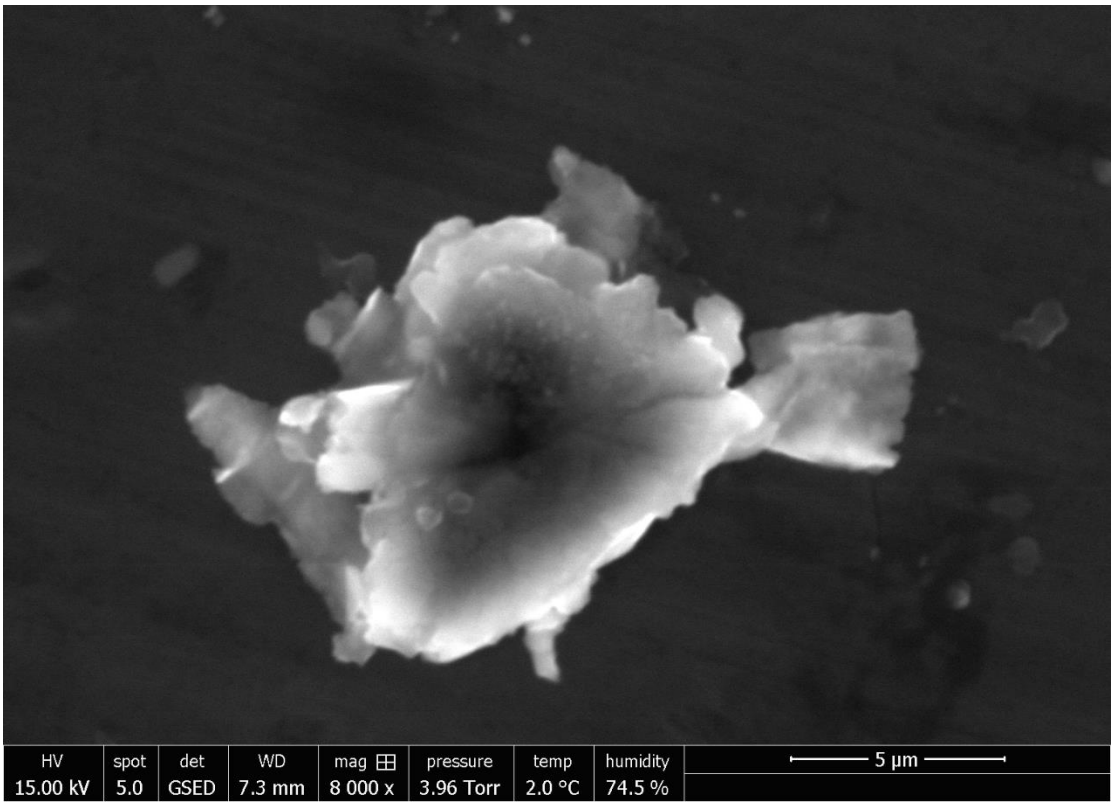

Figure A25: Environmental scanning electron micrographs of the mixture of BSM (1mg/mL) and teicoplanin (12.5 mg/mL)

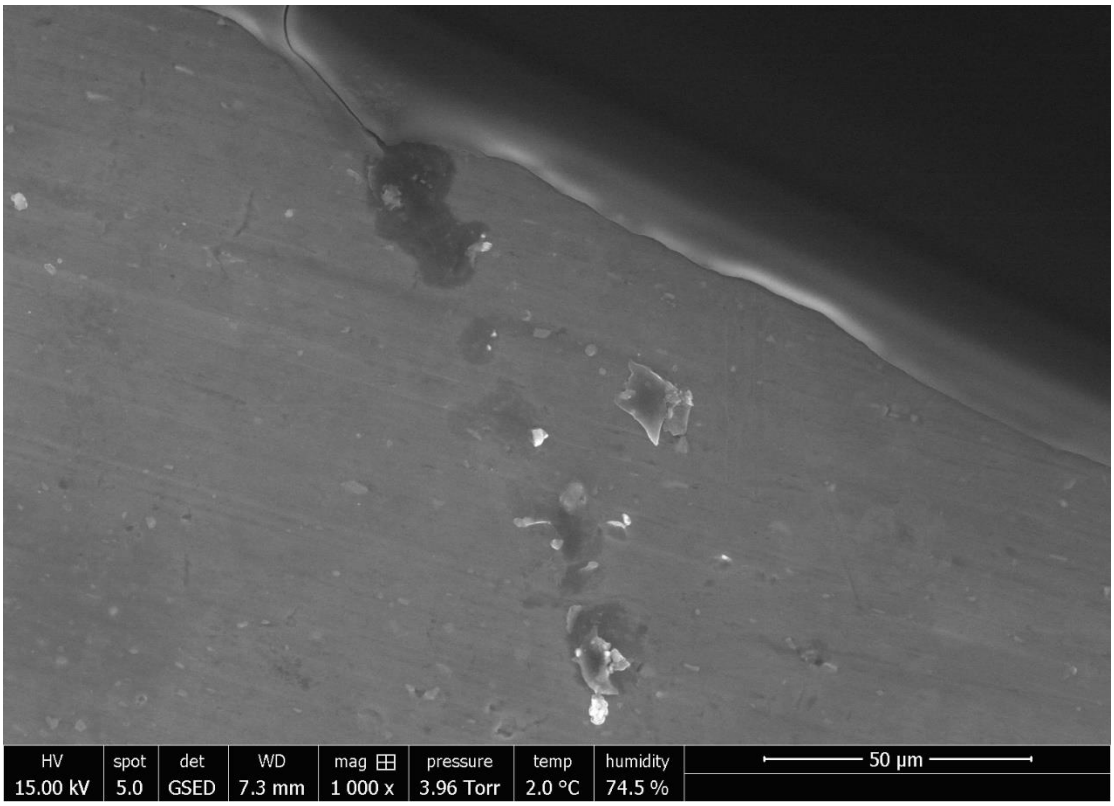

Figure A26: Environmental scanning electron micrographs of the mixture of BSM (1mg/mL) and teicoplanin (12.5 mg/mL)

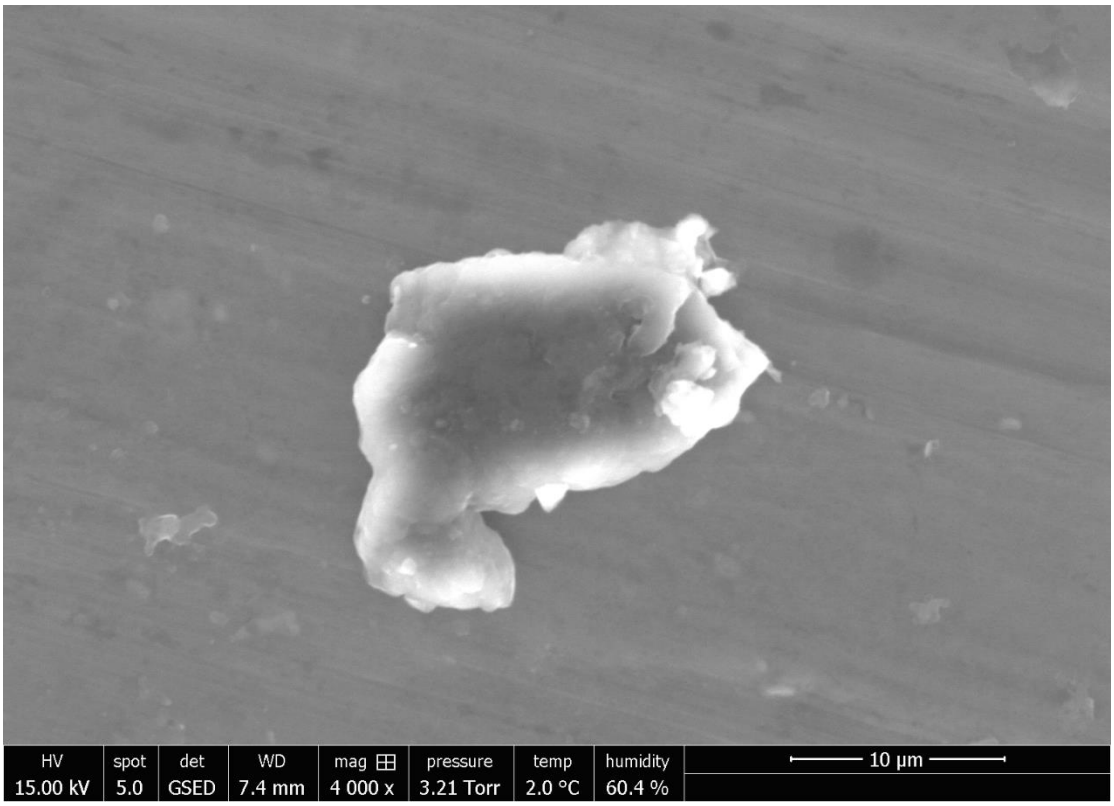

Figure A27: Environmental scanning electron micrographs of the mixture of BSM (1mg/mL) and teicoplanin (12.5 mg/mL)